DIFFUSION AND CONVECTIVE MIXING OF COMPONENTS IN NATURALLY FRACTURED RESERVOIRS

By Victor H. Arana O.

ProQuest LLC.
789 East Eisenhower Parkway
P.O. Box 1346
Ann Arbor, MI 48106 – 1346

A thesis submitted to the Faculty and Board of Trustees of the Colorado School of Mines in partial fulfillment of the requirements for the degree of Doctor of Philosophy (Petroleum Engineering).

Golden, Colorado

Date Sept 26, 2001

Signed: Victor Arana

Victor H. Arana O.

Approved: Hossein Kazemi

Dr. Hossein Kazemi
Thesis Advisor

Ramona M. Graves

Dr. Ramona Graves
Thesis Co-Advisor

Golden, Colorado

Date September 27, 2001

Craig W. Van Kirk

Dr. Craig W. Van Kirk
Professor and Head
Department of Petroleum Engineering

ABSTRACT

Diffusion, in addition to convective mixing, can be an important contributor to component mixing in naturally fractured petroleum reservoirs. The primary objective of this dissertation is to study the significance of the diffusive mixing of nitrogen in such reservoirs in the presence of convective flow induced by injection of nitrogen as well as production of reservoir fluids.

The heart of this dissertation is a numerical model that includes molecular, thermal and pressure diffusion effects, both before and after nitrogen injection. The temperature gradient is assumed to be constant and invariant. The fractured porous media for this study is conceptualized by a dual-continuum approach in which vertical or subvertical fractures are adjacent to the matrix blocks of reservoir rock. Nitrogen is injected at the top of the fracture and oil is produced at the bottom.

The numerical model is a compositional simulator, where pressure and saturations are treated implicitly and composition is treated explicitly. A comprehensive evaluation of important interacting parameters (including fracture orientation, vertical matrix permeability, and matrix porosity) was conducted. The results led to three important conclusions. (1) At virgin reservoir conditions, thermal and pressure diffusion effects contribute to the initial steady-state compositional gradient to some extent. (2) Diffusive mixing of nitrogen is significant only in the low velocity regions of the reservoir such as the interior of the matrix blocks. (3) Hydrodynamic dispersion, that is, the combination of molecular diffusion and mechanical dispersion, is the main cause of fluid mixing in the high-velocity regions of the reservoirs.

TABLE OF CONTENTS

LIST OF FIGURES

LIST OF TABLES

ACKNOWLEDGMENTS

I would like to thank my advisor Dr. Hossein Kazemi who furthered my understanding of reservoir simulation, and who taught me to see obstacles in a simple way – he told me so many times "Victor, make your life simple." I will keep it in mind. It was an honor for me to work under his engaged and expert guidance. I am very appreciative.

I am also greatly indebted to Dr. Ramona Graves, my co-adviser, who helped me in crucial moments and provided me many useful comments.

My gratitude is further extended to my committee members: Dr. J. Fanchi, Dr. E. Ozkan, and Dr. T. Ohno. Special gratitude goes to Dr. N. Hurley, who helped me immensely in editing the final version of my thesis.

I am indebted to Dr. Craig Van Kirk, Head of Petroleum Department, for his ever-present and timely moral support.

Also, I want to thank Pemex-Exploration-Production for the financial support during my stay at CSM. Finally, I would like to thank Dr. Fernando Rodriguez, manager of reservoirs at Pemex, for being interested in what I was doing.

Dedicated to my wife, Dalia, and
our lovely sons, Irvin and Elliot, for giving me the
chance to finish this work.

CHAPTER 1

INTRODUCTION

Numerical simulation is the most practical reservoir engineering tool to study compositional multiphase flow in naturally fractured reservoirs. Compositional simulators were developed for predicting the phase and compositional behavior of petroleum reservoirs during the production phase of the reservoir as well as during hydrocarbon gas injection. Multiphase compositional simulators are also needed to study specific EOR reservoir process, including nitrogen and carbon dioxide injection.

Our ability to exploit a petroleum reservoir system depends on how well the system is understood. The goal of any study is to enhance our understanding of such systems. In general, one uses reservoir models to decipher the interaction of several competing phenomena in an effort to arrive at a practical analysis of the system. Furthermore, modeling of complex fluid flow through porous media is difficult. This difficulty increases when the system is inhomogenous. Such is definitely the case of most naturally fractured petroleum reservoirs, where fractures are responsible for fluid transport to the wellbore while the rock matrix acts mainly as a storage medium that feeds the fractures.

For modeling naturally fractured petroleum reservoirs on a global scale, it is common to use either the dual-porosity or dual-porosity/permeability approach. In the dual-porosity

approach, the fracture network is a treated as a continuum while matrix blocks are treated as discontinuous discrete units embedded in the fracture network. The two are linked by a matrix-fracture transfer function. In the dual-porosity/permeability approach, both matrix and fractures are continuous and are still linked by a matrix-fracture transfer function. For modeling reservoir performance on a local scale, a simpler approach is to model a fractured porous media as a single matrix block with an adjacent fracture. This approach is a good fine-scale representation of a fractured reservoir since it allows one to show more details of the fluid flow between the fracture and the matrix block.

It has long been common to inject inert gas into naturally fractured, volatile-oil reservoirs. Doing so can improve recovery by maintaining reservoir pressure, displacing oil, and/or vaporizing the intermediate components of the oil. As the injected gas is not initially at equilibrium with the reservoir oil, the contact between the phases results in mass transfer, or diffusion. There are three types of mass transfer mechanisms: molecular, thermal, and pressure diffusion (also known as gravitational segregation). Molecular diffusion is the tendency to mix due to concentration or chemical potential gradient. Thermal diffusion is the tendency to separate components under a temperature gradient. Pressure diffusion results in component separation by pressure gradient. With respect to molecular diffusion, there are three types: gas-gas, liquid-liquid and gas-liquid diffusion. In a multi-component system, the tendency of molecular diffusion to equalize composition may be impeded by thermal and pressure diffusion. In a naturally fractured

petroleum reservoir, when the fluid contained in both fracture and matrix blocks develop a compositional gradient, molecular diffusion tends to equalize matrix and fracture fluid composition. Diffusion stops when a final thermodynamic equilibrium is reached in both media. It can be a slow process. Molecular diffusion coefficients in gases are one or two orders of magnitude larger than liquids. Gas-liquid diffusion coefficients are about the same as those used for liquids. In general, pressure and thermal diffusion in porous media are small because pressure and temperature gradients and their respect coefficients are small.

In addition to diffusion, dispersion (another important part of the mixing phenomena) can be related to the distribution in travel times that results when a fluid passes through a porous media. When two miscible fluids are brought into contact with an initially sharp front separating them, a transition zone develops across the initial front. The two fluids slowly diffuse into each other and, after some time, develop a diffused mixed zone. This mixing process is independent of whether or not a convective current exists in the medium. If, however, the two fluids are also flowing, as is the case in the exploitation of a real reservoir, then a different sort of mixing, known as convective mixing, will occur. Convective mixing is caused by a non-uniform velocity field, which, in turn, may be caused by the morphology of the medium, the fluid flow condition, and the chemical or physical interactions with the solid surface of the medium.

On a microscopic scale, the two most important mechanisms contributing to mixing are convective mixing and diffusion. When studying compositional gradient before production, diffusive fluxes have to be considered. In practice, one usually combines the molecular diffusion and mechanical dispersion into a single process known as hydrodynamic dispersion.

Unlike nonfractured porous media where diffusion is generally insignificant, in naturally fractured reservoirs diffusion can be very important. Dispersive flux through fractures rapidly increases the contact area for diffusion and, therefore, accentuates compositional differences between matrix and fracture fluid. When an inert gas is injected into a naturally fractured reservoir, the composition of both the fracture and the matrix fluids must be understood to predict gas breakthrough in producing wells. This can be done with the help of a compositional numerical simulator.

Numerical models can be used to simulate a variety of scenarios. For example, the composition of the fluid phases within the reservoir can be calculated before any field project is initiated. Furthermore, the model can provide the distribution and composition of produced fluid as well as the amount of inert gas that must be injected at a certain period of time to maintain pressure.

Compositional simulation models are further used to simulate processes for which the

black oil assumptions are weak or invalid. The compositional models describe the fluid contained in the reservoir as a mixture of components. Gas-oil phase properties and equilibrium ratios are calculated from pressure- and composition-dependent correlation or from an equation of state (EOS). For each component in the fluid mixture, a compositional multiphase flow simulator consists of a mass conservation equation, flow equations and thermodynamic equilibrium constrains and specific constrains regarding mole fractions, saturations, and pressures. These equations result in a set of partial differential equations to be solved. An important characteristic of these equations is their strong nonlinearity, which requires solution by numerical methods. In the numerical methods, the continuous character of a given equation in time and space is changed to a set of discrete equations by using finite difference method. Ultimately, the result is a nonlinear system of algebraic equations where the Newton-Raphson method can be used to linearize the equations. Then, any linear equation solver can be used to arrive at the solution iteratively.

Assuming a matrix block with an adjacent fracture as our fractured porous medium, a numerical simulator works in the following manner. It breaks the reservoir into two systems: one, a system of matrix cells and the other, a system of fracture cells. Most of the flow to the wells occurs through the fracture network with high permeability that contains a relatively small fluid volume. The bulk of the hydrocarbon fluid is contained within the matrix cells. The fluids within each cell are considered to be in equilibrium at

the cell pressure and temperature. The change of reservoir condition over time is investigated by determining average values in each cell during successive time steps. As the reservoir is depleted, fluids are expelled from the matrix into the fracture, which conveys them to the producing wells.

The set of equations simulating compositional multiphase flow results in a system of ($2nc$+6) equations, with the same number of unknowns for each cell. Here, *nc* stands for the number of components, or pseudo-components, used to represent the fluid. The unknowns, also known as primary variables, are three pressures, three saturations, and *nc* molar fractions for each component in each phase, namely, oil and gas.

Reservoir compositional simulators are used to predict the performance of those fluids within a reservoir in which their volumetric properties are a function of pressure, temperature, and composition, that is, volatile oil and gas and condensate. They are the best computational tools for forecasting depletion of volatile oil, gas and condensate reservoirs, injection of inert gases and others. Although used for many years, reservoir simulation still presents some areas in need of improvements.

An important issue in compositional simulation is fluid phase behavior. The behavior of a hydrocarbon mixture at reservoir and surface conditions is determined by its chemical

composition as well as by the prevailing pressure and temperature. This behavior is of prime consideration in the development and management of reservoirs, thus, affecting all aspects of petroleum exploration and production.

In general, the behavior of a hydrocarbon mixture can be determined from an equation relating pressure, temperature, and volume, that is, an equation of state (EOS). An EOS can be used to describe fluid phase behavior over a wide range of pressure, temperature, and composition values.

The effect of diffusion on fractured reservoirs has not been well understood. This work attempts to shed a new light on the subject and provide a method for simulating molecular, thermal, and pressure diffusion in naturally fractured reservoirs. But the ultimate objective is to study the significance of diffusion and convective mixing of components in naturally fractured petroleum reservoirs both before and after production. This is accomplished by developing a compositional multiphase simulator with the following characteristics: composition is treated explicitly while pressure and saturation are evaluated implicitly. Molecular, thermal, and pressure diffusions are considered as well as mechanical dispersion. Several conditions are assumed and numerical results are obtained. Emphasis is placed on demonstrating the effect of (1) fracture orientation, (2) vertical permeability in matrix, and (3) matrix porosity.

It will be demonstrated that when injecting nitrogen into a volatile oil in naturally fractured reservoirs, the above factors can be of considerable importance to analyzing diffusion and convective mixing in such reservoirs. In view of the large number of parameters, however, no attempt was made to develop a complete parametric study.

CHAPTER 2

LITERATURE REVIEW

Reservoir simulation has been used since the early days of petroleum engineering. The objective of reservoir simulation is to understand the chemical, physical, and fluid flow processes occurring in a petroleum reservoir and thereby optimizing hydrocarbon recovery. Different compositional models have been developed to model different processes by characterizing the composition of reservoir fluid. This is done through the use of a finite number of components, resulting in a strongly coupled system of nonlinear partial differential equations and constraining equations.

There have been numerous advances since the early works of Kazemi et al. (1969,1976, 1979) on numerical simulation of naturally fractured reservoirs both in single- and multi-phase flow. Also we have seen many improvements in practical approaches to compositional simulation as reported by Kazemi (1978) and Fussell and Fussel (1979).

Regarding the fractured reservoir issue, emphasis has been placed on the study and modeling of the various processes that occur in the matrix-to-fracture transfer of fluids. Compositional flow in reservoirs, on the other hand, has undergone advances in the optimization to solve thermodynamic equilibrium equations and nonlinear sets of flow differences equations.

In this chapter a brief literature review is presented, including available models to conceptualize a fractured reservoir, the evolution of compositional simulators, and the state of knowledge of diffusion in nonfractured and fractured porous media. The conclusion of this chapter presents a discussion of the problem to be solved.

The literature shows the existence of three models to conceptualize a fractured porous media: dual-porosity, dual-porosity/dual-permeability, and the single block with an adjacent fracture approach. A brief discussion of each follows.

Expanding upon the theory of fluid flow in fractured porous media developed by Barenblatt et al. (1960), Warren and Root (1963) introduced the concept of dual-porosity models into petroleum reservoir engineering. The dual-porosity approach has become the most widely accepted technique for the simulation of naturally fractured reservoirs on a large scale. In this approach, the reservoir is represented by two systems, fracture and matrix. The fracture system represents the interconnected network of fractures that contributes to primary fluid flow. The discontinuous matrix system represents rock pore volume containing the majority of the storage in the reservoir and acting as source or sink to the fractures.

Kazemi (1969) was the first to incorporate the dual-porosity concept into a numerical model with subsequent extension to simulation of multiphase fluid flow (1976, 1979) for large-scale applications. Since that time, numerical modeling of naturally fractured reservoirs using dual-porosity models has been the subject of numerous investigations. The papers by Gilman and Kazemi (1983) and Hill and Thomas (1983) provide new contributions to the practical aspects of reservoir simulation.

The dual-porosity/dual permeability formulation, unlike the dual-porosity model, allows both matrix-to-matrix and fracture-to-fracture flow between grid cells. The works presented by Hill and Thomas (1985) and Gilman and Kazemi (1988) are among the formulations using the dual-porosity/dual-permeability approach to simulate fractured reservoirs.

The single block concept has also been the subject of much research. Yamamoto et al. (1971) used this concept to study a single matrix block under several boundary conditions. The dual-continuum approach presented by Festoy and Van Golf-Racht (1989) to simulate gravity drainage is similar to the single block concept. A single block approach better represents the actual flow taking place between the matrix and the fracture. Each point in the reservoir has the properties of either the matrix or the fracture system. This is a more physical representation of the reservoir. It is not, however, appropriate for an analytical solution of the pressure distribution in the reservoir. The

single block approach is used in reservoir simulation to discretize both matrix and fractures. In other words, the domain is divided by cells that have either matrix properties or fracture properties. Other authors have used this formulation to simulate different processes in fractured reservoirs, among them Fung (1991), who analyzed block-to-block processes. In addition, Sonier et al. (1988) and Rossen and Shen (1989) have used the dual-continuum approach to simulate different processes in fractured reservoirs.

Compositional reservoir simulations are important tools for predicting the performance of oil recovery when the oil and gas undergo mass transfer during the recovery process. These processes include (1) nitrogen injection into a volatile oil, (2) enhanced oil recovery from oil reservoirs by CO_2 injection, and (3) enriched gas injection. Several authors have studied multiphase compositional flow in naturally fractured reservoirs. Early compositional simulators were based on K-values that were expressed as a function of pressure, for example, Yamamoto et al. (1971). More recently, cubic equations of state such as those of Redlick-Kwong or Peng-Robinson appear to be more popular for the correlation of fluid properties (Firoozabadi, 1999). Two compositional simulators that utilize an equation of state for thermodynamic equilibrium and fluid properties calculations are described by Fussel and Fussel (1979) and Coats (1980). Coats (1989) has also developed a compositional model to simulate such flow in fractured reservoirs. His model is fully implicit and accounts for molecular diffusion.

Phase behavior models are used extensively in the petroleum industry, especially in compositional simulation. An important consideration in applying a phase behavior model to reservoir simulation studies is the wide range of composition and pressure needed to produce a real mixture of hydrocarbons. By far the most used equation of state in reservoir simulation is the Peng-Robinson equation of state (PR-EOS). The PR-EOS appeared in 1976 and since then most simulators have used this equation to compute PVT properties.

In general, there is a vast body of literature on molecular diffusion, especially for two components. On the other hand, thermal diffusion and pressure diffusion literature is scarce. Perkins and Johnston (1963) provided a review of molecular diffusion and dispersion in porous media. Sigmund (1976) provided a procedure for the practical computation of molecular diffusion coefficients. Van Golf-Racht (1982) and Saidi (1987) provided a good explanation of molecular diffusion and, in general, of fractured reservoirs; however, these two works did not present any discussion regarding thermal and pressure diffusion. Da Silva and Belery (1989) showed the importance of considering molecular diffusion as a recovery mechanism in fractured reservoirs. They showed a simple method, based on the Sigmund's procedure, to compute molecular diffusion coefficients. They used a single block model to demonstrate that molecular diffusion is an important process that has to be accounted for, especially in fractured reservoirs. Belery and Da Silva (1990) presented a study of the effect of diffusion in the compositional

gradient in a reservoir of the North Sea, demonstrating that thermal diffusion can affect compositional grading.

Bedrikovetski (1993) conducted studies of compositional variation in thermal and gravitational fields. He pointed out that the effect of thermal diffusion in the mixing of components is much less important than that of dispersive mixing for a mixture in motion. It is the only work to make reference to this critical issue.

Both Jacqmin (1990) and Riley and Firoozabadi (1998) studied the effect of natural convection and diffusion on the composition variation in hydrocarbon reservoirs. Their studies address compositional variation in homogeneous porous media. Riley and Firoozabadi (1998) showed that thermal diffusion can affect composition variation in horizontal and vertical directions in hydrocarbon reservoirs.

Similarly, Ghorayeb and Firoozabadi (2000) conducted a numerical study of natural convection and diffusion in fractured porous media. They found that the effect of diffusion on compositional variation could be important for small fracture apertures. Firoozabadi et al. (2000) use the irreversible thermodynamic theory to provide a procedure for the computation of thermal and pressure diffusion coefficients.

The literature review so far is notable for two important facts: (1) The analysis of diffusion is conducted under static conditions without sources or sinks, in other words, prior to exploiting the reservoir and (2) the time necessary to see such effects is great, thousand of years or more, that is, geological time. To the best of our knowledge, none of the above works have treated the behavior of diffusion under a convective motion of fluids, that is, when wells are producing/injecting fluids.

As stated earlier, the primary objective of this work is to study the significance of diffusive mixing of nitrogen in naturally fractured reservoirs -- both short term and long term. Additionally, I have attempted to formulate and explore the effect of gas-to-liquid molecular diffusion between fracture-filled gas and the adjacent matrix block.

CHAPTER 3

MATHEMATICAL FORMULATION

For compositional multiphase flow, three forces must be properly accounted for: viscous, gravity, and capillary. In addition, if an inert gas is injected, diffusion and dispersive processes must be included to quantify for mass transfer between phases.

Most compositional simulators are written in terms of moles rather than masses, since phase behavior equations are usually written in terms of moles. Water is generally treated differently. The assumption often made is that both fluids are immiscible. Considering this assumption, separate mass conservation equations are written for the water component and hydrocarbon components.

As noted in Chapter One, there are several approaches to conceptualizing and modelling a fractured porous media. They include: dual-porosity, dual-porosity/dual-permeability and single block approaches. The single block, also known as dual-continuum approach, is a more physical representation of a fractured reservoir. What follows is a brief discussion of the single block model, with a description of mass transport mechanisms as well as the equations that govern the compositional multiphase flow in porous media.

3.1 Dual-continuum Approach

The dual-porosity theory developed by Barenblatt et al. (1960) and introduced to the petroleum industry by Warren and Root (1963), assumes that the bulk of flow takes place in the fractures. The matrix acts only as a storage medium for the reservoir fluids, and transfer functions describe the flow from the matrix to the fracture network. Mathematically, the dual-porosity theory assumes that a point in the reservoir consists of both matrix and fracture continua.

A dual-continuum approach is a more realistic approach to account for the actual flow taking place between the matrix and the fracture. Each point in the reservoir has the properties of either matrix or fracture system. This is a more physical representation of the reservoir. In a dual-continuum approach, cells represent both matrix and fractures. Different properties are assigned to each medium. In other words, the fractured porous media consists of a matrix block with an adjacent fracture. The space domain is discretized and each cell becomes either matrix or fracture (Fig 3.1).

3.2 Mass Transport Mechanisms

According to Charbeneau (2000), there are three basic physical mechanisms by which miscible and immiscible fluids are transported through porous media: convective

transport (also know as advective); molecular transport (also known as diffusion); and mechanical dispersion. The combination of molecular diffusion and mechanical dispersion in a single term is called hydrodynamic dispersion, or convective mixing. A brief description of each mechanism follows.

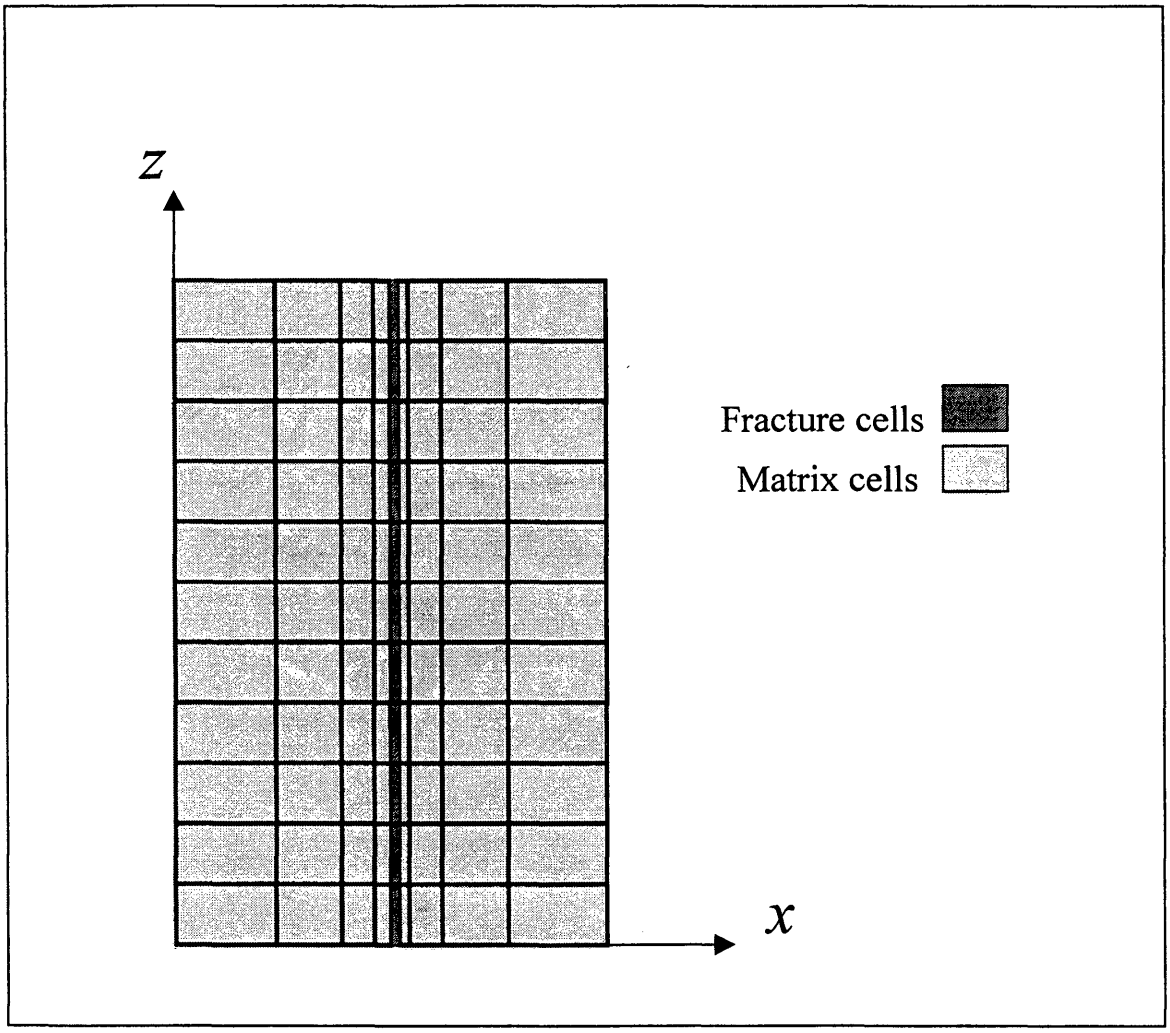

Figure 3.1 Single Matrix Block with a Centralized Fracture

3.2.1 Convective Transport

Convective transport is the movement of a component (contaminant) as it is carried along within bulk fluid movement. Convection, the most significant mass transport process, results from differences in fluid potential. In some literature, it is called advective transport because, strictly speaking, convection refers to fluid motion caused by temperature differences. In this work, however, we will adopt the term convective transport.

3.2.2 Molecular Transport

Diffusion is the process of mass transport associated with random molecular motion. Bird et al. (1960) showed that molecular transport mainly consists of three forms of diffusion: molecular diffusion, thermal diffusion, and pressure diffusion. Molecular diffusion is the tendency to mix due to composition gradient. Thermal diffusion is the tendency to separate components under a temperature gradient. Pressure diffusion is the separation of components by pressure gradient. Pressure diffusion thus plays an important role in cases where a centrifuged force is used. Since molecular transport is associated with molecular motion instead of bulk fluid movement, diffusion does not result in mass transport over large distances. Its effects are purely local.

3.2.3 Mechanical Dispersion

Mechanical dispersion is associated both with bulk velocity fluid movement and with the presence of a porous medium. Two basic mechanisms drive dispersion in macroscopically homogeneous, microscopically disordered porous media, and arise in the pore-level velocity field forced on the flowing fluid by the irregularity of pore space (Sahimi 1995). The first mechanism is kinematic: adjacent particles in one channel can follow different paths leading to a different channel. These particles may later come together in another channel. The result is a wide variation in the lengths of the streamlines and their transverse separation. The second mechanism is dynamic: particles nearest the wall of the pore channel move more slowly than those nearest the channel center. The variations of the pore dimension cause the particle to move at different speeds. Heterogeneities in permeability thus allow fluid particles to move at different speeds, even when the pressure gradient is uniform.

3.2.4 Convective Mixing

When two miscible fluids are in contact with an initially sharp front separating them, a transition zone develops across the initial front. The two fluids slowly diffuse into one another and, after some time, form a diffused mixed zone. This mixing process is independent of whether or not a convective flow exists in the medium. If, however, the

two miscible fluids are in contact and flowing, as might be the case during the exploitation of a reservoir, experience shows that these fluids spread more rapidly than as a result of pure molecular diffusion. This spreading phenomenon is called convective mixing. Convective mixing is the combination of both diffusion and mechanical dispersion. It is also known as hydrodynamic dispersion.

3.3 Mathematical Model

The equations governing compositional multiphase flow in porous media arise from three sources, (Lake et al., 1984), (Kazemi,1999):

1. Material balance describing component flow, that is, *nc* flow equation for each component *c* for each hydrocarbon phase, namely, gas and oil. Also, one mass balance equation for the water.

2. Phase equilibrium relationship, that is, *nc* thermodynamic equilibrium equation for the equilibrium between hydrocarbon phases.

3. Constraint equations that require the phase saturations to sum to unity and the mole fraction in each phase to sum to unity. Besides, it is necessary to relate water, oil and gas pressure, that is, capillary pressures relationships.

Expressions for each of the previous points follow this discussion.

3.4 Fluid Flow Governing Equations

From a mathematical point of view, compositional reservoir simulators consist of a set of partial differential equations and a set of algebraic equations, both with the appropriate initial and boundary conditions.

The partial differential equations, taking into account Darcy's law, describe the molar conservation for each component of the reservoir fluid system. Component transport caused by capillary, gravity, and diffusion-dispersion is taken into account. The compositional multiphase flow equations are developed in Appendix A.

The same notation used by Kazemi and Gilman (1993) is followed. The equations describing the compositional multiphase flow in porous media, assuming the double-continuum approach, are as follow.

Hydrocarbon components,

$$\nabla \cdot \left[J_{c,o}^{*} + J_{c,g}^{*} + J_{c}^{GL} \right] + \nabla \cdot \left[x_c \xi_o \frac{kk_{ro}}{\mu_o} \left(\nabla p_o - \gamma_o \nabla D \right) + y_c \xi_g \frac{kk_{rg}}{\mu_g} \left(\nabla p_g - \gamma_g \nabla D \right) \right] + \left[x_c \xi_o \bar{q}_o + y_c \xi_g \bar{q}_g \right] = \frac{\partial}{\partial t} \left[\phi \left(x_c \xi_o S_o + y_c \xi_g S_g \right) \right] \quad (3.1)$$

where $c = 1,2,\ldots,nc$

In the first bracket of Equation 3.1, $J^{*}_{c,o}$ and $J^{*}_{c,g}$ represent the summation of both diffusive flux and mechanical dispersion terms in the oil and gas phase, respectively. The gas-liquid diffusion is represented by J^{GL}_{c} and it is expressed in such a way because the compositional gradient is expressed slightly different than gas-gas or liquid-liquid diffusion. The second bracket represents the convective flow term, the third term is the source or sink, and the term on the right hand side is the accumulation term.

Because the hydrocarbon phase is assumed to be insoluble with the water phase, the water equation can be treated as mass balance instead of molar balance.

Water phase,

$$\nabla \cdot \left[\frac{kk_{rw}}{B_w \mu_w} \left(\nabla p_w - \gamma_w \nabla D \right) \right] = \frac{\partial}{\partial t} \left[\phi b_w S_w \right] \qquad (3.2)$$

The thermodynamic equilibrium equations are expressed in the form of an equality between the fugacity of each component in both oil and gas phases.

$$f_{c,o} = f_{c,g} \qquad c = 1,2,\ldots, nc \qquad (3.3)$$

Fugacities are obtained using the Peng-Robinson equation of state (PR-EOS). Their computations are shown in Chapter Five.

The two mole fraction constraints are:

$$\sum_{c=1}^{nc} x_c = 1 \tag{3.4}$$

and

$$\sum_{c=1}^{nc} y_c = 1 \qquad c = 1,2,\ldots, nc. \tag{3.5}$$

The saturation constraint is:

$$S_o + S_g + S_w = 1 \tag{3.6}$$

Capillary pressure establishes the relation between the pressures of phases:

$$Pc_{go} = p_g - p_o \tag{3.7}$$

and

$$Pc_{wo} = p_o - p_w \tag{3.8}$$

The equations governing compositional multiphase flow in porous media are given by the set of Equations (3.1) to (3.8). This equation system consists of a set of ($2nc$ + 6)

equations with the same number of unknowns. The (2*nc*+6) unknowns are $(p_o, p_g, p_w, S_o, S_g, S_w, x_1, x_2, ..., x_{nc}, y_1, y_2, ..., y_{nc})$.

As was established in the Equation (3.1), $J^*_{c,o}$ and $J^*_{c,g}$ are the summation of both diffusive fluxes of component *c* and mechanical dispersion in the oil and gas phase, respectively. J^{GL}_c represents the gas-liquid diffusion term of the component *c*. Because these three terms are very important in the present study, they deserve a more detailed discussion.

3.5 Diffusive Flux and Hydrodynamic Dispersion

In compositional multiphase flow, the total molar flux of a given component consists of convective flux, resulting from the fluid velocity and diffusive flux, as a result of the concentration, temperature, and pressure gradients. This diffusive flux consists of three terms: molecular, thermal and pressure diffusion. With respect to molecular diffusion, there are three forms of transferring mass between phases, namely, gas-gas, liquid-liquid, and gas-liquid diffusion. Molecular diffusion is important where a compositional gradient exists. Thermal diffusion plays an important role in processes where a temperature gradient exists. Pressure diffusion becomes important in centrifuge experiments, where the generated force can separate components, (Fried and Combarnous, 1975).

Belery and Da Silva (1990) and Ghorayeb and Firoozabadi (1998) have provided expressions to compute the diffusive flux in porous media,

$$J_{c,p} = -\phi S_p \xi_p \left[D^M_{c,p} \nabla x_{c,p} + D^T_{c,p} \nabla T + D^P_{c,p} \nabla p \right] \qquad (3.9)$$

where $c = 1,2,\ldots,nc$, and $p = o, g$.

D^M, D^T, and D^P are the molecular, thermal, and pressure diffusion coefficients, respectively. In addition, they showed procedures to compute these multipliers in a relatively easy fashion. Chapter Five will demonstrate how these terms are computed.

In Equation 3.9, the first term inside the brackets is known as the ordinary or molecular diffusion. Note that this term does not allow gas-liquid molecular diffusion. The second term is the thermal diffusion, also known as the Soret effect, which is the tendency to separate components due to a difference in temperature. The third term is the pressure diffusion, or gravitational diffusion. $D^M_{c,p}$ is the effective molecular diffusion coefficient in porous medium. The effective diffusion coefficient is smaller than the molecular diffusion coefficient, because the diffusing component or contaminant must follow a complex path through the porous media. In this work, an extension of Sigmund's procedure made by Da Silva and Belery (1989) is used to compute the multicomponent molecular diffusion coefficient. This method is illustrated in Chapter Five.

Thermal diffusion has been established as part of the diffusive flux. Thermal diffusion arises because of the presence of a temperature gradient, either vertical or horizontal, in the porous media. Thermal diffusion is the tendency to separate under a temperature gradient; therefore, the tendency provided by molecular diffusion to equalize composition can be impeded by thermal and pressure diffusion.

If we want to quantify gas-liquid molecular diffusion, it is necessary to add one term given by

$$J_c^{GL} = -\left[D_c^{GL}\nabla C_{c,GL}\right] \tag{3. 10}$$

where D^{GL} is the gas-liquid diffusion coefficients and $\nabla C_{c,GL}$ represents the concentration gradient of component c for gas diffusing from the fracture into oil in the matrix. The gas-liquid diffusion coefficient is computed as a harmonic average of both gas and liquid molecular coefficients, that is,

$$\left[\frac{D_c^{GL}}{\Delta x}\right]_{f-m} = \frac{2D_{c,o,m}D_{c,g,f}}{D_{c,o,m}\Delta x_f + D_{c,g,f}\Delta x_m} \qquad c = 1,2,...,nc \tag{3. 11}$$

Following the form of the molecular diffusion term in Equation 3.9, the concentration gradient for the case of gas-liquid molecular diffusion is given by

$$C_{c,g} - C_{c,o} = \left(\phi S_g \xi_g y_c\right)_f - \left(\phi S_o \xi_o x_c\right)_m \qquad c = 1,2,...,nc \tag{3. 12}$$

In Equation 3.12, the subscripts *f* and *m* stand for fracture and matrix, respectively. Generally, the first term in Equation 3.12 is larger than the second term; therefore, gas-liquid diffusion will take place. Also, note that gas-liquid diffusion is only allowed for the interface between fracture cells and the adjacent cells in the matrix block. In the interior nodes of the matrix block, the gas and liquid (if present) are in equilibrium; therefore, the net diffusion rate is zero. Renner (1988) used a similar experiment where CO_2 was in contact with an oil-saturated core. He determined molecular diffusion coefficients between CO_2 and the liquid hydrocarbon. He provided a correlation of the molecular diffusion coefficient as a function of liquid viscosity, molecular weight of gas, specific molar volume of gas, pressure and temperature of the system.

As was pointed out, mechanical dispersion is associated with both bulk velocity fluid movement and the presence of the porous medium.

In practice, one usually combines molecular diffusion and mechanical dispersion into a single hydrodynamic dispersion coefficient. Because of mechanical dispersion, hydrodynamic dispersion will depend upon direction. Then, according to Bear (1972), Kazemi (1993), and Charbeneau (2000), the hydrodynamic dispersion term is given by:

$$\mathbf{K}_{c,p,x} = D^{M}_{c,p,x} + \frac{\tilde{\alpha}_L v^2_{p,x} + \tilde{\alpha}_T \left(v^2_{p,y} + v^2_{p,z}\right)}{\phi S_p \left|\vec{v}_p\right|} \qquad c=1,2,\ldots,nc; \text{ and } p=o,g. \tag{3.13}$$

Thus, considering mechanical dispersion, Equation 3.9 becomes

$$J^{*}_{c,p} = -\phi S_p \xi_p \left[\mathbf{K}_{c,p} \nabla x_{c,p} + D^{T}_{c,p} \nabla T + D^{P}_{c,p} \nabla p\right] \tag{3.14}$$

In Equation 3.13, $\tilde{\alpha}_L$ and $\tilde{\alpha}_T$ are the longitudinal and transversal dispersivity factors, respectively. It is important to mention that these two dispersivity factors are scale dependent. $D^{M}_{c,p}$ is the effective molecular diffusion coefficient for porous media. Similar expressions can be obtained for y and z. Consequently, the effective molecular diffusion coefficient for porous media in Equation 3.9 combined with the mechanical dispersion term becomes $\mathbf{K}_c$, which is known as hydrodynamic dispersion coefficient given by Equation 3.13. When mechanical dispersion (second term of Equation 3.13) is ignored, Equation 3.14 collapses to Equation 3.9.

3.6 Initial and Boundary Condition

Any formulation of flow through porous media is incomplete if the initial and boundary conditions are not specified. Here, initial conditions define the pressure, saturation, and composition distribution at time equal to zero. Boundary conditions specify the ways in which the reservoir interacts with its surroundings.

3.6.1 Initial Conditions

It is assumed that gravitational equilibrium exists at time equal to zero. In addition, composition and pressure at a certain reference level are known, and the gas-oil contact and water-oil contact are also known. An important point is that at gravitational equilibrium conditions, convective flow vanishes. From Darcy's law:

$$\frac{kk_{rp}}{\mu_p}\left(\nabla p_p - \gamma_p \nabla_p\right) = 0 \qquad p=o,g,w. \tag{3. 15}$$

In a horizontal plane, located at any height from the reference level,

$$\frac{\partial p_p}{\partial x} = 0 \tag{3.16a}$$

and

$$\frac{\partial p_p}{\partial y} = 0 \tag{3.16b}$$

Equations 3.16a and 3.16b mean that under equilibrium conditions, pressure on a horizontal plane holds constant. At the same conditions, Equation 3.15 becomes

$$\frac{\partial p_p}{\partial z} - \gamma_p = 0 \tag{3. 17}$$

This means that the vertical distribution of pressure is given by the column fluid weight. That is,

$$p_p(x,y,z,t=0) = p_p^0(z) \tag{3. 18}$$

Therefore, knowing the reference pressure, $p_{p,ref}$, measured at reference depth, z_{ref}, it is possible to compute the pressure at any point in the reservoir.

Integrating Equation 3.17, it becomes

$$\int_{p_{p,ref}}^{p_p} dp_p = \int_{z_{ref}}^{z} \gamma_p(p)dz \tag{3.18a}$$

Then,

$$p_p = p_{p,ref} + \bar{\gamma}_p\left(\bar{p}_p\right)\left[z - z_{ref}\right] \tag{3. 19}$$

where the sub-index p stands for oil, gas, and water.

Fluid composition can be known from a representative sample taken at some level of reference, 0, before the exploitation of the reservoir begins. That is,

$$x_c(x_0, z_0) = x_{c,0} \qquad c = 1,2,\ldots,nc. \tag{3. 20}$$

3.6.2 Boundary Conditions

In case of boundary conditions, the cross-section is assumed to be bounded by an impermeable rock, so that the total mass flux for all components vanishes at the boundaries. That is,

$$\left(\nabla p_p - \gamma_p \nabla D\right)_S = 0 \tag{3.21a}$$

$$J^*_{c,p} \Big|_S = 0 \qquad c = 1,2, \ldots, nc. \tag{3.21b}$$

where S means along the boundary contour of the domain that represents the reservoir and p stands for oil, o, or gas, g.

In the case of internal boundaries, for example, a well, two conditions are commonly specified,

a. Constant flow rate. Darcy's law can express this condition as

$$\left(p_p - p_{wf}\right) = \frac{\mu_p q_p}{IP\left(k_{rp}\right)} \qquad p = o, g \tag{3. 22}$$

where IP is the productivity index. Equation 3.22 represents the variation in the flowing well pressure, p_{wf}, at constant flow rate.

b. Pressure

In this case the pressure is specified in the well. That is,

$$p_p(well,t) = p_p(t)_{well} \qquad p = o,\ g \tag{3.23}$$

This means that the well will produce at constant pressure with a variation in the flow rate.

CHAPTER 4

NUMERICAL FORMULATION

Some of the differential equations that result from fluid flow through porous media are nonlinear. Because of the nonlinearity, a numerical technique is necessary to obtain an approximate solution to these equations. The transport equations presented in the previous chapter can be solved by the finite differences method. This technique replaces all derivatives by the finite-difference approximations resulting in a set of nonlinear algebraic equations. Then, by using the iterative Newton-Raphson method, the resultant set of equations can be solved by any linear equation solver, (Minkowycz et al., 1988).

In this chapter, the equations governing the multiphase compositional flow through porous media are approximated by the finite difference method. After using the Newton-Raphson method, the resulting matrix is reduced by matrix operations.

4.1 Discretization of the Flow Equations

Discretization of any partial differential equation by finite difference method consists of changing its continuum domain to a discrete domain in all its independent variables. In our case, flow through porous media, the spatial and time domains are replaced by a network of discrete points. The approximate partial differential equations are then written

for each of these discretized points. The system of algebraic equations is solved by a suitable technique, providing an approximate solution to the dependent variables at each of the nodes and at discrete points in time. The approximations of Equations 3.1 to 3.8 in finite differences are developed in Appendix B.

The finite difference approximation of the component hydrocarbon is written as follows:

$$\Delta\left[J^{*}_{c,o} + J^{*}_{c,g} + J^{GL}_{c}\right]^{n+1}_{ik} + \Delta\left[x_c T_o \left(\Delta p_o - \gamma_o \Delta D\right)\right]^{n+1}_{ik} + \Delta\left[y_c T_g \left(\Delta p_g - \gamma_g \Delta D\right)\right]^{n+1}_{ik} + \left(x_c \xi_o q_o + y_c \xi_g q_g\right)^{n+1}_{ik} = \frac{V_{r,ik}}{\Delta t} \Delta_t \left[\phi\left(x_c \xi_o S_o + y_c \xi_g S_g\right)\right]_{ik} \quad (4.1)$$

where $c = 1, 2, 3, \ldots nc.$

The water equation is written as follows:

$$\Delta\left[T_w \left(\Delta p_w - \gamma_w \Delta D\right)\right]^{n+1}_{ik} = \frac{V_{r,ik}}{\Delta t} \Delta_t \left[\phi b_w S_w\right]_{ik} \quad (4.2)$$

The equilibrium thermodynamic equations are:

$$\left(f_{co}\right)^{n+1}_{ik} = \left(f_{cg}\right)^{n+1}_{ik} \qquad c = 1, 2, 3, \ldots nc. \quad (4.3)$$

Constraints also have to be discretized:

$$Pc^{n+1}_{go,ik}\left(S_g\right) = p^{n+1}_{g,ik} - p^{n+1}_{o,ik} \quad (4.4)$$

$$Pc^{n+1}_{wo,ik}\left(S_w\right) = p^{n+1}_{o,ik} - p^{n+1}_{w,ik} \quad (4.5)$$

$$\left(S_o + S_g + S_w\right)_{ik}^{n+1} = 1 \tag{4. 6}$$

$$\left(\sum_{c=1}^{nc} x_c\right)_{ik}^{n+1} = 1 \tag{4. 7}$$

$$\left(\sum_{c=1}^{nc} y_c\right)_{ik}^{n+1} = 1 \tag{4. 8}$$

where : $i = 1, 2, ...I$; $k = 1, 2, ... K$; $n = 0, 1, 2 ...$

Equations defined by 4.1 to 4.8 constitute a set of ($2nc$ + 6) non-linear algebraic equations with the same number of unknown variables, namely $\left(p_o, p_g, p_w, S_o, S_g, S_w, x_1, x_2, ..., x_{nc}, y_1, y_2, ..., y_{nc}\right)$

Using the constrained relationships, one can eliminate some unknowns and therefore some equations. Five equations can be simplified by performing the following substitution:

Equations 4.4 to 4.8 can be written as:

$$p_g = p_o + Pc_{go} \tag{4. 9}$$

$$p_w = p_o - Pc_{wo} \tag{4. 10}$$

$$S_o = 1 - S_g - S_w \tag{4. 11}$$

$$x_{nc} = 1 - \sum_{c=1}^{nc-1} x_c \tag{4. 12}$$

$$y_1 = 1 - \sum_{c=2}^{nc} y_c \tag{4. 13}$$

Therefore, substituting Equations 4.9 to 4.13 into Equations 4.1 and 4.2, five unknowns and five equations are eliminated.

In summary, the system of algebraic nonlinear equations given by Equations (4.1) to (4.8) consists of a set of ($2nc$ + 1) equation with the same number of unknowns for every node (i,k) and every time step n+1.

4.2 Solution and Linearization of the Discretized Equations

Equations 4.1 to 4.8 are nonlinear and are solved by the Newton-Rapshon procedure. In Appendix C, the Newton-Raphson method is described in detail. The set of Equations 4.1 to 4.8 is linearized in two stages. First, a prelinearization is done in the convective and diffusive terms in Equation 4.1. The composition is treated explicitly in such terms. In other words, the composition is treated implicitly in the accumulative term. Second, the resultant system of equations is linearized by the Newton-Raphson method.

The first linearization of the flow equation is performed by treating both diffusive and dispersion terms as well as the composition in the convective term explicitly, at the previous time step. Composition in the remaining source and accumulative terms are treated implicitly. With regard to the oil phase, this is expressed as

$$x_c^{n+1} \cong x_c^n \qquad c = 1,2,...nc \tag{4. 14}$$

For example, the oil transmissibility is now dependent of the following variables:

$$T_o\left(p_o, S_g, S_w, x_1,..., x_{nc}\right)^{n+1} \cong \; T_o\left(\left[p_o, S_g, S_w\right]^{n+1}, \left[x_1,..., x_{nc}\right]^n\right)$$

Therefore, the residual functions of Equation 4.1 and Equation 4.2 are,

For hydrocarbon components:

$$F_{c,ik}^{n+1} = \Delta\left[J_{o,c}^* + J_{g,c}^* + J_c^{GL}\right]^n + \Delta\left[x_c^n T_o^\theta \left(\Delta p_o^{n+1} - \gamma_o^\theta \Delta D\right)\right]_{ik} + \Delta\left[y_c^n T_g^\theta \left(\Delta p_o^{n+1} - \Delta Pc_{go}^{n+1} - \gamma_g^\theta \Delta D\right)\right]_{ik}$$
$$+ \left[x_c \xi_o q_o + y_c \xi_g q_g\right]_{ik}^{n+1} - \frac{V_{r,ik}}{\Delta t} \Delta_t \left[\phi\left(x_c \xi_o \left(1 - S_g - S_w\right) + y_c \xi_g S_g\right)\right]_{ik} = 0 \tag{4. 15}$$

For the water phase:

$$F_{w,ik}^{n+1} = \Delta\left[T_w\left(\Delta p_o - \Delta Pc_{wo} - \gamma_w \Delta D\right)\right]_{ik}^{n+1} - \frac{V_{r,ik}}{\Delta t} \Delta_t \left[\phi b_w S_w\right]_{ik} = 0 \tag{4. 16}$$

The residual function for the equilibrium thermodynamic equation is given by

$$G_{c,ik}^{n+1} = \left(f_{co}\right)_{ik}^{n+1} - \left(f_{cg}\right)_{ik}^{n+1} = 0 \tag{4. 17}$$

where $c = 1, 2, 3,..., nc$; $i = 1, 2, ...I$; $k = 1, 2, ... K$;

Notice that Equations 4.9 to 4.13 have been substituted into Equations 4.15 and 4.16.

In Equation 4.15, the superscript θ means that p_o, S_g, S_w are evaluated at $n+1$ and composition at n. For instance, the functionality of the oil phase transmissibility is

$$T_o^{\theta} = T_o\left(p_o^{n+1}, S_g^{n+1}, S_w^{n+1}, x_c^n\right) \tag{4. 18}$$

The system of equations obtained after applying the above partial prelinearization is then solved by Newton-Raphson method, (Minkowycz et al., 1988). First, let us define the following vectors to simplify the notation:

$$W = \left[p_o, S_g, S_w\right] \tag{4. 19}$$

$$X = \left[x_1,..., x_{nc-1}\right] \tag{4. 20}$$

$$Y = \left[y_2,..., y_{nc}\right] \tag{4. 21}$$

Therefore, the functionality of the residual Equations 4.15 to 4.17 for the node (i,k) are the following:

Hydrocarbon components:

$$F_{c,i,k}^{n+1} = F_{c,i,k}\left([W]_{i,k-1}, [W]_{i-1,k}, [W,X,Y]_{i,k}, [W]_{i+1,k}, [W]_{i,k+1}\right)^{n+1} \tag{4.22}$$

Water component:

$$F_{w,i,k}^{n+1} = F_{w,i,k}\left([W]_{i,k-1}, [W]_{i-1,k}, [W]_{i,k}, [W]_{i+1,k}, [W]_{i,k+1}\right)^{n+1} \tag{4.23}$$

Thermodynamic equilibrium:

$$G_{c,i,k}^{n+1} = G_{c,i,k}\left([W,X,Y]_{i,k}\right)^{n+1} \tag{4.24}$$

where $c = 1, 2, 3, ..., nc.$; $i = 1, 2, ...I$; $k = 1, 2, ... K$;

The Newton-Raphson procedure can be applied to solve any consistent set of nonlinear equations. In this work, there are $2nc + 1$ equations in $2nc + 1$ unknowns for each of N_b nodes. The total number of nodes is given by $N_b = I \times K$; where I and K are the total number of cells in x- and z-direction, respectively The equations to be solved are in residual form, as shown by Equations 4.22 to 4.24, and each equation may depend on any of the $2nc + 1$ variables, namely $\left(p_o, S_g, S_w, x_1, ..., x_{nc-1}, y_2, ..., y_{nc}\right)$

The Newton-Raphson procedure yields:

$$[J]^{\nu} \delta U^{\nu+1} = -R^{\nu} \tag{4.25}$$

where ***J***, for our case, is the Jacobian matrix of size $[(2nc+1) \times N_b] \times [(2nc+1) \times N_b]$. $\delta U = U^{v+1} - U^v$ are the iterative changes of the unknown variables. U is the vector of unknowns of size $[(2nc+1) \times N_b]$ and R is the residual vector of size $[(2nc+1) \times N_b]$.

The unknowns and residual vectors can be ordered in a different fashion. Hashem (1998) showed an efficient way of ordering both the equations and the unknowns. In this work, the following order has been chosen:

The vector of unknowns is given by:

$$U = \left(U_1, U_2, ..., U_{N_b}\right)^T \tag{4. 26}$$

and

$$R = \left(R_1, R_2, .., R_{N_b}\right)^T; \tag{4. 27}$$

where

$$U_j = \left(W, X, Y\right)_j^T$$

and

$$R_j = \left(F_w, F_1, ..., F_{nc}, G_1, ..., G_{nc}\right)_j^T; \qquad j = 1, 2, \ldots, N_b$$

In general, the form of matrix 4.25, for a standard ordering shown by Fig 4.1a, will have a pentadiagonal structure, as shown by Fig 4.1b.

For 2- dimensions the system of equations (4.25) can be written as:

$$E^{\nu}_{i,k}\delta U^{\nu+1}_{i,k-1} + C^{\nu}_{i,k}\delta U^{\nu+1}_{i-1,k} + A^{\nu}_{i,k}\delta U^{\nu+1}_{i,k} + B^{\nu}_{i,k}\delta U^{\nu+1}_{i+1,k} + D^{\nu}_{i,k}\delta U^{\nu+1}_{i,k+1} + = -R^{\nu}_{i} \qquad (4.28)$$

$i = 1, 2, ...I$; $k = 1, 2, ... K$; $\nu = 1,2,\ldots,$

where $A,B,C,D,$ and E are submatrix of size $(2nc + 1)\times(2nc + 1)$. The elements of $E,C,A,B,$ and D are the derivatives of the residual functions with respect to the unknowns in node $(i,k-1)$; $(i-1,k)$; (i,k); $(i+1,k)$; and $(i,k+1)$ respectively. The elements of the matrix A,B,C,D and E are given in Appendix D.

Notice that $\delta U^{\nu+1} = U^{\nu+1} - U^{\nu}$ and $U = (W,X,Y)^T$.

By taking advantage of the structure of the Jacobian matrix, its size of $[(2nc+1) \times N_b] \times [(2nc+1) \times N_b]$ can be reduced to a size of $[3 \times N_b] \times [3 \times N_b]$. In other words, one has to solve for the 2-dimensional problem a pentadigonal matrix of size $[N_b \times N_b]$, whose elements are submatrices of size (3 × 3). Next, a detailed procedure to reduce the Jacobian matrix is presented.

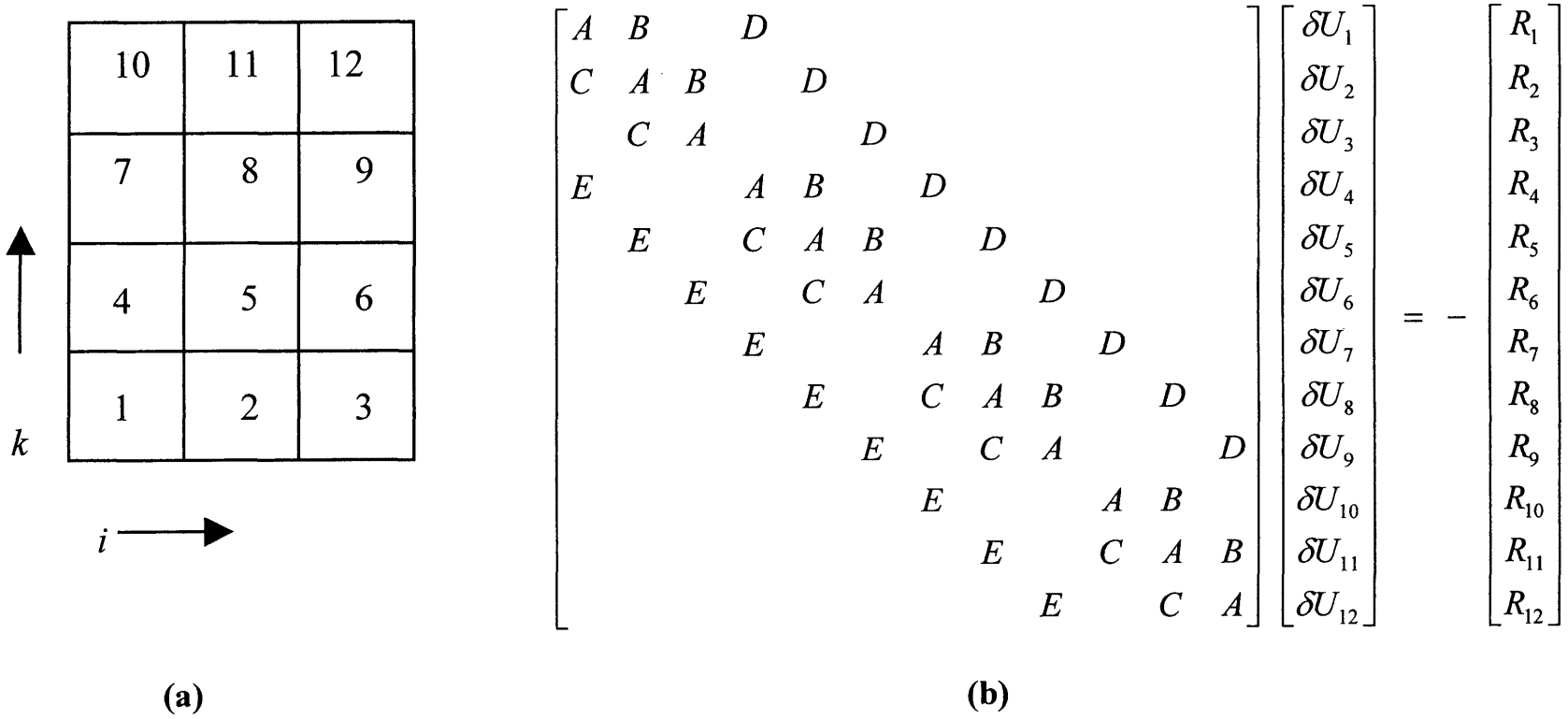

Figure 4.1 (a) Standard Ordering. (b) Matrix structure for 2-dimension case.

4.3 Reduction of the Linearized Discretized Equations

By taking advantage of its matrix structure, the system of Equations 4.28 can be reduced to a system of size (3 × 3) per node. First, in order to reduce the system from ($2nc$ + 1)×($2nc$ + 1) to (nc + 1)×(nc + 1) equations per node, the nc thermodynamic equilibrium equations have to be coupled to the flow equations. For simplicity, the reduction will be done for the 1-dimensional case. Extension to the 2-dimensional case is straightforward. Therefore, the Equation 4.28 can be written as:

$$\begin{bmatrix} C_{ul} & [0]_{ur} \\ [0]_{ll} & [0]_{lr} \end{bmatrix}_i^{\nu} \begin{bmatrix} \delta U_u \\ \delta U_l \end{bmatrix}_{i-1}^{\nu+1} + \begin{bmatrix} A_{ul} & A_{ur} \\ A_{ll} & A_{lr} \end{bmatrix}_i^{\nu} \begin{bmatrix} \delta U_u \\ \delta U_l \end{bmatrix}_i^{\nu+1} + \begin{bmatrix} B_{ul} & [0]_{ur} \\ [0]_{ll} & [0]_{lr} \end{bmatrix}_i^{\nu} \begin{bmatrix} \delta U_u \\ \delta U_l \end{bmatrix}_{i-1}^{\nu+1} = -\begin{bmatrix} R_u \\ R_l \end{bmatrix}_i^{\nu} \quad (4.29)$$

The submatrices and subvectors are defined consistently. Submatrices with subscript *ul* are (nc+1)×(nc+1), *ur*- submatrices are (nc+1)×(nc), *ll*- submatrices are (nc)×(nc+1), *lr*-sub-matrices are (nc)×(nc). The subvector δU is partitioned as (δU_u ,δU_l). The residual function vector has been split it up in two vectors (R_u ,R_l).

For a mixture represented by four components, the matrices and vectors in Equation 4.29 can be written as:

$$\delta U_u = [\delta W, \delta x_1, \delta x_2] \quad (4.30)$$

$$\delta U_l = [\delta x_3, \delta Y] \quad (4.31)$$

$$R_{u,i,k} = \left(R_w, R_1, R_2, R_3, R_4\right)^T_{i,k} \tag{4. 32}$$

$$R_{l,i,k} = \left(G_1, G_2, G_3, G_4\right)^T_{i,k} \tag{4. 33}$$

Notice that the vector δX has been substituted by its elements, $\delta W = \left[\delta p_o, \delta S_g, \delta S_w\right]$, and $\delta Y = \left[\delta y_2, \delta y_3, \delta y_4\right]$.

The set of Equations 4.29 can be written as

$$C^{\nu}_{ul,i}\delta U^{\nu+1}_{u,i-1} + A^{\nu}_{ul,i}\delta U^{\nu+1}_{u,i} + A^{\nu}_{ur,i}\delta U^{\nu+1}_{l,i} + B^{\nu}_{ul,i}\delta U^{\nu+1}_{u,i+1} = -R^{\nu}_{u,i} \tag{4. 34}$$

and

$$A^{\nu}_{ll,i}\delta U^{\nu+1}_{u,i} + A^{\nu}_{lr,i}\delta U^{\nu+1}_{l,i} = -R^{\nu}_{l,i} \tag{4. 35}$$

Solving Equation 4.35 for $\delta U^{\nu+1}_{l,i}$ in terms of $\delta U^{\nu+1}_{u,i}$:

$$\delta U^{\nu+1}_{l,i} = -\left[A^{\nu}_{lr}\right]^{-1} R^{\nu}_{l,i} - \left[A^{\nu}_{lr}\right]^{-1} A^{\nu}_{ll,i}\delta U^{\nu+1}_{u,i} \tag{4. 36}$$

Substituting Equation 4.36 into Equation 4.35 :

$$C^{\nu}_{ul,i}\delta U^{\nu+1}_{u,i-1} + A^{*\nu}_{ul,i}\delta U^{\nu+1}_{u,i} + B^{\nu}_{ul,i}\delta U^{\nu+1}_{u,i+1} = -R^{*\nu}_{u,i} \tag{4. 37}$$

where

$$A^{*\nu}_{ul,i} = A^{\nu}_{ul,i} - A^{*\nu}_{ur,i}A^{\nu}_{ll,i} \tag{4. 38}$$

and

$$R^{*\nu}_{u,i} = R^{\nu}_{u,i} - A^{\nu*}_{ur,i} R^{\nu}_{l,i} \tag{4. 39}$$

The superscript (*) means that the elements in that matrix or vector have been modified.

Equation 4.37 can be written as:

$$\begin{bmatrix} c_{ul} & [0]_{ur} \\ c_{ll} & [0]_{lr} \end{bmatrix}^{\nu}_{i} \begin{bmatrix} \delta u_u \\ \delta u_l \end{bmatrix}^{\nu+1}_{i-1} + \begin{bmatrix} a_{ul} & a_{ur} \\ a_{ll} & a_{lr} \end{bmatrix}^{\nu}_{i} \begin{bmatrix} \delta u_u \\ \delta u_l \end{bmatrix}^{\nu+1}_{i} + \begin{bmatrix} b_{ul} & [0]_{ur} \\ b_{ll} & [0]_{lr} \end{bmatrix}^{\nu}_{i} \begin{bmatrix} \delta u_u \\ \delta u_l \end{bmatrix}^{\nu+1}_{i-1} = -\begin{bmatrix} r_u \\ r_l \end{bmatrix}^{\nu}_{i} \tag{4. 40}$$

where

$$\delta u_u = [\delta W]^T \tag{4. 41}$$

$$\delta u_u = [\delta x_1, \delta x_2]^T \tag{4. 42}$$

$$R^{*}_{u} = [r_u, r_l]^T \tag{4. 43}$$

The set of Equations 4.40 can be written as:

$$c^{\nu}_{ul,i} \delta u^{\nu+1}_{u,i-1} + a^{\nu}_{ul,i} \delta u^{\nu+1}_{u,i} + a^{\nu}_{ur,i} \delta u^{\nu+1}_{l,i} + b^{\nu}_{ul,i} \delta u^{\nu+1}_{u,i+1} = -r^{\nu}_{u,i} \tag{4. 44}$$

and

$$c^{\nu}_{ll,i} \delta u^{\nu+1}_{u,i-1} + a^{\nu}_{ll,i} \delta u^{\nu+1}_{u,i} + a^{\nu}_{lr,i} \delta u^{\nu+1}_{l,i} + b^{\nu}_{ll,i} \delta u^{\nu+1}_{u,i+1} = -r^{\nu}_{l,i} \tag{4. 45}$$

Solving for $\delta u^{\nu+1}_{u,ik}$ in Equation 4.45 :

$$\delta u_{l,i}^{\nu+1} = -\left[a_{lr}^{\nu}\right]^{-1} r_{l,i}^{\nu} - \left[a_{lr}^{\nu}\right]^{-1} c_{ll,i}^{\nu} \delta u_{u,i-1}^{\nu+1} - \left[a_{lr}^{\nu}\right]^{-1} a_{ll,i}^{\nu} \delta u_{u,i}^{\nu+1} - \left[a_{lr}^{\nu}\right]^{-1} b_{ll,i}^{\nu} \delta u_{u,i+1}^{\nu+1} \tag{4.46}$$

Substituting Equation 4.46 into Equation 4.44:

$$c_{ul,i}^{*\nu} \delta u_{u,i-1}^{\nu+1} + a_{ul,i}^{*\nu} \delta u_{u,i}^{\nu+1} + b_{ul,i}^{*\nu} \delta u_{u,i+1}^{\nu+1} = -r_{u,i}^{*\nu} \tag{4.47}$$

where

$$c_{ul,i}^{*\nu} = c_{ul,i}^{\nu} - a_{ur,i}^{\nu} \left[a_{lr,i}^{\nu}\right]^{-1} c_{ll,i}^{\nu} \tag{4.48}$$

$$a_{ul,i}^{*\nu} = a_{ul,i}^{\nu} - a_{ur,i}^{\nu} \left[a_{lr,i}^{\nu}\right]^{-1} a_{ll,i}^{\nu} \tag{4.49}$$

$$b_{ul,i}^{*\nu} = b_{ul,i}^{\nu} - a_{ur,i}^{\nu} \left[a_{lr,i}^{\nu}\right]^{-1} b_{ll,i}^{\nu} \tag{4.50}$$

$$r_{u,i}^{*\nu} = -r_{u,i}^{\nu} + a_{ur,i}^{\nu} \left[a_{lr,i}^{\nu}\right]^{-1} r_{l,i}^{\nu} \tag{4.51}$$

The system of Equations given by 4.47 consists of three equations with three unknowns per node *i*. The unknowns are $\left(\delta p_o, \delta S_g, \delta S_w\right)_i$.

4.4 Source Terms

In the equation governing the multiphase compositional flow through porous media, the presence of a source/sink was indicated by q_p, $p = o,g$. These represent production or injection for the entire block. A brief discussion on the treatment of the sources and sinks in this work follows.

Flow rates are considered at surface conditions. It is assumed that the molar flow rate at reservoir conditions is equal to the molar flow rate at surface conditions. That is,

$$Q_r = Q_s \tag{4. 52}$$

In Equation 4.52, the subscripts s and r stand for surface and reservoir conditions, respectively. The molar flow rate at surface condition, Q_s, is defined as

$$Q_s = q_{os}\xi_{os} + q_{gs}\xi_{gs} \tag{4. 53}$$

Considering the mole fraction of the liquid phase, L, and the mole fraction of vapor, V, the molar flow rate at surface conditions can be expressed as

$$q_{os}\xi_{os} = L_s Q_s = L_s Q_r \tag{4. 54}$$

and

$$q_{gs}\xi_{gs} = V_s Q_s = V_s Q_r \tag{4. 55}$$

where

$$L_s + V_s = \frac{n_l}{n} + \frac{n_v}{n} = 1$$

Similarly, for a single layer, the molar flow rate at reservoir conditions, Q_r, is

$$Q_r = q_o\xi_o + q_g\xi_g \tag{4. 56}$$

Substituting Equation 4.56 into Equations 4.54 and 4.55, they become:

$$q_{os}\xi_{os} = L_s\left(q_o\xi_o + q_g\xi_g\right) \tag{4. 57}$$

and

$$q_{gs}\xi_{gs} = V_s\left(q_o\xi_o + q_g\xi_g\right) \tag{4. 58}$$

By using Darcy's law, one can obtain the volumetric flow rate at reservoir conditions as follows:

$$q_p = IP\frac{k_{rp}}{\mu_p}\left(p_p - p_{wf}\right) \tag{4. 59}$$

where $p = o,g,w$ and p_{wf} is the bottom hole pressure. IP is the productivity index.

Equation 4.59 can be used to compute the volumetric flow rate needed in Equations 4.57 and 4.58. Two possibilities exist: (1) constant flow rate and (2) constant bottom hole pressure. Let us analyze the first case. If the volumetric flow rate is constant, then the bottom hole pressure must change. Therefore, equations 4.57 and 4.58 become:

For oil,

$$\frac{q_{os}\xi_{os}}{L_s} = IP\left[\xi_o\frac{k_{ro}}{\mu_o}\left(p_o - p_{wf}\right) + \xi_g\frac{k_{rg}}{\mu_g}\left(p_g - p_{wf}\right)\right] \tag{4. 60}$$

For gas,

$$\frac{q_{gs}\xi_{gs}}{V_s} = IP\left[\xi_o \frac{k_{ro}}{\mu_o}\left(p_o - p_{wf}\right) + \xi_g \frac{k_{rg}}{\mu_g}\left(p_g - p_{wf}\right)\right] \tag{4.61}$$

Assuming that the pressure drop is the same for both phases:

$$\Delta p = p_o - p_{wf} = p_g - p_{wf} \tag{4.62}$$

Then, Equation 4.60 becomes

$$\Delta p = p_o - p_{wf} = \frac{q_{os}\xi_{os}}{L_s(IP)\left[\xi_o \frac{k_{ro}}{\mu_o} + \xi_g \frac{k_{rg}}{\mu_g}\right]} \tag{4.63}$$

Regarding the oil phase, Equation 4.59 becomes:

$$q_o = IP \frac{k_{ro}}{\mu_o} \frac{\Theta}{\Psi} \tag{4.64}$$

where

$$\Theta = \frac{q_{os}\xi_{os}}{L_s} \tag{4.65}$$

and

$$\Psi = IP\left[\xi_o \frac{k_{ro}}{\mu_o} + \xi_g \frac{k_{rg}}{\mu_g}\right] \tag{4.66}$$

Similarly an expression for the gas flow rate can be obtained in a straightforward manner. By using a global composition obtained from properties at reservoir condition, Kazemi et al. (1978) provided the following expression:

$$z_{c,well} = \frac{x_c \xi_o q_o + y_c \xi_g q_g}{\xi_o q_o + \xi_g q_g} \tag{4. 67}$$

It is assumed that composition, $z_{c,well}$, is the same that enters into the separators, that is,

$$z_{c,surf} = z_{c,well} = \frac{x_c \xi_o q_o + y_c \xi_g q_g}{\xi_o q_o + \xi_g q_g} \tag{4. 68}$$

Substituting Equations 4.60 and 4.61 into Equation 4.68, it results

$$z_{c,surf} = \frac{x_c \xi_o \left[IP \frac{k_{ro}}{\mu_o} \Delta p \right] + y_c \xi_g \left[IP \frac{k_{rg}}{\mu_g} \Delta p \right]}{\xi_o \left[IP \frac{k_{ro}}{\mu_o} \Delta p \right] + \xi_g \left[IP \frac{k_{rg}}{\mu_g} \Delta p \right]} = \frac{\left[\frac{x_c \xi_o k_{ro}}{\mu_o} + \frac{y_c \xi_g k_{rg}}{\mu_g} \right]}{\left[\frac{\xi_o k_{ro}}{\mu_o} + \frac{\xi_g k_{rg}}{\mu_g} \right]} \tag{4. 69}$$

To determine molar densities and mole fraction of phases, a flash calculation at surface conditions can be performed by using the global composition, $z_{c,surf}$.

Let us discuss the second possibility, where bottom hole pressure is constant. For this case, the computation of flow rates is direct. Equation 4.64 becomes

$$q_o = IP\frac{k_{ro}}{\mu_o}\left(p_o - p_{wf}\right) \tag{4.70}$$

Equations 4.64 and 4.70 are used in the simulator.

4.5 Algorithm for solving the Discretized Equations

In order to solve the reduced system of Equations 4.47, one has to do the following:

1. Compute the elements of the submatrices $c^*_{ul,i}, a^*_{ul,i}, b^*_{ul,i}$ given by Equations 4.48, 4.49, and 4.50, respectively, as well as the vectors $r^*_{u,k}$, given by Equation 4.51.
2. Solve the system 4.47 to determine $\delta u_u = \left(\delta p_o, \delta S_g, \delta S_w\right)_i^T$. In this work the NSPIV subroutine to solve the pentadiagonal system is used, (Sherman, 1980).
3. Solve the Equation 4.46 to determine $\delta u_l = \left(\delta x_1, \delta x_2, ..., \delta x_{nc-2}\right)_i^T$. Then, the vector $\delta U_{u,i}$ is obtained, as shown in Equation 4.30.
4. Having obtained $\delta U_{u,i}$, one can use the Equation 4.36 to obtain $\delta U_{l,i}$
5. Having obtained all unknowns given by vectors U_u and U_l, that is, $U_i = \left(U_u, U_l\right) = \left(p_o, S_g, S_w, x_1, x_2, ..., x_{nc-1}, y_2, y_3, ..., y_{nc}\right)^T$, convergence is verified.

CHAPTER 5

FLUID AND ROCK PROPERTIES

The objective of this chapter is to present a brief discussion of how rock and fluid properties are computed. This chapter is divided in two parts. The first part is related to rock properties. The second part will address all those properties related to the compositional fluid to be used in this work.

5.1 Rock Properties

Reservoir rocks constitute a porous environment within which hydrocarbons and water are found. Knowledge of the petrophysical and hydrodynamic properties of reservoir rocks are of fundamental importance to any simulation study and, in general, to petroleum engineering. This type of data can be acquired from two major sources, namely: samples of rock (cores) and geophysical measurements (well logs) including formation tests. In the following, computation of the main rock properties is presented.

5.1.1 Absolute Permeability

Permeability depends only on the characteristics of the porous media. It is independent of fluid properties. It measures the capacity of the porous medium to transmit fluids under

the action of a pressure gradient. The permeability, k, has dimensions of squared length. In petroleum engineering, k is often measured in Darcy units. This definition remains valid in the case of a fractured reservoir. However, in the presence of two systems –that is, matrix and fracture– permeability may be identified as matrix permeability, fracture permeability, and system permeability. Due to its importance in this work, they deserve a brief discussion.

Fracture permeability is associated with the hydraulic conductivity measured during the flow of fluid through a single fracture or through a fracture network, independent of the rock matrix. It is the conductivity of a single channel or a group of channels. Bear (1993) and Aguilera (1990) showed that permeability in the fracture can be expressed as a cubic law given by

$$k_f = \alpha f_a^2 \qquad (5.1)$$

where α is a constant and f_a is the fracture aperture. The above expression is known as the cubic law equation (because the flow rate is proportional to f_a^3). Witherspoon et al. (1980) have demonstrated the range of validity of the cubic law in a fractured rock.

Matrix permeability can be obtained from a sample without fractures. By using conventional cylindrical cores, the permeability –based on Darcy's equation– is expressed by,

$$k = \frac{q\mu L}{A\Delta p} \tag{5.2}$$

where q, μ, A, L and Δp are the flow rate, viscosity, cross section area, length, and pressure drop, respectively.

If the sample has some fractures, which in general is the case, what is obtained is the total permeability of the system, and not the single permeability of matrix or fractures. In addition, permeability can be obtained from well testing; the difference between this value and that obtained from a sample are the scale: well testing provides permeability of some radius of investigation and sample analysis provides permeability for that particular sample.

The permeability definition just described implies that the formation is fully saturated with a single fluid, that is, that the saturation of a particular fluid is 100%. Such permeability is called absolute permeability.

5.1.2 Relative Permeability

When more than one fluid flows through the porous network in a rock, it is necessary to introduce a new term called relative permeability. Relative permeability is the ratio of the effective permeability of a given fluid at a fixed saturation to the absolute permeability.

The bounds on relative permeability are $1 \geq k_r \geq 0$. Experiments can be performed to determine its dependence on phase saturation.

In the general case where water, oil, and gas are flowing simultaneously at a point, one requires three-phase relative permeability. This permeability (Thomas, 1982) is based on the following assumption: relative permeability to water is a function of water saturation, $k_{rw}(S_w)$; relative permeability to gas is a function of gas saturation, $k_{rg}(S_g)$; and relative permeability to oil is a function of both gas and water saturation, $k_{ro}(S_g, S_w)$. Consequently, k_{rw} and k_{rg} are simply determined from the two-phases water-oil and gas-oil relative permeability data, respectively. k_{ro} can be computed, for example, by using the Stone's correlation (Aziz and Settari, 1979 ; Kazemi, 1999) given by

$$k_{ro} = k^*_{row}\left(\frac{k_{row}}{k^*_{row}} + k_{rw}\right)\left(\frac{k_{rog}}{k^*_{row}} + k_{rg}\right) - \left(k_{rw} + k_{rg}\right) \qquad (5.3)$$

In Equation 5.3, k_{row} and k_{rog} are the values obtained from the water-oil and gas-oil relative permeability curves, respectively, and k^*_{row} is the relative oil permeability in the presence of water evaluated at residual water saturation (end point). Notice that when water saturation is immobile and k_{row} =1.0, the equation collapses to the gas-oil relative oil permeability k_{rog}.

5.1.3 Capillary Pressure

Capillary pressure is the pressure difference between the interfaces of two immiscible fluids. If capillary pressure is a positive number, then it is the non-wetting phase minus the wetting phase pressure, that is, $Pc = p_{nw} - p_w$. Therefore, for a gas-oil system with oil as the wetting phase we have

$$Pc_{go} = p_g - p_o \tag{5.4}$$

and for a water-oil phase with water as the wetting phase,

$$Pc_{wo} = p_o - p_w \tag{5.5}$$

Experimental research has shown that capillary pressure can be represented as a function of one of the phase saturations, that is,

$$Pc_{wo} = P(S_w) \tag{5.6}$$

and

$$Pc_{go} = P(S_g) \tag{5.7}$$

The above equations apply to the matrix block in a fractured reservoir. In this work the capillary pressure in the fracture is neglected.

5.1.4 Porosity

Porosity is defined as the ratio of the connected void volume (pore volume) and fractures to the bulk volume of the formation rock. Connected porosity is a measure of the fluid capacity of the rock. If one assumes that porosity is a function of pressure, then from the definition of pore compressibility, c_r (sometimes called rock compressibility), we have (Graves, 2000):

$$c_r = c_b + c_\phi \tag{5.8}$$

Assuming negligible bulk compressibility, c_b, it becomes

$$c_r = c_\phi = \frac{1}{\phi}\frac{\partial \phi}{\partial p} \tag{5.8a}$$

Equation 5.8a can be integrated. Then porosity can be related to rock compressibility and pressure by,

$$\phi = \phi_o e^{c_r(p-p_o)} \tag{5.9}$$

The exponential in equation 5.9 can be expressed as $e^x = 1 + \frac{x}{1!} + \frac{x^2}{2!} + ... + \frac{x^n}{n!}$. Then, considering the first two terms, it becomes:

$$\phi = \phi_o[1 + c_r(p - p_o)] \qquad (5.10)$$

where the subscript *o* represents a reference point. Thus, porosity decreases as pressure does.

5.1.5 Tortuosity and Dispersivity Factors

Tortuosity is a characteristic of a porous medium, usually defined as the ratio of the true length of the flow path of a fluid particle and the straight-line distance between the starting and finishing point of that particle's motion. Therefore, tortuosity depends on porosity. If porosity is low, tortuosity is large. In classical models of flow in porous media, tortuosity is often treated as an adjustable parameter. The tortuosity factor is used to modify the molecular diffusion coefficient, adapting it for use in porous media.

In the fluid flow through porous media, the transit time of a fluid particle between entrance and exit planes depends on the path that it follows through the pore space. Some particles passing the entrance plane at the same instant will arrive at the exit plane by a set of different paths with a distribution of transit times. Therefore, an injected

component will spread in the mean-flow direction as it passes through the medium. The resulting distribution is a measure of longitudinal dispersion in a porous media.

In the same way, particles passing simultaneously through a restricted area of the entrance plane will not totally follow the mean flow to the exit plane, but rather, will be dispersed in the transverse direction as well. That is, the particles and the paths traveled will have a wider distribution of exit location than entrance location. Therefore, a contaminant front will also spread laterally on the way to the exit plane. The distribution of these transit times for crossing the system at a given transverse plane is a measure of transverse dispersion in a porous medium.

Experiments have shown that longitudinal dispersion is greater than transversal dispersion by one or two orders of magnitude. In addition, longitudinal and transversal dispersivity factors are scale dependent (Figure 5.1; Gelhar et al., 1992; Sahimi, 1995).

5.1.6 Temperature Gradient

In general, there is a variable temperature gradient within the hydrocarbon reservoir in a vertical direction. In some reservoirs, there may also be a temperature gradient in a horizontal direction. Bottom-hole temperature can be recorded with a Drill Stem Test (DST), which is generally performed on exploration wells.

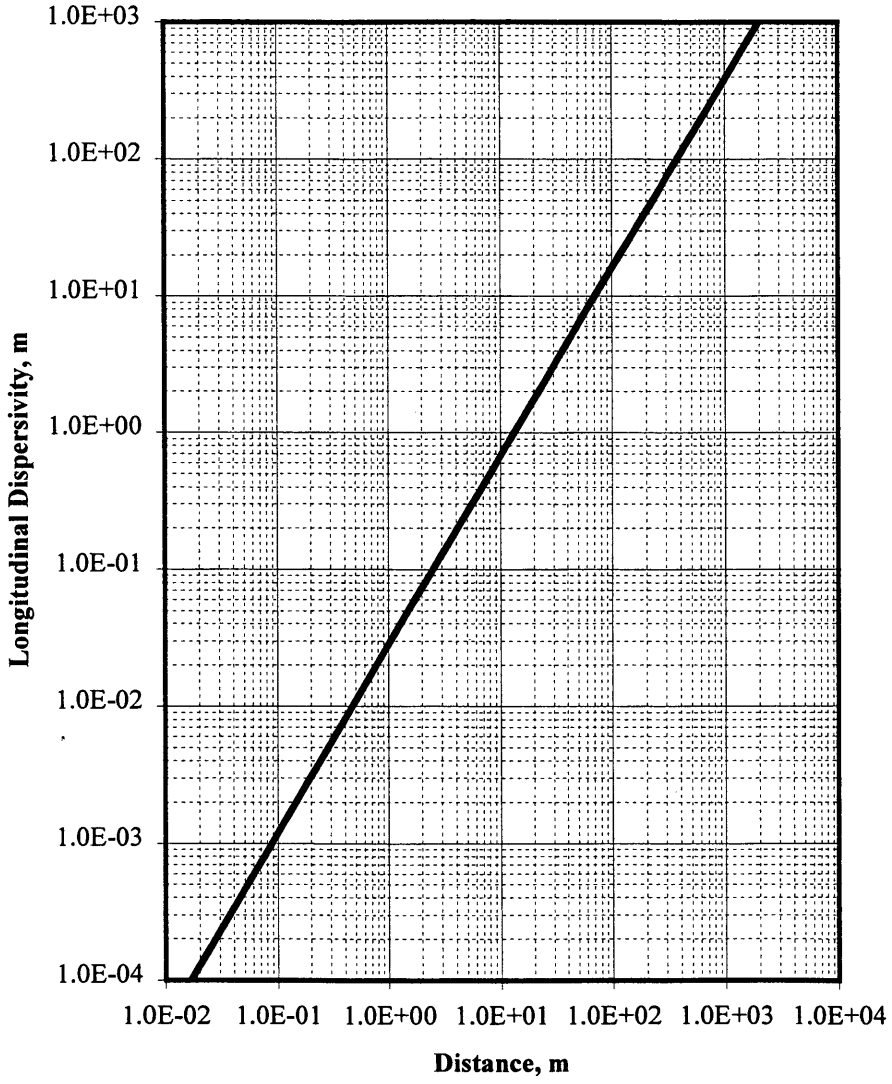

Fig 5.1 Longitudinal Dispersivity as a Function of Distance (after Sahimi, 1995)

In this work, the temperature gradient is held constant and fixed and is expressed as follows:

$$\widetilde{T} = \widetilde{T}_z(z - z_0) + \widetilde{T}_0 \qquad (5.\ 11)$$

T_0 and z_0 are the temperature and depth at the reference level and T_z is the temperature gradient in the z-direction.

5.2 Phase Behavior and Fluid Properties

A compositional phase behavior model must be able to predict all PVT data by using the composition, pressure, and temperature of the reservoir fluid. The phase behavior models must be evaluated and tuned against the measured PVT data prior to being used in reservoir simulation. In general, any equation of state can be used to describe the fluid phase behavior. Following is a detailed discussion of the Peng-Robinson equation, then a flash calculation and saturation pressure, followed by a discussion of how the different fluid properties will be computed including density, viscosity, molecular diffusion coefficient, thermal diffusion ratio and pressure diffusion coefficient.

5.2.1 Peng-Robinson Equation of State

Equations of state (EOS) are basically developed for pure components. They are, however, applied to multicomponent systems by using mixing rules to determine their parameters for mixture. They have received wide acceptance in the petroleum industry both because of their simplicity and their ability to predict accurately the phase behavior of oil-gas systems. The EOS is used in compositional simulation to compute fugacities and fluid properties. There are many equations of state and correlations available in the literature. In this work, the discussion given by Michelsen and Heidemenn (1981) and Nghiem and Li (1989) is followed. They represent most of the EOS by the equation:

$$p = \frac{RT}{v-b} - \frac{a}{(v+\delta_1 b)(v+\delta_2 b)} \tag{5. 12}$$

δ_1 and δ_2 are constants, and v is the molar volume. The mixture parameters a and b are given by the following mixing rules:

$$a = \sum_{i=1}^{nc}\sum_{j=1}^{nc} x_i x_j a_{ij} \tag{5. 13}$$

$$b = \sum_{i=1}^{nc} x_i b_i \tag{5. 14}$$

The values of a_{ij} are obtained from

$$a_{ij} = (a_i a_j)^{0.5}(1.0 - \kappa_{ij}) \tag{5. 15}$$

In Equation 5.15, κ_{ij} represent the interaction coefficients between components i and j. The pure-component parameters a_{ij} and b_i are obtained from the critical properties and acentricities of the pure component, that is,

$$a_{ij} = \Omega_a R^2 T^2 \frac{T_{ci}^2}{p_{ci}} \left[1.0 + m_i \left(1.0 - \left(\frac{T}{T_{ci}} \right)^{0.5} \right) \right]^2 \tag{5.16}$$

$$m_i = m(\omega_i) \tag{5.17}$$

$$b_i = \Omega_b R \frac{T_{ci}}{p_{ci}} \tag{5.18}$$

the constants Ω_a and Ω_b are determined from the critical condition of the pure component.

For the two frequently used EOS, the constants are given in Table 5.1. After introducing the dimensionless parameters:

$$A = \frac{ap}{(RT)^2} \tag{5.19}$$

$$B = \frac{bp}{RT} \tag{5.20}$$

Table 5.1 Constants for equation of state

	δ_1	δ_2	Ω_a	Ω_b	$m(\omega_i)$
SRK-EOS	1.0	0.0	0.42748	0.08664	$0.480+1.574\omega_i-0.176\omega_I^2$
PR-EOS	1+1.414	1-1.414	0.45724	0.07780	$0.37464+1.54226\omega_i-0.26992\omega_i^2$

Equation 5.12 can be written as a cubic equation in terms of the compressibility factor Z, as follows:

$$Z^3-[\delta_1\delta_2 B+1]Z^2+\lfloor A-(\delta_1+\delta_2)B-(1-2\delta_1\delta_2)B^2\rfloor Z-\lfloor AB+\delta_1\delta_2(B^3+B^2)\rfloor=0 \quad (5.21)$$

In general, equation 5.21 is applied separately to each phase, and if there are three real roots for the phase compressibility factor Z, the largest real root is taken when considering the vapor phase and the smallest positive root when considering the liquid phase.

5.2.2 Fugacity

The fugacity is a measure of the tendency of a component to escape from the phase. Fugacity is used more than Gibbs free energy in petroleum engineering applications, specifically, for phase equilibrium calculations.

At constant temperature, the chemical potential, μ, for a pure substance reduces to

$$\left[\frac{\partial \mu_i}{\partial p}\right]_T = v \tag{5. 22}$$

Where μ and v are the chemical potential and molar volume, respectively. Then, from the ideal gas equation, v is computed as:

$$v = \frac{RT}{p} \tag{5. 23}$$

Then, Equation 5.22 for a pure substance i becomes

$$\left[\frac{\partial \mu_i}{\partial p}\right]_T = \frac{RT}{p} \tag{5. 24}$$

Integrating Equation 5.24 at constant temperature, results in:

$$\mu_i - \mu_i^o = RT \ln p - RT \ln p^o \tag{5. 25}$$

Equation 5.25 provides a simple relation for the change of chemical potential of a pure ideal gas when its pressure changes from p^o to p.

According to Prausnit et al. (1986), Lewis generalized the above equation for applications to real systems by defining a corrected pressure function f, called fugacity, as follows:

$$\mu_i - \mu_i^o = RT \ln f_i - RT \ln f_i^o \qquad (5.26)$$

where superscript o means a reference state. For an ideal gas, the fugacity is equal to its pressure, and the fugacity of each component is equal to its partial pressure.

Because both μ_i^o and f_i^o are fixed at the same pressure and temperature, at equilibrium all μ's are identical, thus, f_i must also be identical to say that the system is at equilibrium.

In Appendix E it is demonstrated that at equilibrium the chemical potentials are equal in all phases in the system. Then writing Equation (E.14) for the component i in two phases, with all reference states being at the same temperature, the equality of the chemical potential at equilibrium results in:

$$f_i^I = f_i^{II} \qquad (5.27)$$

That is, the fugacity of each component is equal in all phases in a system at equilibrium. Fugacity can be imagined as a measure of the escaping tendency of molecules from one phase to an adjacent phase. Therefore, in a multicomponent system, if the fugacity of a

component in two adjacent phases is the same, those two phases will be in equilibrium with no transfer of molecules from one phase to another.

The fugacity f_i can be related to measurable properties using thermodynamic relationships (Edmister and Lee, 1984):

$$\ln\phi_i = \frac{1}{RT}\int_V^\infty \left[\left(\frac{\partial p}{\partial n_i}\right)_{T,V,n_{j\neq i}} - \frac{RT}{V}\right] dV - \ln Z \tag{5.28}$$

where

$$\phi_i = \frac{f_i}{x_i p} \tag{5.29}$$

$$Z = \frac{pv}{RT} \tag{5.30}$$

and $i = 1, 2, \ldots, nc$.

Integration of Equation 5.28 gives the following expression for fugacity:

$$\ln\phi_i = \frac{b_i}{b}(Z-1) - \ln(Z-B) - \frac{1}{\delta_2-\delta_1}\frac{A}{B}\left[\frac{2\sum_{j=1}^{nc} x_i a_{ij}}{a} - \frac{b_i}{b}\right]\ln\left(\frac{Z+\delta_2 B}{Z+\delta_1 B}\right) \tag{5.31}$$

Derivation of Equation 5.31 is in Appendix E.

5.2.3 Saturation Pressure Calculation

Computing the saturation pressure and comparing it with the pressure of the system usually determines the single-phase region. The saturation pressure calculation consists of determining the pressure at which liquid and gas phases are in equilibrium. Given a specific temperature, there are two cases: (1) bubble pressure and (2) dew pressure. In the bubble pressure calculation, the mole fraction of liquid phase, L, and the mole fraction of component c in the liquid phase are:

$$L = 1.0 \quad \text{and} \quad z_c \equiv x_c \quad c = 1,2,\ldots, nc. \tag{5.32}$$

For the dew point, the above conditions become:

$$V = 1.0 \quad \text{and} \quad z_c \equiv y_c \quad c = 1,2,\ldots, nc. \tag{5.33}$$

The global molar fraction of component c is given by

$$z_c = Lx_c + Vy_c \tag{5.34}$$

where

$$\sum_{c=1}^{nc} z_c = 1.0 \tag{5.35}$$

The above problem is modeled through the following equilibrium conditions:

$$f_{c,L} - f_{c,V} = 0 \tag{5.36}$$

and the restrictive equations:

$$\sum_{c=1}^{nc} x_c = 1 \quad \text{or} \quad \sum_{c=1}^{nc} y_c = 1 \tag{5.37}$$

Equations 5.32 to 5.37 result in a system of (nc+1) nonlinear equations that must be solved iteratively for both cases, namely, bubble pressure and dew pressure. The unknown variables are $(p_b, y_1, y_2, ..., y_{nc})$ for bubble pressure and $(p_d, x_1, x_2, ..., x_{nc})$ for dew pressure.

This work follows a procedure similar to that of Nghiem and Li (1983) and Abhvani and Beaumont (1987). Both authors combined successive substitution, SS, with the Newton-Raphson method, NRM. A brief discussion of these methods follows.

The mentioned approach begins with the SS, followed by the NRM. First, given temperature, type of fluid, and composition, one estimates the pressure and composition of the forming phase. Second, estimated K-values are used to flash the mixture at the specified pressure and temperature. The K-values for the first iteration can be estimated by

$$K_c = \frac{y_c}{x_c} \qquad c = 1,2, \ldots, nc \tag{5.38}$$

or

$$K_c = \frac{\exp\left[5.37(1+\omega_c)\left(1-T_{rc}^{-1}\right)\right]}{p_{rc}} \tag{5.39}$$

At this point, liquid and vapor fugacities are determined from the phase composition, and new estimates for K values are obtained by

$$K_c^{l+1} = \frac{\phi_{c,L}}{\phi_{c,V}} = \frac{\dfrac{f_{c,L}}{x_c p}}{\dfrac{f_{c,V}}{y_c p}} = \frac{f_{c,L}}{f_{c,V}}\frac{y_c}{x_c} = \frac{f_{c,L}}{f_{c,V}}K_c^l \qquad c = 1,2,\ldots,nc \tag{5.40}$$

The corrected values for composition are

$$y^{l+1} = K_c^{l+1}x_c = \frac{f_{c,L}}{f_{c,V}}y_c \tag{5.41}$$

It is assumed this procedure is converged when

$$\left|1-\sum_{c=1}^{nc} y_c^{l+1}\right| \le \varepsilon \qquad \text{and} \qquad \left|y_c^{l+1}-y_c^l\right| \le \varepsilon \tag{5.42}$$

If the SS method shows poor convergence, one can adjust the pressure by the following empirical criteria, (Branco and Rodriguez, 1994):

$$\sum_{c=1}^{nc} y_c^{l+1} > 1 \quad \text{then} \quad p^{l+1} = Cp^l \quad \text{where} \quad 1.05 < C < 1.5$$

$$\sum_{c=1}^{nc} y_c^{l+1} < 1 \quad \text{then} \quad p^{l+1} = Cp^l \quad \text{where} \quad 0.80 < C < 0.98$$

If the convergence is not reached at a specified number of iteration, the algorithm switches to the Newton-Raphson method. In this work, the number of iterations for the SS is 15.

The residual functions for the NRM are given by

$$G_c = f_{c,L} - f_{c,V} \tag{5.43}$$

Then, the Jacobian matrix has the following form:

$$\begin{bmatrix} \frac{\partial G_1}{\partial p} & \frac{\partial G_1}{\partial y_2} & \frac{\partial G_1}{\partial y_3} & \cdots & \frac{\partial G_1}{\partial y_{nc}} \\ \frac{\partial G_2}{\partial p} & \frac{\partial G_2}{\partial y_2} & \frac{\partial G_2}{\partial y_3} & \cdots & \frac{\partial G_2}{\partial y_{nc}} \\ \cdot & \cdot & \cdot & & \cdot \\ \frac{\partial G_{nc}}{\partial p} & \frac{\partial G_{nc}}{\partial y_2} & \frac{\partial G_{nc}}{\partial y_3} & \cdots & \frac{\partial G_{nc}}{\partial y_{nc}} \end{bmatrix} \begin{bmatrix} \delta p \\ \delta y_2 \\ \cdot \\ \delta y_{nc} \end{bmatrix} = - \begin{bmatrix} G_1 \\ G_2 \\ \cdot \\ G_{nc} \end{bmatrix} \tag{5.44}$$

where

$$\frac{\partial G_c}{\partial p} = \frac{\partial f_{c,L}}{\partial p} - \frac{\partial f_{c,V}}{\partial p} \tag{5.45}$$

and

$$\frac{\partial G_c}{\partial y_j} = -\frac{\partial f_{c,V}}{\partial y_j} \qquad c = 1, 2, \ldots, nc; \qquad j = 2,3, \ldots, nc \tag{5.46}$$

The procedure is assumed converged when

$$\sum_{c=1}^{nc} \left(\frac{f_{c,L}}{f_{c,V}} - 1 \right)^2 < \varepsilon \tag{5.47}$$

A procedure for the computation of the dew point can be obtained similarly.

5.2.4 Flash Calculations

In reservoir simulation, the reservoir is commonly divided into a number of grid cells. The fluids within each cell are considered to be in equilibrium at the cell pressure and temperature. The change of reservoir conditions with time is investigated by determining the average values in each cell during each successive time steps. The number of equations describing the equilibrium between the phases increases with the number of components. The common method of reducing the computational time is to group fluid components describing the fluid by a few pseudo-components (Danesh, 1998).

A flash calculation basically consists of determining the composition of each phase, namely gas and liquid, as the pressure is reduced. A two-phase flash problem seeks to find the number of moles in the gas, V, and liquid phase, L, given the number of moles of feed, F, the mole fraction of components in the feed z_c, c = 1,2,…,nc, and pressure and temperature. Then, if one mole of mixture is flashed at pressure p and temperature T, the total material balance is,

$$L + V = 1 \tag{5.48}$$

Where L is the molar fraction of liquid phase and V is the molar fraction of vapor phase.

The balance for each component is

$$z_c = x_c L + y_c V \tag{5.49}$$

Where c = *1,2,..,nc.*, and z_c, x_c, y_c are mole fractions of the component c in the total mixture, liquid phase, and vapor phase, respectively.

The material balance is under the following constrains,

$$\sum_{c=1}^{nc} z_c = 1 \tag{5.50}$$

$$\sum_{c=1}^{nc} x_c = 1 \tag{5.51}$$

$$\sum_{c=1}^{nc} y_c = 1 \tag{5.52}$$

At equilibrium, the fugacity of any component, c, in the vapor phase is equal to that in the liquid phase. The equality of fugacity can be expressed by the equilibrium ratio, K_c, as given by

$$K_c = \frac{y_c}{x_c} = \frac{\phi_{c,L}}{\phi_{c,V}} \tag{5.53}$$

Equations 5.48 to 5.53 provide the required $2nc+2$ independent equations to determine the $2nc+2$ unknowns, namely x_c, y_c, L, and V.

Combining Equations 5.48 to 5.53 results in

$$x_c = \frac{z_c}{K_c + L(1 - K_c)} \tag{5.54}$$

and

$$y_c = \frac{K_c z_c}{K_c + L(1 - K_c)} \tag{5.55}$$

Combining the above equations, one obtains the expression known as the Rachford-Rice equation. This equation is given by Danesh (1998).

$$F(L)=\sum_{c=1}^{nc}\frac{z_m(K_m-1)}{K_m+L(1-K_m)}=0 \tag{5.56}$$

Notice that Equation 5.56 must be solved iteratively. The method of successive substitution, SS, can be used to solve iteratively the above system. Such a method involves the following steps (Firoozabadi, 1999):

1) Estimate the initial value of K_c at the fixed temperature and pressure. The Wilson's correlation can be used for this purpose, such equation is given by

$$K_c=\frac{\exp\left[5.37(1+\omega_c)\left(1-1/T_{rc}\right)\right]}{p_{rc}} \tag{5.57}$$

where T_{rc} and p_{rc} are the reduced temperature and reduced pressure of component c, respectively.

2) Solve Equation 5.56 for L. This can be done using the Newton-Raphson method.

3) Calculate x_c and y_c from Equations 5.54 and 5.55, then the compressibility factors of both phases can be computed from an equation of state.

4) Calculate fugacities of liquid and gas.

5) Update K_c. The update is given by

$$K_c^{l+1} = K_c^l \frac{f_{c,L}}{f_{c,V}} \qquad c = 1,2, \ldots, nc$$

6) Test the convergence. For example:

$$\sum_{c=1}^{nc} \left(\frac{f_{c,L}}{f_{c,V}} - 1 \right) < \varepsilon$$

The number of iterations depends on the proximity to the critical point. The SS method explained in this section allows the detection of the single-phase region without computing the saturation pressure. However, it has poor convergence near the critical point. The Newton-Raphson method can also be used to solve the above problem, however, because of the overshoot, the Newton-Raphson iteration may fail to converge when the initial estimate is not a good estimate of the solution of the system of linear equation. We will use the SS methods together with the Newton-Raphson method to improve the convergence (Fussel and Yanosik ,1978 ; Abhvani and Beaumont,1987).

Another important issue, beyond satisfying the equilibrium conditions, is the stability criteria. Two-phase stability criteria are simple and have been used routinely (Kazemi, 1999). A three-phases stability test is designed and reported by Michelson (1982). The equilibrium condition given by the equality of fugacities is a necessary but not a sufficient condition. For gas-liquid equilibria, however, the equilibrium is always obtained from the equality of fugacities. This is the case of the present work. The

hydrocarbon system that we chose can only have one or two fluid phases (liquid hydrocarbon, vapor hydrocarbon or both). Therefore, stability test for the presence of the third phase is not needed (that is, liquid-liquid or vapor-liquid-liquid). Furthermore, two-phase stability is handled implicitly in the code.

5.2.5 Minimum Variable Newton-Raphson (MVNM)

The method of successive substitution (SS) and the Newton-Raphson method (NRM) have limitations, however they have desirable features. The SS method, unlike NRM, does not require good initial estimates of K_c values. However, the rate of convergence in the critical region is extremely slow. The NRM has quadratic convergence whereas the SS method has a linear rate of convergence. As was established above, the NRM may fail to converge when the initial estimate is not a good estimate.

The combination of SS and NRM is a good choice and has the desirable features of both, Abhvani and Beaumont (1987) and Fussel and Yanosik (1978) introduced iterative methods that used both schemes: SS and NRM. They called it minimum variable Newton-Raphson method (MVNR). The objective of the MVNR method is to minimize the set of iteration variables for which simultaneous iteration is required and use the Newton-Raphson method for the correction step. A brief discussion of the MVNR method follows.

The mathematical model for a flash liberation is given by Equations (5.37) to (5.40). The set of unknowns are $(x_1, x_2, ..., x_{nc}, y_1, y_2, ..., y_{nc}, L, V)$. The MVNR method divides the above system into two sets: a set identified as iteration variable and a set identified as dependent variable. If the fluid system is predominantly liquid, then the set of iteration variables would be $(y_1, y_2, ..., y_{nc}, V)$ and it is referred to as the *V- y* iteration. On the other hand, if the fluid system is predominately vapor, then the set of iteration variables would be $(x_1, x_2, ..., x_{nc}, L)$ and it is referred to as the $L - x$ iteration. The first estimates for either the *V-y* or *L-x* iteration are the values of the variables calculated at the previous pressure.

V- y Iteration

For this group, the constraint equation is

$$\sum_{c=1}^{nc} y_c = 1 \tag{5. 58}$$

Using the above equation, one can express the following equation

$$y_1 = 1 - \sum_{c=2}^{nc} y_c \tag{5. 59}$$

Then the set of iteration variables become $(y_2, y_3, ..., y_{nc}, V)$. The overall material balance and the component material balance may be written as

$$L = 1 - V \tag{5.60}$$

and

$$x_c = \frac{z_c - V y_c}{L} \qquad c = 1,2,\ldots,nc \tag{5.61}$$

The set of dependent variables is $(x_1, x_2, ..., x_{nc}, y_1, L)$. The remaining *nc* equilibrium equations will be used to define the residual function for the *nc* iteration variables as follows

$$G_c = f_{c,L} - f_{c,V} \qquad c = 1,2,\ldots,nc \tag{5.62}$$

The resulting system of equations is solved by the NRM. The Jacobian matrix has the following form:

$$\begin{bmatrix} \frac{\partial G_1}{\partial V} & \frac{\partial G_1}{\partial y_2} & \frac{\partial G_1}{\partial y_3} & \cdots & \frac{\partial G_1}{\partial y_{nc}} \\ \frac{\partial G_2}{\partial V} & \frac{\partial G_2}{\partial y_2} & \frac{\partial G_2}{\partial y_3} & \cdots & \frac{\partial G_2}{\partial y_{nc}} \\ \cdot & \cdot & \cdot & \cdot & \cdot \\ \cdot & \cdot & \cdot & \cdot & \cdot \\ \frac{\partial G_{nc}}{\partial V} & \frac{\partial G_{nc}}{\partial y_2} & \frac{\partial G_{nc}}{\partial y_3} & \cdots & \frac{\partial G_{nc}}{\partial y_{nc}} \end{bmatrix} \begin{bmatrix} \delta V \\ \delta y_2 \\ \cdot \\ \cdot \\ y_{nc} \end{bmatrix} = - \begin{bmatrix} G_1 \\ G_2 \\ \cdot \\ \cdot \\ G_{nc} \end{bmatrix} \tag{5.63}$$

where $\delta V = V^{l+1} - V^{l}$ represents the iterative change of V. The rest of the variables are defined similarly.

The elements in Equation (5.63) are given by

$$\frac{\partial G_c}{\partial V} = \frac{\partial}{\partial V}\left[f_{c,L} - f_{c,V}\right] = \sum_{j=2}^{nc} \frac{\partial}{\partial x_j}\left[f_{c,L} - f_{c,V}\right]\frac{\partial x_j}{\partial V} = \sum_{j=2}^{nc} \frac{\partial f_{c,L}}{\partial x_j}\frac{\partial x_j}{\partial V} \tag{5.64}$$

and

$$\frac{\partial x_j}{\partial V} = \frac{\partial}{\partial V}\left[\frac{z_j - V y_j}{L}\right] = \frac{L\left(-y_j\right) + \left(z_j - V y_j\right)}{L^2} = \frac{x_j - y_j}{L} \tag{5.65}$$

Substituting Equation 5.65 into Equation 5.64 results in:

$$\frac{\partial G_c}{\partial V} = \frac{1}{L}\sum_{j=2}^{nc} \frac{\partial f_{c,L}}{\partial x_j}\left(x_j - y_j\right) \tag{5.66}$$

The remaining elements are given by

$$\frac{\partial G_c}{\partial y_j} = \frac{\partial}{\partial y_j}\left[f_{c,L} - f_{c,V}\right] = \frac{\partial f_{c,L}}{\partial x_j}\frac{\partial x_j}{\partial y_j} - \frac{\partial f_{c,V}}{\partial y_j} = -\frac{V}{L}\frac{\partial f_{c,L}}{\partial x_j} - \frac{\partial f_{c,V}}{\partial y_j} \tag{5.67}$$

where c = 1,2,…,nc and j = 2,3,…,nc.

Once the set of iteration variables have been obtained $\left(y_2, y_3, ..., y_{nc}, V\right)$, then the set of dependent variables $\left(x_1, x_2, ..., x_{nc}, y_1, L\right)$ is computed from Equations 5.59, 5.60 and 5.61.

Abhvani and Beaumont (1987) have shown that the combination of both methods, SSI and MVNR, is the best approach to perform a flash calculation.

5.2.6 Density and Viscosity

Compositional simulators calculate the densities from an EOS, as seen earlier. The most popular is the Peng-Robinson equation of state. At the calculated equilibrium conditions, a compressibility factor, Z, is calculated. This provides the mass density by the following equation:

$$\rho_p = \frac{pM}{Z_p RT} \tag{5.68}$$

where

$$M = \sum_{c=1}^{nc} x_c M_c \tag{5.69}$$

the molar density is given by

$$\xi_p = \frac{p}{Z_p RT} \tag{5.70}$$

where the subscript p stands for phase. Notice that the inverse of Equation 5.70 provides the molar volume, v.

Viscosity can also be calculated through some correlations relating it to density. In this work, the Lorenz et al. (1964) correlation was used.

The Lorenz correlation expresses the viscosity as a function of pressure, temperature and composition of the fluid and it is given by:

$$\mu = \mu^o + \frac{\left[a_o + a_1\xi_r + a_2\xi_r^2 + a_3\xi_r^3 + a_4\xi_r^4\right]^4 - a_5}{\lambda} \tag{5. 71}$$

where $a(0:5) = (0.1023,0.023364,0.058533,-0.040758,0.0093324,0.0001)$

The auxiliary terms μ^o, ξ_r , and λ are given by

$$\lambda = \frac{\left[\sum_{c=1}^{nc} x_c T_{C,c}\right]^{\frac{1}{6}}}{\left[\sum_{c=1}^{nc} x_c M_c\right]^{\frac{1}{2}}\left[\sum_{c=1}^{nc} x_c p_{C,c}\right]^{\frac{2}{3}}} \tag{5. 72}$$

$$\mu^o = \frac{\sum_{c=1}^{nc}\left(x_c \mu_c^o M_c^{0.5}\right)}{\sum_{c=1}^{nc}\left(x_c M_c^{0.5}\right)} \tag{5. 73}$$

if $T_{r,c} < 1.5$

$$\mu_c^o \chi_c = 34\times10^{-5} T_{r,c}^{0.94} \tag{5. 74}$$

if $T_{r,c} > 1.5$

$$\mu_c^o \chi_c = 17.78 \times 10^{-5} \left(4.58 T_{r,c} - 1.67\right)^{\frac{5}{8}} \tag{5.75}$$

where

$$\chi_c = \frac{T_{C,c}^{\frac{1}{6}}}{M_c^{\frac{1}{2}} p_{C,c}^{\frac{2}{3}}} \tag{5.76}$$

and $T_{r,c} = \frac{T}{T_{C,c}}$ is this the reduced temperature of component c.

The units for this correlation are: $p_{C,c}$ (atm), T(K), ξ (lb-mol/ft^3), v(ft^3/lb-mol), μ(cp). Molecular weight must be in consistent units.

5.2.7 Molecular Diffusion Coefficient

Molecular diffusion coefficients are computed by the method given by Da Silva and Belery (1989). This method is based on the published work of Sigmund (1976).

For two mixtures of fluid brought into contact, the average mixture corresponds to the final equilibrium state after equalization of concentration gradients. These two mixtures represent the composition in two adjacent grid cells. If w represents the fraction of fluid 1 in the mixture, an overall composition is then given by:

$$z_i = w z_{i1} + (1 - w) z_{i2} \tag{5.77}$$

The average mixture molar density can be expressed as a harmonic average,

$$\xi_i = \frac{\xi_{i1}\xi_{i2}}{w\xi_{i2} + (1-w)\xi_{i1}} \tag{5. 78}$$

Using the component critical molar volume v_{ci} and the Equation 5.77, the mixture critical molar density is given by:

$$\xi_{i,c} = \frac{\sum_{i=1}^{nc} z_i v_{c,i}^{2/3}}{\sum_{i=1}^{nc} z_i v_{c,i}^{5/3}} \tag{5. 79}$$

The key parameter characterizing the mixture is the reduced molar density defined as:

$$\xi_{i,r} = \frac{\xi_i}{\xi_{i,c}} \tag{5. 80}$$

The diffusion coefficients for the binary system are related to pressure, temperature and composition through the Hirschfelder equation (Bird et al.,1960):

$$\xi_i^o D_{ij}^o = \frac{2.2648\times10^{-5}}{\sigma_{ij}^2 \Omega_{ij}} \left(\frac{1}{M_i} + \frac{1}{M_j} \right)^{1/2} T^{1/2} \tag{5. 81}$$

In Equation 5.81, the collision diameters σ and the collision integral Ω of the Lennard-Jones potential are given by

$$\sigma_i = 0.1866 v_{i,c}^{1/3} Z_{i,c}^{-6/5} \tag{5.82}$$

$$\sigma_{i,j} = 0.5(\sigma_i + \sigma_j) \tag{5.83}$$

$$\varepsilon_i = 65.3 T_{i,c} Z_{i,c}^{18/5} \tag{5.84}$$

$$\varepsilon_{ij} = (\varepsilon_i \varepsilon_j)^{1/2} \tag{5.85}$$

$$T_{ij} = \frac{T}{\varepsilon_{ij}} \tag{5.86}$$

$$\Omega_{ij} = \frac{1.06036}{T_{ij}^{0.15610}} + 0.1930 e^{-0.47935 T_{ij}} + 1.03587 e^{-1.52996 T_{ij}} + 1.76474 e^{-3.89411 T_{ij}} \tag{5.87}$$

Equation 5.81 is not valid for high pressure encountered in hydrocarbon reservoirs. A correction has to be done by using the following equation:

$$D_{ij} = \frac{\xi_m^o D_{ij}^o}{\xi_m} \pi \tag{5.88}$$

where π is given by

For $\xi_{mr} < 3$, $\pi = 0.99589 + 0.096016 \xi_{mr} - 0.22035 \xi^2_{mr} + 0.032874 \xi^3_{mr}$

For $\xi_{mr} > 3$, $\pi = 0.18839 e^{(2-\xi_{mr})}$

Finally, the effective diffusion coefficient for each component of the mixture is estimated on the basis of Wilke's equation (Sigmund, 1976):

$$D_i^M = \frac{1 - z_i}{\sum_{\substack{j=1 \\ j \neq i}}^{nc} z_j D_{ij}^{-1}} \tag{5. 89}$$

In summary, effective diffusion coefficient is a function of temperature, fluid critical properties, composition, and fluid molar densities.

5.2.8 Thermal Diffusion Coefficient

Because of the small magnitude of the phenomena, measurements of the thermal diffusion ratio are difficult to make. It is therefore necessary to compute it from theoretical models. While these models are subject to uncertainty, due to the absence of experimental data they are the only source with which to compute the thermal diffusion ratio.

The thermal diffusion ratio is a measure of the magnitude of thermal diffusion. Firoozabadi's model was implemented in this work (Firoozabadi et al., 2000). Neglecting cross diffusion effects, the expression to compute the thermal diffusion ratio is

$$k_i^T = \frac{M_i x_i M_{nc} x_{nc}}{MRT} \left[\frac{Q_i^*}{M_i} - \frac{Q_{nc}^*}{M_{nc}} \right] \tag{5. 90}$$

where $i=1,2,...,nc-1$.

Then, according to Belery and Da Silva (1990), the thermal diffusion coefficient is given by

$$D_c^T = \frac{D_c^M k_c^T}{T} \qquad c = 1,2,\ldots\ nc\text{-}1 \qquad (5.91)$$

In Equation 5.90, Q^* is the net heat of transport of component c. This term is given by

$$Q_c^* = -\frac{\Delta\overline{u}_c}{\tau_c} + \left[\sum_{j=1}^{nc} \frac{x_c \Delta\overline{u}_j}{\tau_j}\right] \frac{\overline{v}_c}{\sum_{j=1}^{nc} x_j \overline{v}_j} \qquad c=1,2,...,nc. \qquad (5.92)$$

In Equation 5.92, $\overline{u}$ and $\overline{v}$ are the partial molar internal energy and the partial molar volume, respectively, and they are computed from the PR-EOS. τ is the ratio of the energy of vaporization and the energy of viscous flow of component c (Glasstone et al., 1941). In the determination of Q^*, Firoozabadi's model assumes the value of 4.0 for τ. In this work, a value of 3.5 was used. Equations to calculate molar properties as well as partial molar properties are shown in Appendix E.

5.2.9 Pressure Diffusion Coefficient

In Equation 3.9, the term $D^P{}_i$ represents the pressure diffusion coefficient. This study utilizes the method presented by Firoozabadi et al. (2000). Neglecting the cross-diffusion process, the pressure diffusion coefficient is given by

$$D_i^P = \frac{L_{ii}}{\xi T M_{nc} x_{nc}} \left[\sum_{j=1}^{nc-1} x_j \bar{v}_j + \frac{M_{nc} x_{nc}}{M_i} \bar{v}_i - \frac{1}{\xi} \right] \qquad i = 1,2,\ldots\ nc\text{-}1 \qquad (5.93)$$

where the coefficients, L_{ii} are given by

$$\sum_{l=1}^{nc-1} \sum_{k=1}^{nc-1} \frac{M_k x_k + M_{nc} x_{nc} \delta_{lk}}{M_k} \frac{\partial \ln f_k}{\partial x_j} \delta_{li} L_{li} = \frac{\xi M_{nc} x_{nc} D_i^M}{R} \qquad i, j = 1,2,\ldots\ nc\text{-}1 \quad (5.94)$$

In Equation 5.94, δ_{li} denotes the Kronecker delta.

5.3 Structure of the Program Code

This section explains briefly the structure of the program code:

1. Input Data: Data include reservoir geology, reservoir geometry, grid structure, basic rock and fluid properties as well as flow rates.
2. Grid Variables: This part in the simulator computes for every numerical cell the following parameters: pore volume, composition, phase pressures and saturations. At the beginning of every timestep, the unknown variables are set equal to their

most recent values, that is, for the first Newton iteration in every time step $U_{i,k}^{n+1,v=1}$ is set equal to $U_{i,k}^{n}$, where v represents the Newton iteration.

3. Fluid and Rock Properties: These calculations include densities, compressibility factors, viscosities, fugacities, diffusion coefficients, relative permabilities, capillary pressure, etc.
4. Jacobian Matrix: Here, calculations include partial derivatives to compute all elements of the the Jacobian Matrix as given in Appendix D and G.
5. Solution Method: The discretized equations are solved by Gaussian elimination method as described in section 4.5.

A brief flow chart is shown in Figure 5.2.

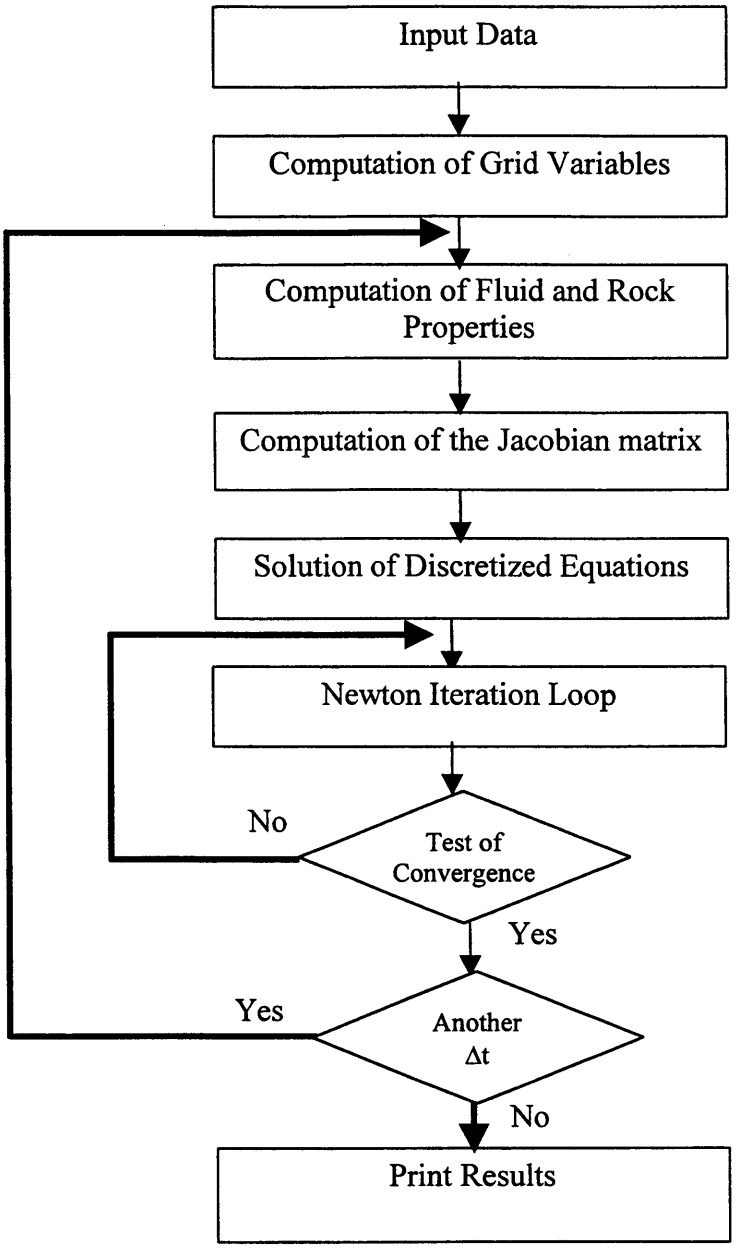

Fig 5.2 Program's Flow Chart

CHAPTER 6

MODEL TESTING AND RESULTS

This chapter presents some results considering molecular, thermal and pressure diffusion, both before and after a petroleum reservoir is exploited. In the first section, the numerical model is tested with some published information. The tests are concerned with initialization of the model, that is, with the effect of diffusion on variation of components before production begins. The subsequent section presents the results of nitrogen injection under different conditions, including fracture orientation, vertical barriers and variation of porosity.

6.1 Model Testing

With no analytical solution available to validate the numerical model, its validity must be verified by comparison only. Model validation was accomplished by running a drawdown test. In addition, published information was used to compare phase behavior, the thermal diffusion ratio and the pressure diffusion multiplier computation.

6.1.1 Drawdown Test

The numerical method was used to generated a drawdown test, which in turn was used to

test the model The change from Cartesian to radial coordinates is straightforward. The validity of the model was established by comparing the value of permeability of the reservoir used to generate the drawdown and the permeability obtained after analyzing the drawdown test. Data used to run the drawdown test are shown in Table 6.1. Figure 6.1 shows a semi-log plot of bottom hole pressure versus time. The slope at early time is given by

$$m = \frac{162.6qB\mu}{kh} \qquad (6.1)$$

From Figure 6.1, the slope m can be obtained and, therefore, the permeability k can be estimated. The value for the slope is m = 4.6. Permeability obtained from equation (6.1) is 9.97 md. The value of permeability used in the numerical model was 10 md.

Table 6.1 Hypothetical Drawdown Test Data

Initial reservoir pressure	21.30 Mpa	(3089.3 psia)
Reservoir thickness	5.0 m	(16.4 ft)
Flow rate	30.0 m^3/day	(188 STB/day)
Formation Vol. Factor	1.52 m^3/m^3	(1.52 Rbl / STB)
Oil viscosity	0.0162 cp	(0.0162 cp)
C1 / C4 / C10	0.5301 / 0.1055 / 0.3644	
Temperature	71 °C	(160 °F)

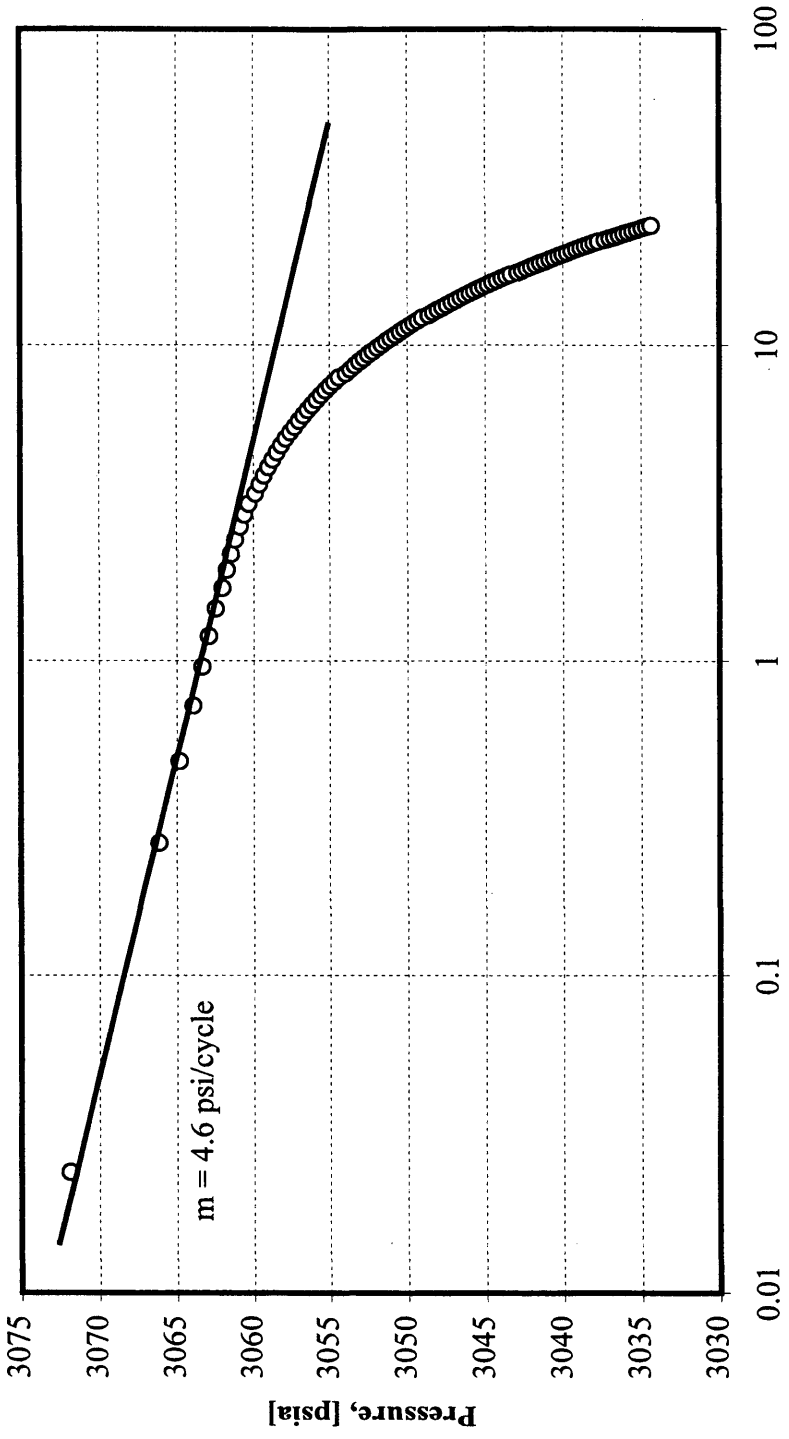

Figure 6.1 Drawdown Test. Bottom Hole Pressure versus Time. Volatile Oil.

6.1.2 Phase Envelope

Published data was used to test the Peng-Robinson EOS. In particular, the work by Boersma and Hagoort (1994) was chosen to validate the EOS. The phase envelope described in that paper is reproduced in this work, and the data used to generate the phase envelope are shown is Table 6.2. Both published and computed results are compared in Figure 6.2. Results obtained in this work are in agreement with the published results.

Table 6.2 Data used to generate the phase envelope

Composition	Mole Fraction	M	Pc (Mpa)	Tc (K)	ω
Nitrogen	0.01	28.013	3.39439	126.2	0.040
Methane	0.64	16.043	4.60016	190.6	0.008
n-butane	0.20	58.124	3.79969	425.2	0.193
n-tetradecane	0.15	198.394	1.62120	694.0	0.679

Binary Interaction Coefficients

Component	Nitrogen	Methane	n-butane	n-tetradecane
Nitrogen	0.0000	0.0289	0.0711	0.1238
Methane	0.0289	0.0000	0.0244	0.0725
n-butane	0.0711	0.0244	0.0000	0.0078
n-tetradecane	0.12385	0.0725	0.0078	0.0000

Reservoir temperature 100 °C (212 °F)

Reservoir pressure 30.2 Mpa (4550 psia)

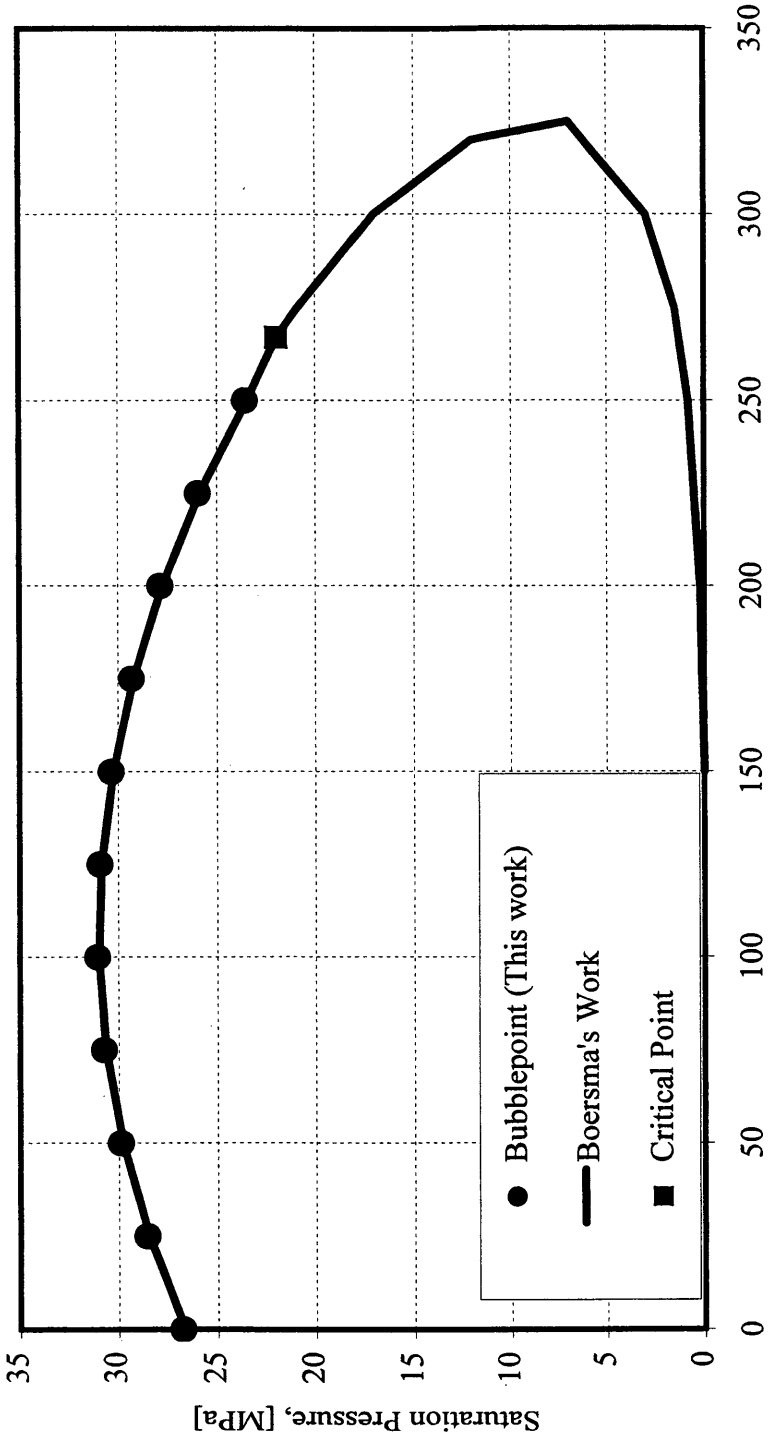

Figure 6.2. Predicted Phase Envelop for initial composition: 1% N2 / 64% C1 / 20% C4 / 15% C14

In addition, example 15.2 given by McCain (1990) is reproduced in this work. Table 6.3 compares results obtained in this work with those published. The results agree.

Table 6.3 McCain's Example

Pressure 1000 psia

Temperature 160 °F

Component	Composition	M	Pc (psia)	Tc (K)	ω
Methane	0.5301	16.043	666.4	343.0	0.0104
n-butane	0.1055	58.124	550.6	765.3	0.1995
n-decane	0.3644	198.394	305.2	1111.7	0.4898

Binary interaction coefficients

	Methane	n-butane	n-decane
Methane	0.00	0.02	0.04
n-butane	0.02	0.00	0.00
n-decane	0.04	0.00	0.00

Composition at 1000 psia and 160 °F

Component	McCain (ex 15-2) x_c	This work x_c	McCain (ex 15-2) y_c	This work y_c
Methane	0.24080	0.24090	0.96130	0.96129
n-butane	0.15170	0.15166	0.03660	0.03664
n-decane	0.60750	0.60744	0.00210	0.00207

Volumetric properties

Property	McCain (ex 15.2)	This work
V	0.4015	0.4012
Z_L	0.3922	0.3921
ρ_L (lb/ft^3)	38.000	38.000
Z_V	0.9051	0.9050
ρ_V (lb/ft^3)	2.9600	2.9650

6.1.3 Molecular Diffusion Coefficient

Computations of the molecular diffusion coefficients are performed to compare the values obtained in this work with those published in the Da Silva and Belery (1989) work. As indicated, the molecular diffusion coefficient was computed using an extension of Sigmund's correlation given by Da Silva and Belery (1989). Both published and computed results are shown in Table 6.4. Again, we can see that the results obtained in this work are in good agreement with published data.

Table 6.4 Comparison of molecular diffusion coefficients for both gas and oil phases

GAS				
P = 4415 psia T = 266 F	Fluid 1	Fluid 2	D (Published) $x10^8$ (m^2/sec)	D(This work) $x10^8$ (m^2/sec)
C1	0.0	84.33	10.15	9.62
C2-C7	0.0	13.93	5.10	4.91
C7	0.0	1.74	2.08	2.07
N2	100	0.00	9.62	9.13
LIQUID				
P = 4415 psia T = 266 F	Fluid 1	Fluid 2	D (Published) $x10^9$ (m^2/sec)	D(This work) $x10^9$ (m^2/sec)
C1	0.07	50.12	5.72	5.41
C2-C7	0.88	17.47	3.28	3.18
C7	60.31	32.41	3.27	3.15
N2	38.74	0.00	5.16	5.04

6.1.4 Thermal Diffusion Ratio

Firoozabadi (2000) has published values of thermal diffusion factors for a mixture of hydrocarbon. These values are different from the thermal diffusion ratio. The thermal diffusion factor and thermal diffusion ratio can be computed by:

$$\alpha_c^T = \frac{1}{MRT}\left[M_{nc}Q_c^* - M_cQ_{nc}^*\right] \tag{6.2a}$$

$$k_c^T = \alpha_c^T x_c x_{nc} \qquad c = 1,2, \ldots, nc\text{-}1 \tag{6. 2b}$$

In equation (6.2a), the heat of transport, Q^*, can be computed by Equation 5.80 as follows,

$$Q_c^* = -\frac{\Delta\overline{u}_c}{\tau_c} + \left[\sum_{j=1}^{nc}\frac{x_c\Delta\overline{u}_j}{\tau_j}\right]\frac{\overline{v}_c}{\sum_{j=1}^{nc}x_j\overline{v}_j} \qquad c=1,2,\ldots,nc. \tag{5.80}$$

In this work, using the procedure described in Chapter Five, the values obtained by Firoozabadi are reproduced. A comparison of both published and computed results is shown in Figure 6.3. In estimating Q^*, Firoozabadi used a value of 4.0 for the ratio between energy of vaporization and energy of viscous flow, τ. In this work, a good match was found for a value of $\tau = 3.5$.

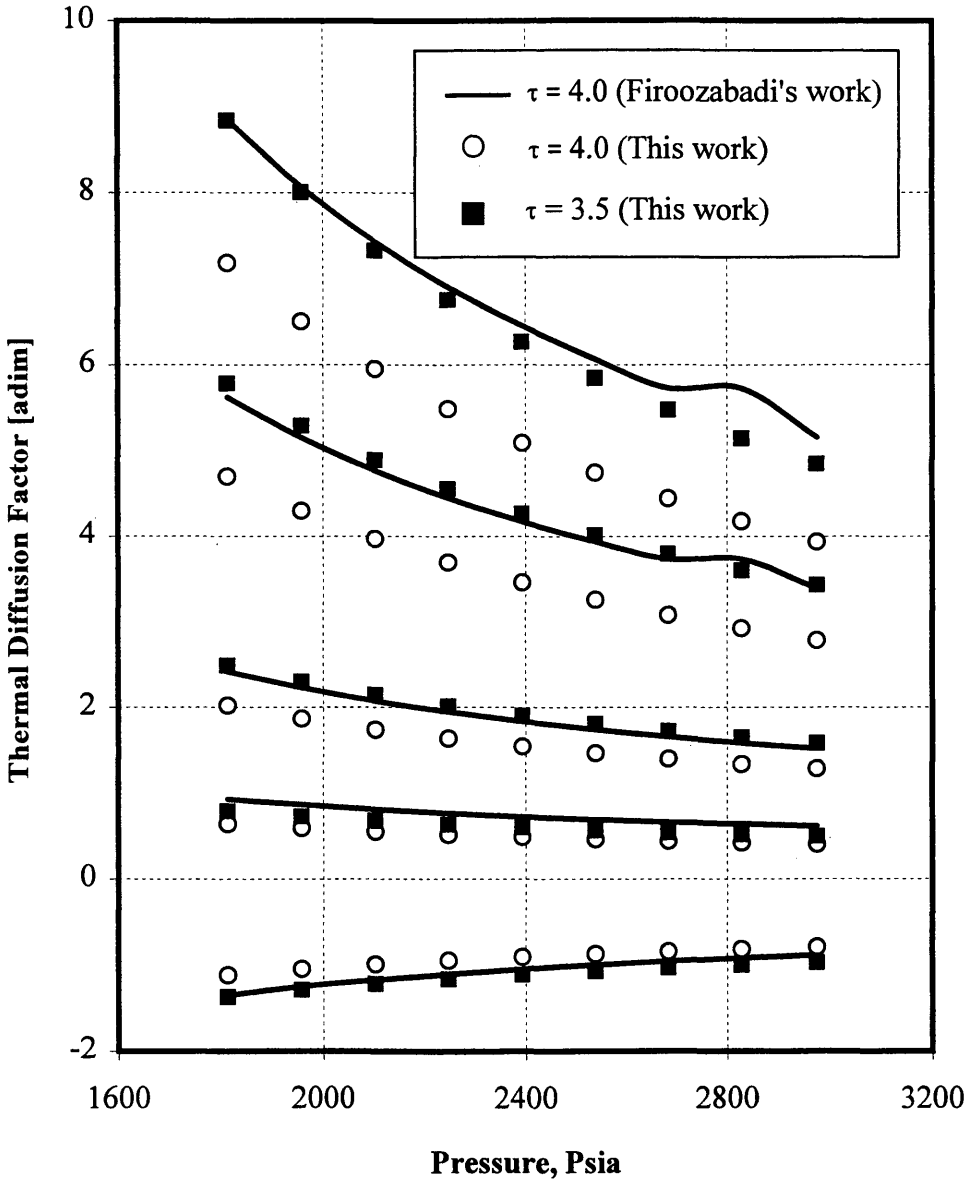

Figure 6.3. Predicted Thermal Diffusion Factor.
C1/C3/C5/C10/C16/C2 (40/12/5/2/1/40% mol)
T = 318 K (113 F).

6.1.5 Pressure Diffusion Coefficient

The coefficient multiplying the pressure gradient in the pressure diffusion term (equation 5.82) was also compared with the published values. Once again, Firoozabadi's work was used as a reference. Table 6.5 shows the information necessary to compute such a coefficient, and the results. Clearly, there is some discrepancy, but in general, they are in good agreement. This small discrepancy is due to the fact that in this work cross-diffusion effects are neglected.

Table 6.5 Comparison of pressure diffusion multiplier

P = 7 MPa T = 315 K	Composition	D^P (Published) x 10^{16} m^2/sec Pa	D^P (Obtained) x 10^{16} m^2/sec Pa
C1	0.25	+ 0.87	+ 0.76
C2	0.25	+ 0.47	+ 0.39
NC4	0.50	--	--

6.2 Effect of the Diffusive Fluxes in the Compositional Gradient.

In general, petroleum reservoirs are not in equilibrium because of the temperature gradient. Recently, Ghorayeb and Firoozabadi (2001) have shown the effect of diffusion on the special variation of components. They concluded that diffusion is an important factor in the computation of the compositional gradient. In this section, a three components model is used to analyze the effect of molecular, thermal and pressure diffusion in the compositional gradient of a fractured reservoir containing a volatile oil without source or sinks. The fractured porous media consists of a single matrix block with a fracture in the middle part, as shown in Figure 6.4. In this work, a synthetic composition is used, and Table 6.6 provides some information, including fluid and rock properties.

Three sets of simulations were performed to quantify the effect of molecular, thermal, and pressure diffusion in the compositional gradient: (1) Simulation assuming molecular diffusion (MD), thermal diffusion (TD), and pressure diffusion (PD). (2) Simulation considering molecular and pressure diffusion; that is, neglecting thermal diffusion. (3) Simulation assuming molecular and thermal diffusion; that is, neglecting pressure diffusion.

Table 6.6 Rock and fluid properties.

Height of matrix block	100 m	328 ft
Width of matrix block	5 m	16.4 ft
Fracture aperture	5 mm	0.016 ft
Initial pressure	30.2 Mpa	4550 psia
Temperature	100 ° C.	212 ° F

Property	Matrix	Fracture
Permeablity	5 mD	20,000 mD
Porosity	0.15	1.0
Res. oil saturation	0.10	0.05
Res. water saturation	0.20	0.05
Tortuosity	1.5	1.0
Long. Dispersivity	10^{-2} m	10^{-2} m
Transv. Dispersivity	10^{-4} m	10^{-4} m

Component	Mole Fraction	D^M (m^2/s)	D^P (m^2/s Pa)
Methane	0.6500	6.02×10^{-9}	$+ 0.39 \times 10^{-16}$
Butane	0.2000	3.20×10^{-9}	
Tetradecane	0.1500	3.0×10^{-9}	$- 0.29 \times 10^{-17}$

Table 6.6 Rock and Fluid Properties.(Cont.)

Relative Permeability and Capillary Pressure Data.

Sg	krg	krog
0.00	0	0.6000
0.05	0.002	0.3200
0.10	0.005	0.1900
0.15	0.012	0.1300
0.20	0.026	0.0850
0.25	0.060	0.0500
0.30	0.105	0.0300
0.35	0.170	0.0180
0.40	0.263	0.0100
0.45	0.400	0.0053
0.50	0.600	0.0029
0.55	0.740	0.0015
0.60	0.840	0.0007
0.65	0.920	0.0003
0.70	1.000	0.0000

Sg	Pcgom(kPa)
0.00	0.00
0.10	0.13
0.20	0.27
0.30	0.45
0.40	0.71
0.50	1.02
0.60	1.50
0.70	2.10
0.77	2.90
0.95	5.9 / 0.8 psi

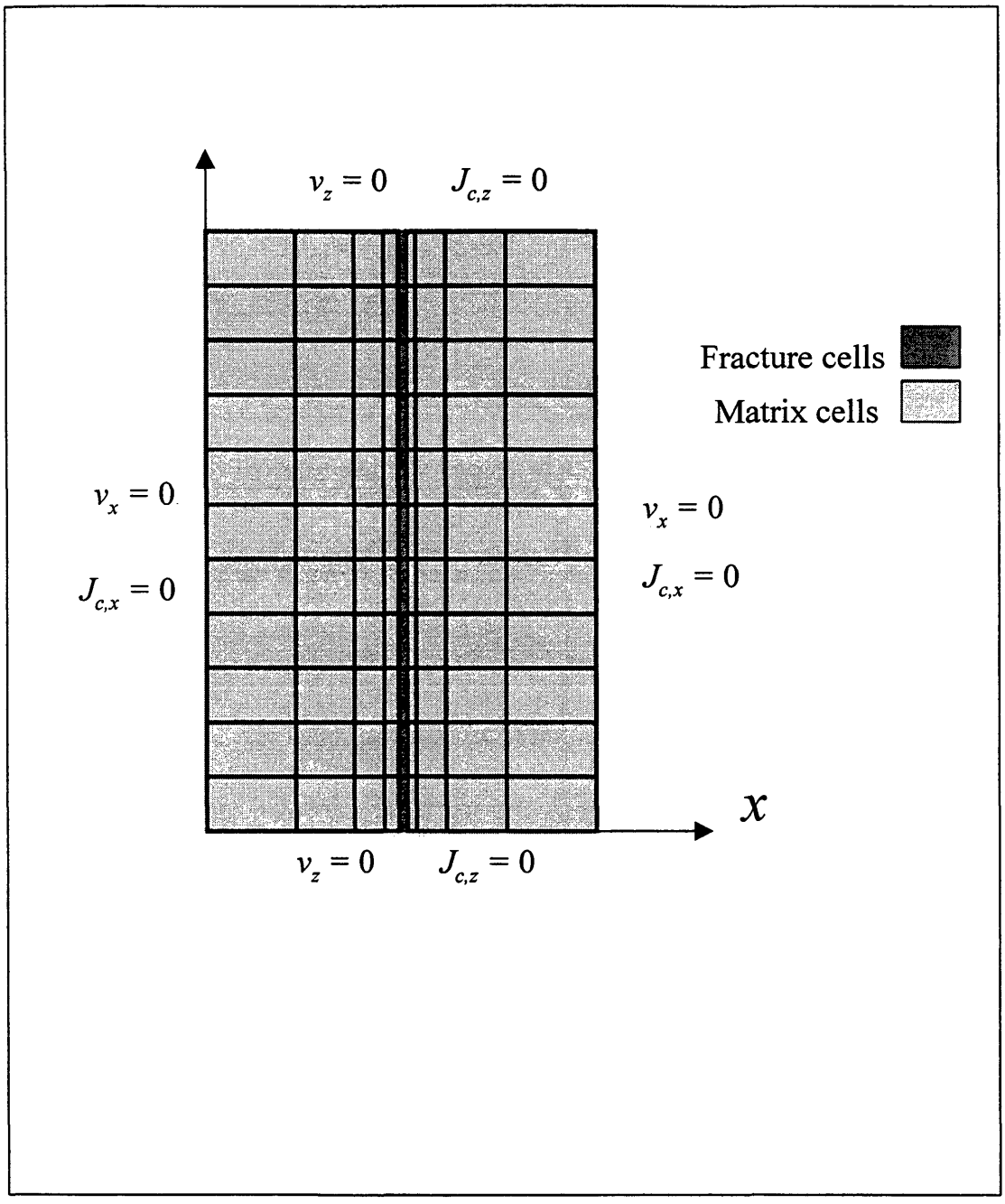

Figure 6.4 Matrix Block with a Fracture in the Middle Part and Boundary Conditions.

6.2.1 Case 1: Considering Molecular Diffusion (MD), Thermal Diffusion (TD), and Pressure Diffusion (PD)

Let us first discuss the case where all diffusive fluxes are considered, that is, molecular, thermal and pressure diffusion. Two pieces of information are important: the thermal diffusion ratio and the pressure diffusion multiplier. These two parameters are computed according to the procedure given in the Chapter Five. The thermal diffusion ratio was computed in a special fashion; see Appendix F for more details. For sake of simplicity, the molecular diffusion coefficient and pressure diffusion multiplier are assumed to be constant. These values are shown in Table 6.6. Simulations were performed from time 0 to 10 x 10^6 days, without any sources or sinks. Under initial conditions, the composition of the mixture is shown is Table 6.6.

Figures 6.5, 6.6, and 6.7 show the composition of C_1, C_4, and C_{14}, respectively, along the vertical fracture. Methane tends to concentrate in the upper part of a reservoir. At 10x10^6 days the values of mole fraction does not change in the fifth decimal, and thus, this composition can be assumed for initialization. The total molar fraction difference for methane is - 0.0015 at 0 m and +0.0015 at 100 m. Composition of butane increases at the bottom and decreases at the top. This trend is mostly due to gravitational segregation (pressure diffusion). Since methane is lighter than butane or tetradecane, it segregates toward the top while butane and tetradecane segregate to the lower part.

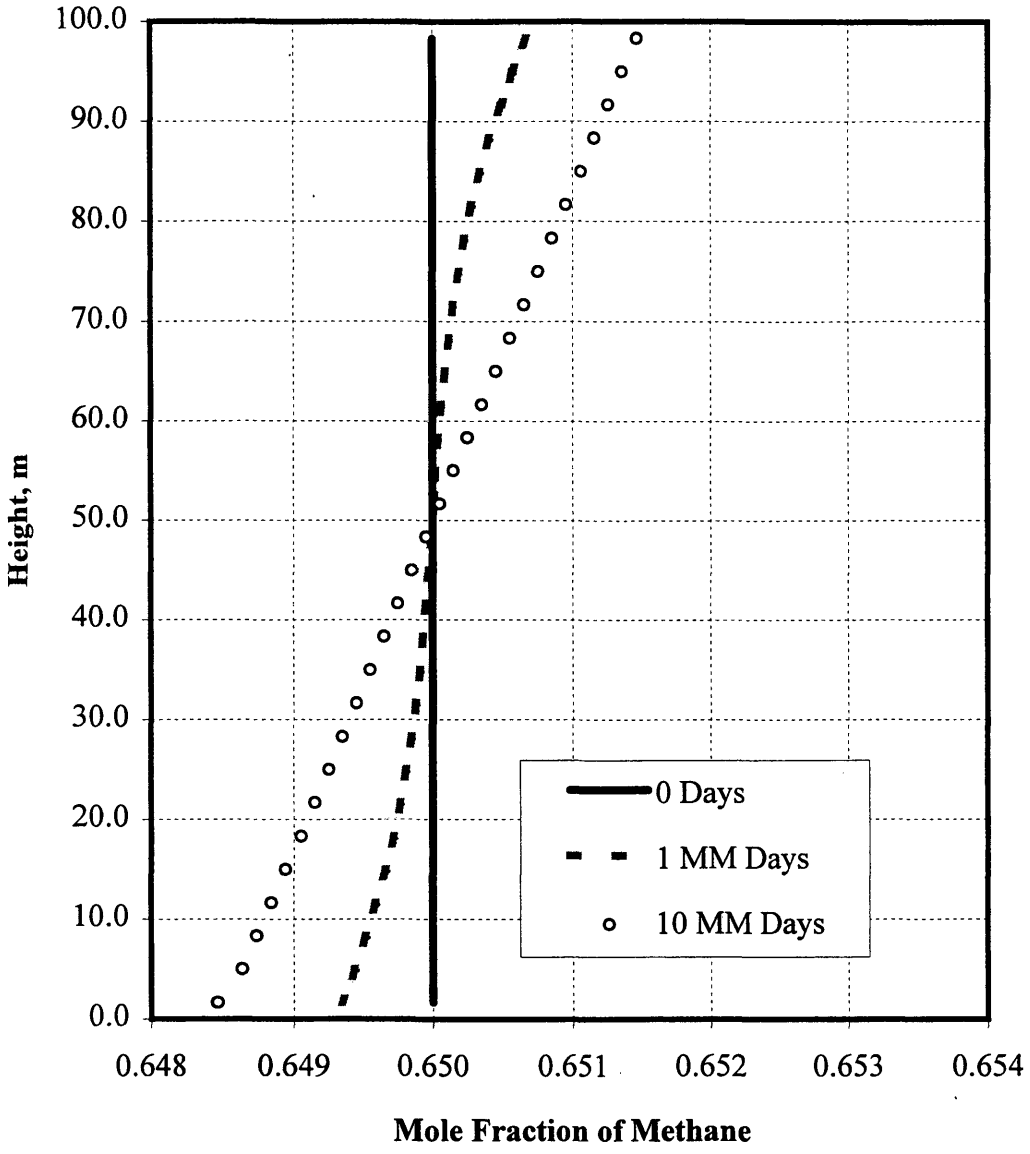

Figure 6.5 Mole Fraction of Methane in the Mixture. Considering Molecular (MD), Pressure (PD), and Thermal Diffusion (TD).

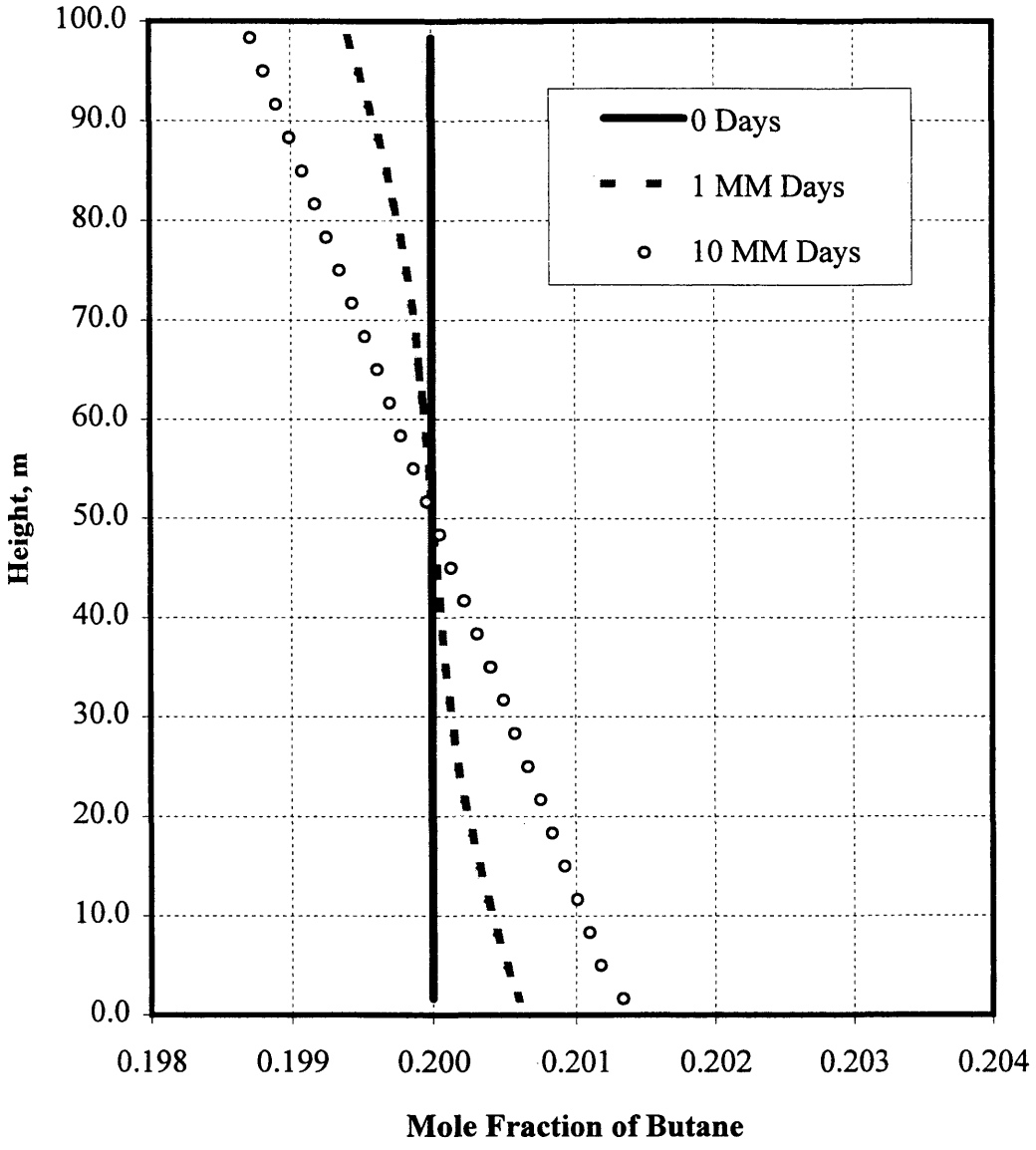

Figure 6.6 Mole Fraction of Butane in the Mixture. Considering Molecular (MD), Pressure (PD), and Thermal Diffusion (TD).

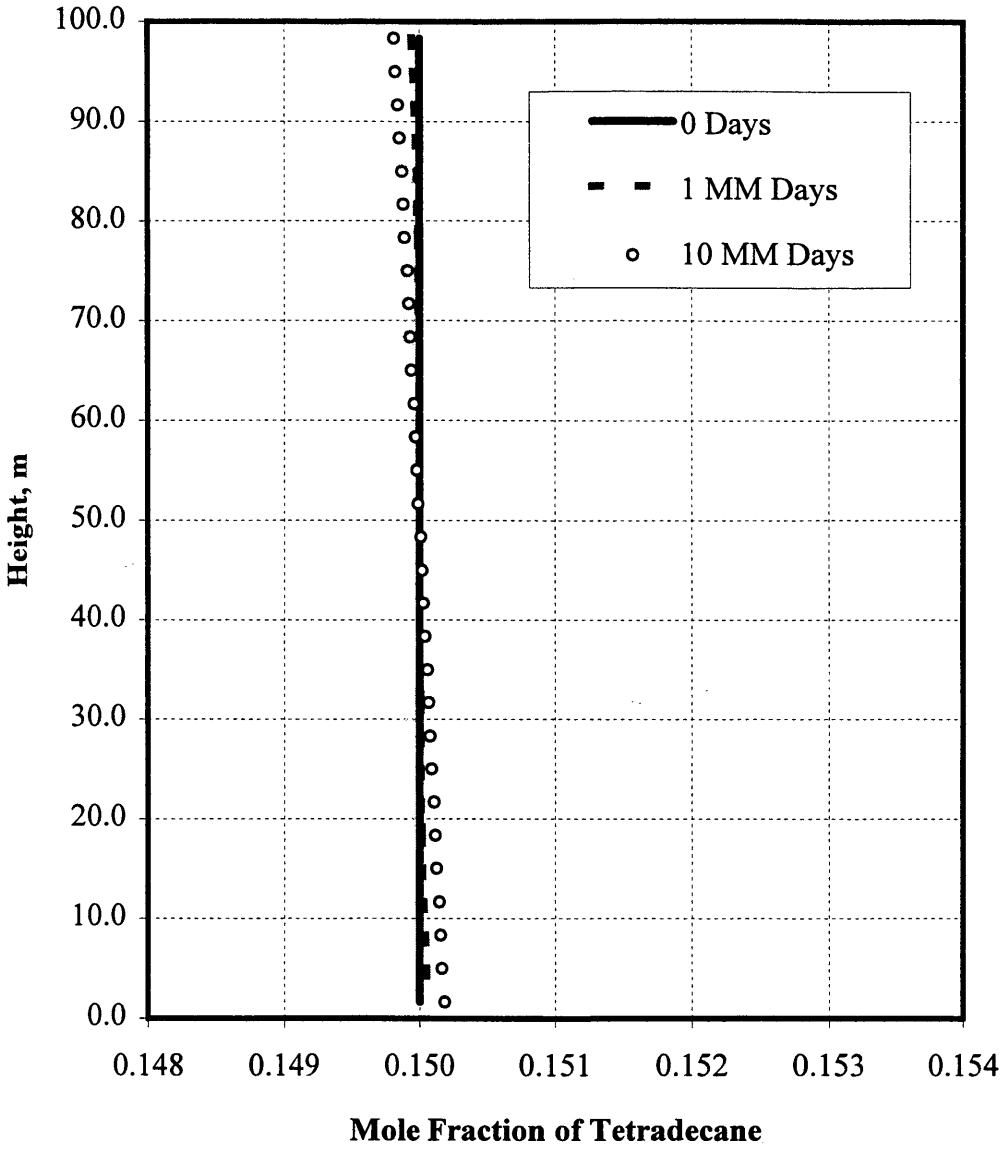

Figure 6.7 Mole Fraction of Tetradecane in the Mixture. Considering Molecular (MD), Pressure (PD), and Thermal Diffusion (TD).

As described in the literature by Danesh (1999), thermal effects are generally opposed to gravity effects. As a result, neglecting TD will result in a smaller amount of methane at the bottom than that shown in Figure 6.5.

Firoozabadi (2000) has shown that the compositional gradient can be totally different for different conditions of pressure and temperature. Furthermore, if the temperature gradient is larger, thermal diffusion can reverse the above behavior.

6.2.2 Case 2: Considering Molecular Diffusion (MD) and Pressure Diffusion (PD)

Before analyzing the compositional gradient when thermal diffusion is neglected, some predictions can be made. First, methane and tetradecane are analyzed; butane is the dependent component. Given that thermal and gravitational effects generally oppose each other, PD will contribute to the concentration of methane at the top while TD will contribute to the concentration of methane at the bottom. In other words, because they act in opposite directions, the concentration of methane at the bottom of the block will decrease when thermal diffusion is neglected. For tetradecane, the roles are inverted. When TD is neglected, PD will contribute to concentrate tetradecane to the bottom.

Figures 6.8, 6.9, and 6.10 show the compositional gradient for methane, butane, and tetradecane, respectively. For purposes of comparison, both cases are included, that is,

MD+PD and MD+TD+PD. We can see that the trends for all components agree with the above analysis. Figure 6.8 shows that the effect of thermal diffusion is to concentrate more methane at the bottom. Pressure diffusion, however, overcomes this effect and so the methane remains concentrated at the top. In the case of tetradecane, TD tends to concentrate it at the top, but with PD still greater than TD, more tetradecane is segregated to the bottom of the block.

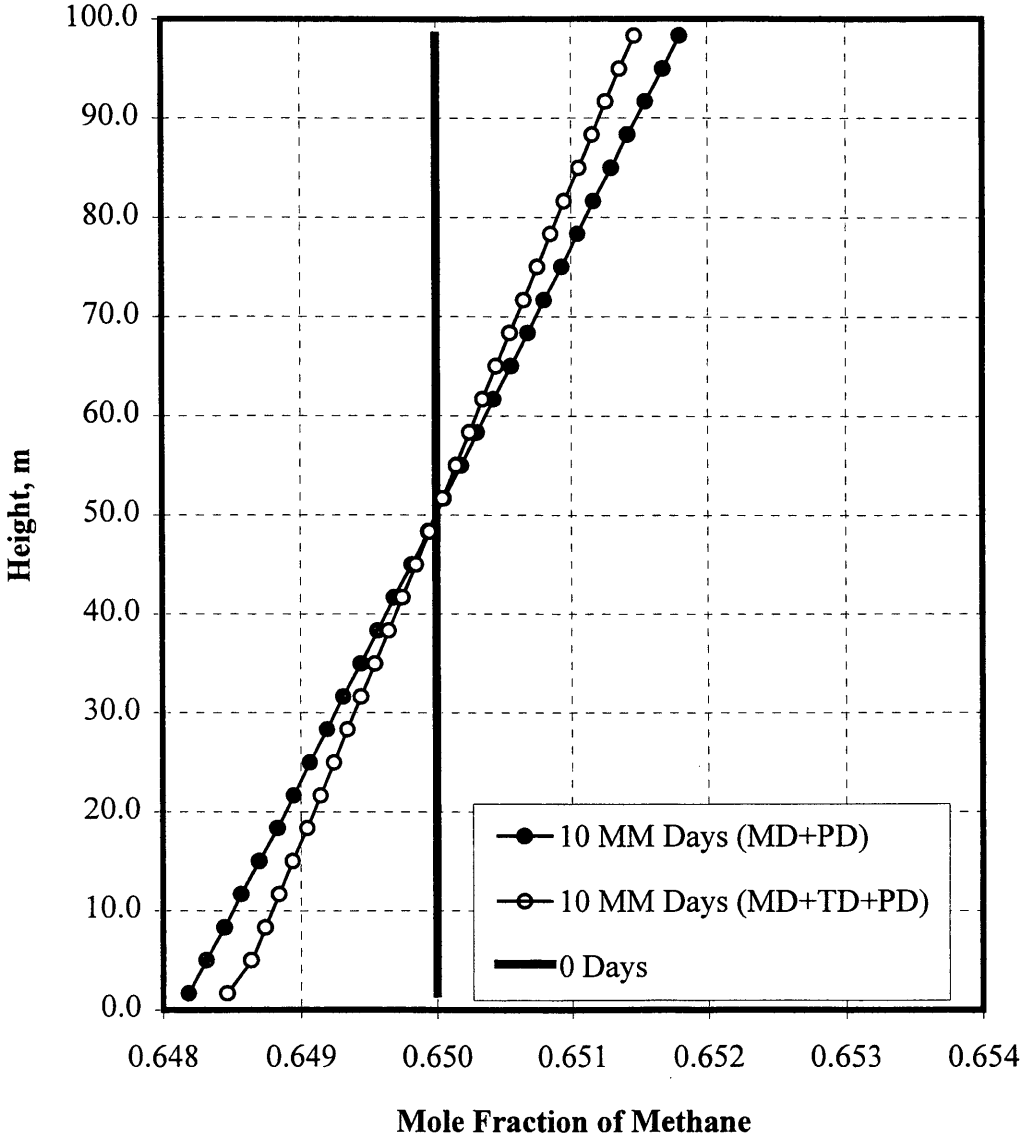

Figure 6.8 Mole Fraction of Methane in the Mixture. Comparing Molecular (MD) and Pressure Diffusion (PD) with Molecular (MD), Thermal (TD) and Pressure Diffusion (PD)

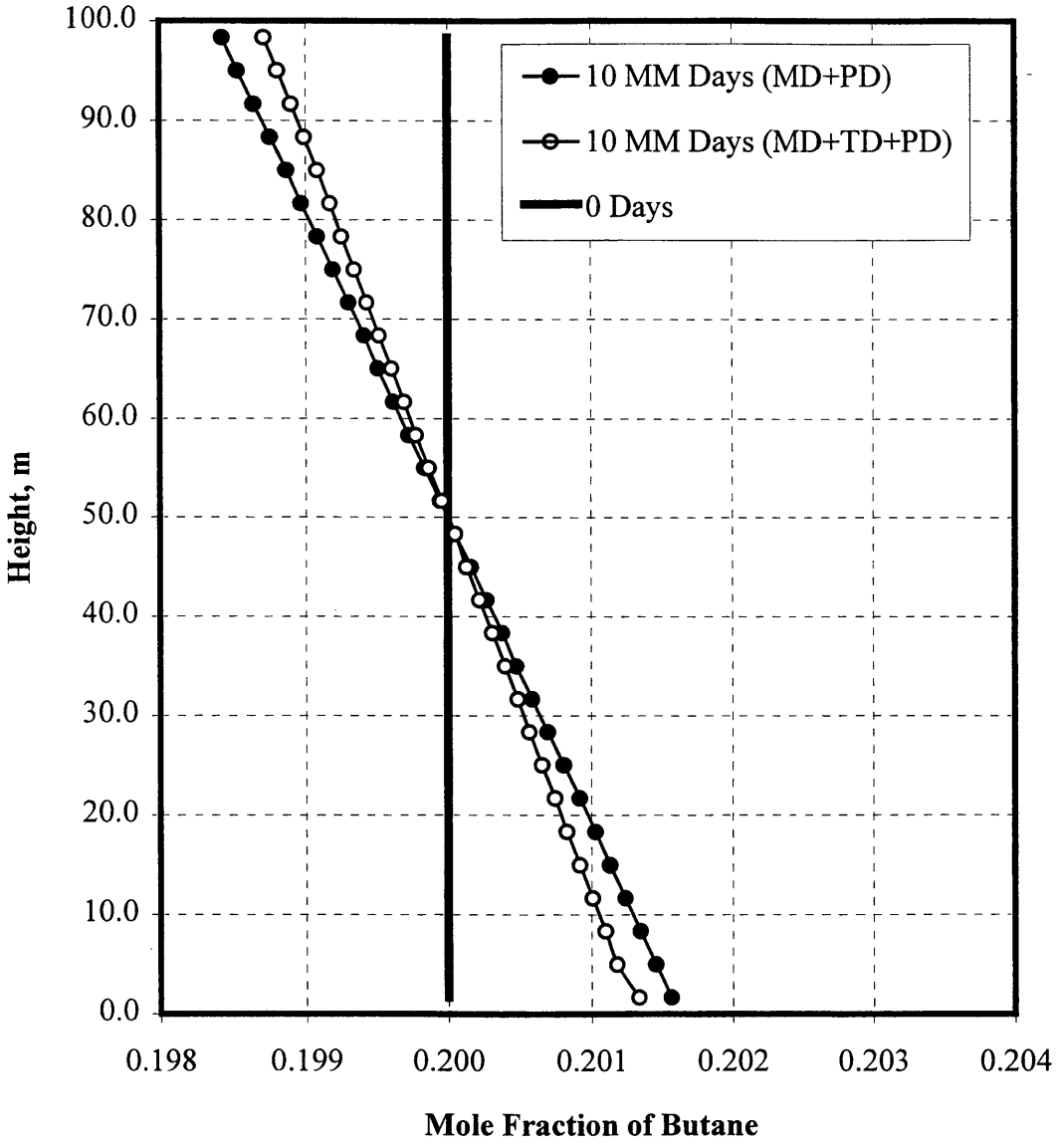

Figure 6.9 Mole Fraction of Butane in the Mixture. Comparing Molecular (MD) and Pressure Diffusion (PD) with Molecular (MD), Thermal (TD) and Pressure Diffusion (PD)

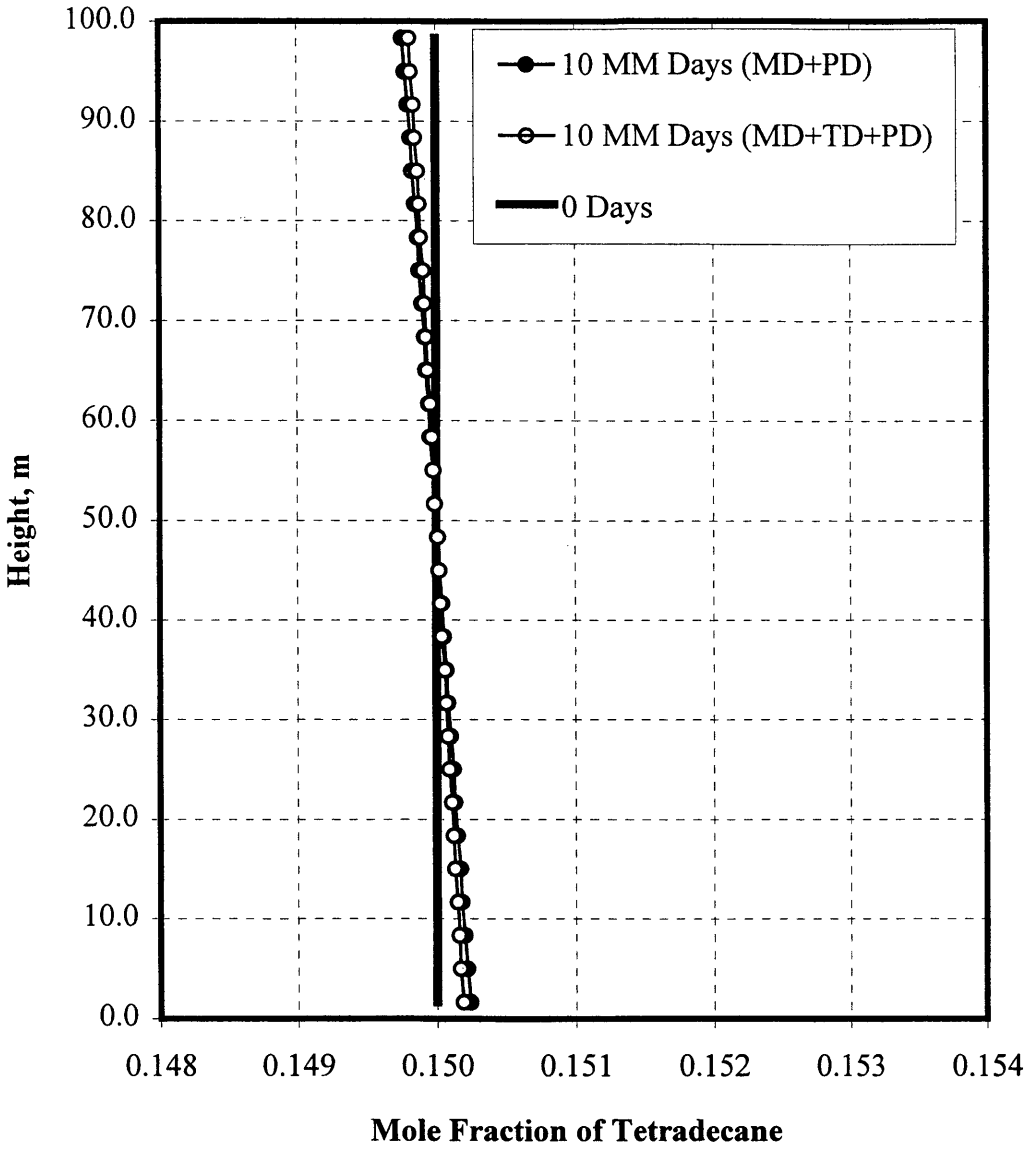

Figure 6.10 Mole Fraction of Tetradecane in the Mixture. Comparing Molecular (MD) and Pressure Diffusion (PD) with Molecular (MD), Thermal (TD) and Pressure Diffusion (PD)

6.2.3 Case 3: Considering Molecular Diffusion (MD) and Thermal Diffusion (TD)

In the third case, pressure diffusion (PD) is suppressed to analyze the effect of thermal diffusion on the compositional variation of components. Figures 6.11, 6.12, and 6.13 show the compositional variations for methane, butane and tetradecane, respectively. Once again, the trends agree with the earlier discussion. Since the thermal diffusion ratio for methane is negative, methane is concentrated at the lower part of the block. We can conclude that pressure diffusion is greater than thermal diffusion by analyzing Figure 6.8 or Figure 6.11. With tetradecane, there is practically no variation in composition when PD is neglected. Notice that the thermal diffusion ratio for tetradecane is ten times smaller than that for methane. In conclusion, for the established conditions, pressure diffusion is greater than thermal diffusion, and it is the dominant term.

Accordingly, we can say that components with negative thermal diffusion ratio, k^T, will segregate to the bottom and components with positive values will concentrate at the top of the block. On the other hand, components with negative pressure diffusion coefficients, $D^P{}_c$, will segregate to the bottom and those with positive values will concentrate at the top of the block. Under specific circumstances, for example, high temperature gradient or conditions near critical point, the above discussion could be invalid.

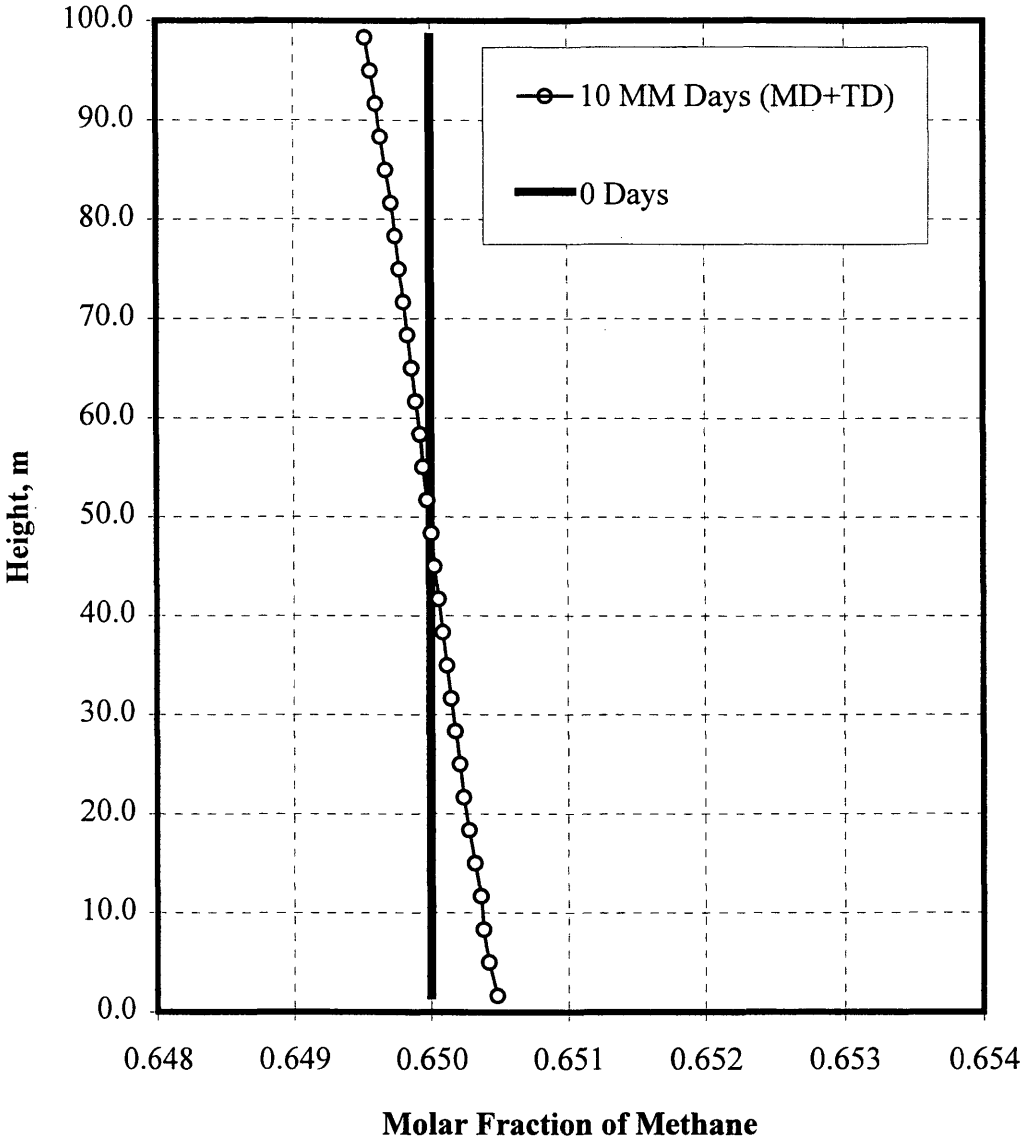

Figure 6.11 Mole Fraction of Methane in the Mixture. Considering Molecular (MD) and Thermal Diffusion (TD).

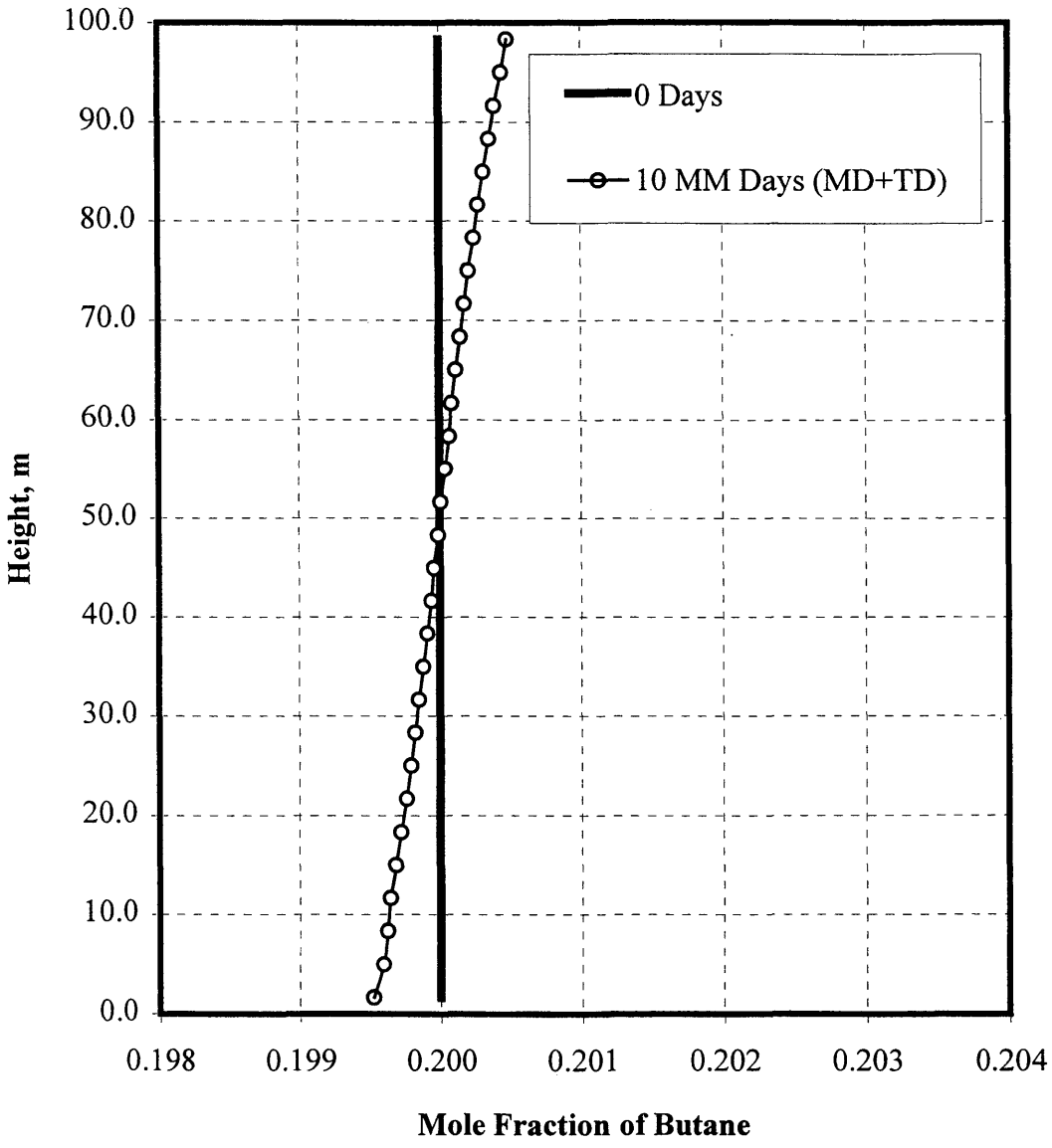

Figure 6.12 Mole Fraction of Butane in the Mixture. Considering Molecular (MD) and Thermal Diffusion (TD).

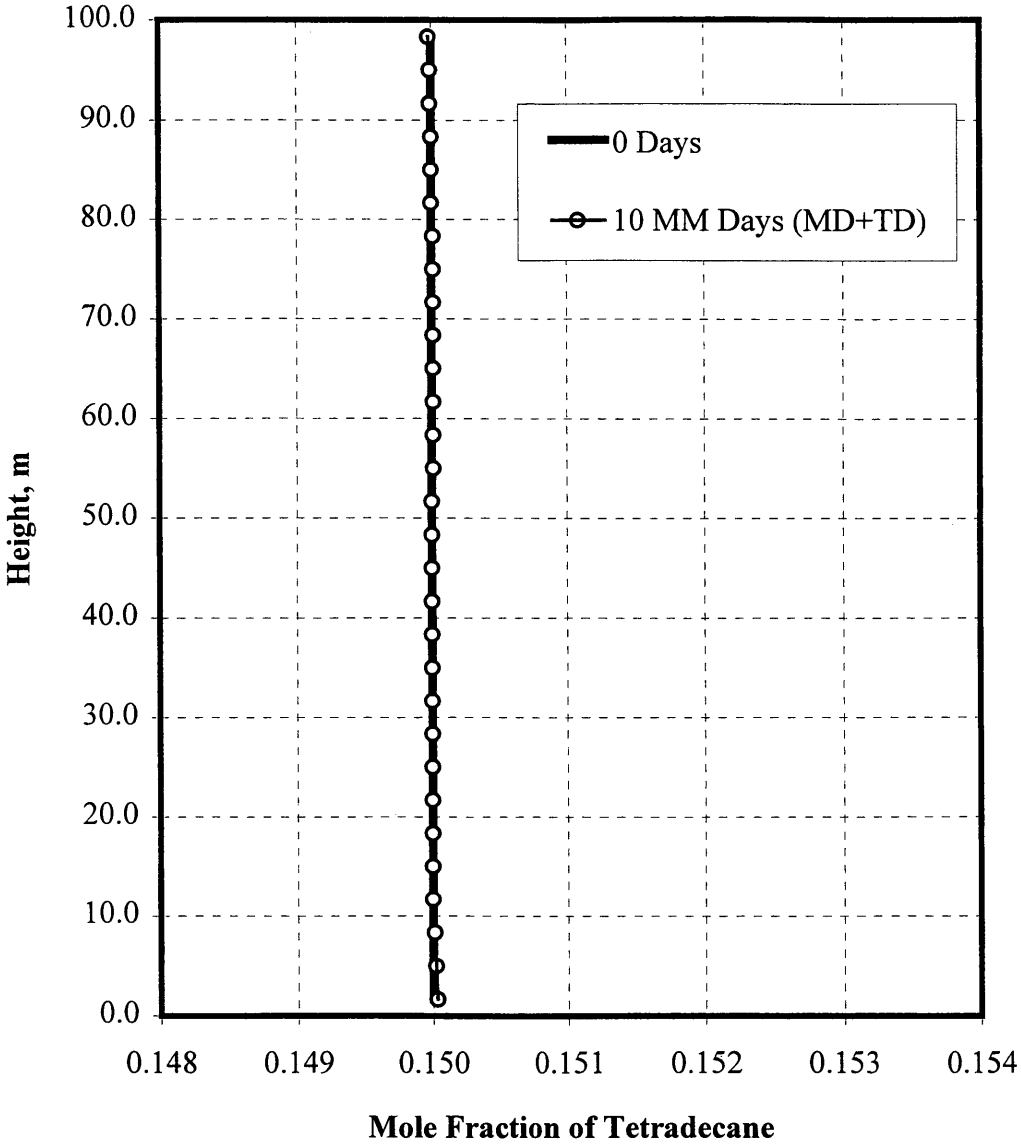

Figure 6.13 Mole Fraction of Tetradecane in the Mixture. Considering Molecular (MD) and Thermal Diffusion (TD).

6.3 Variation of Pressure Saturation with Composition

Let us now discuss the effect of composition variation on saturation pressure. First, from Figure 6.5 or Figure 6.8, it can be seen that C_1 is more concentrated at the top of the block. Since the content of methane in the mixture is considerable (65 %) and since it has the largest vapor pressure value, it is the component that will dictate the trend of saturation pressure along the block. Figure 6.14 shows the saturation pressure for the three cases analyzed. In the first case, considering OD, TD, and PD, the content of methane is larger at the top than at the bottom; the saturation pressure is therefore larger at the top than at the bottom. Recalling the fact that thermal and gravitational effects are generally opposed to each other, let us move onto the second case. For the second case, where thermal diffusion is neglected, there is a lesser amount of methane at the bottom, and the saturation pressure trend is similar but shows a larger positive slope. In the third case, when PD is neglected, the saturation pressure is inverted; it increases with depth as methane does. Both slopes become negative.

Before proceeding, let us discuss the importance of this variation in composition. First, under established conditions, the maximum molar fraction variations between the top and the bottom are 0.003 (0.3 %) for methane, 0.0026 (0.26 %) for butane, and 0.0004 (0.04 %) for tetradecane. Thus, one can conclude that the total molar fraction variation is less than 1%, and therefore, for practical purposes can be neglected. For certain conditions,

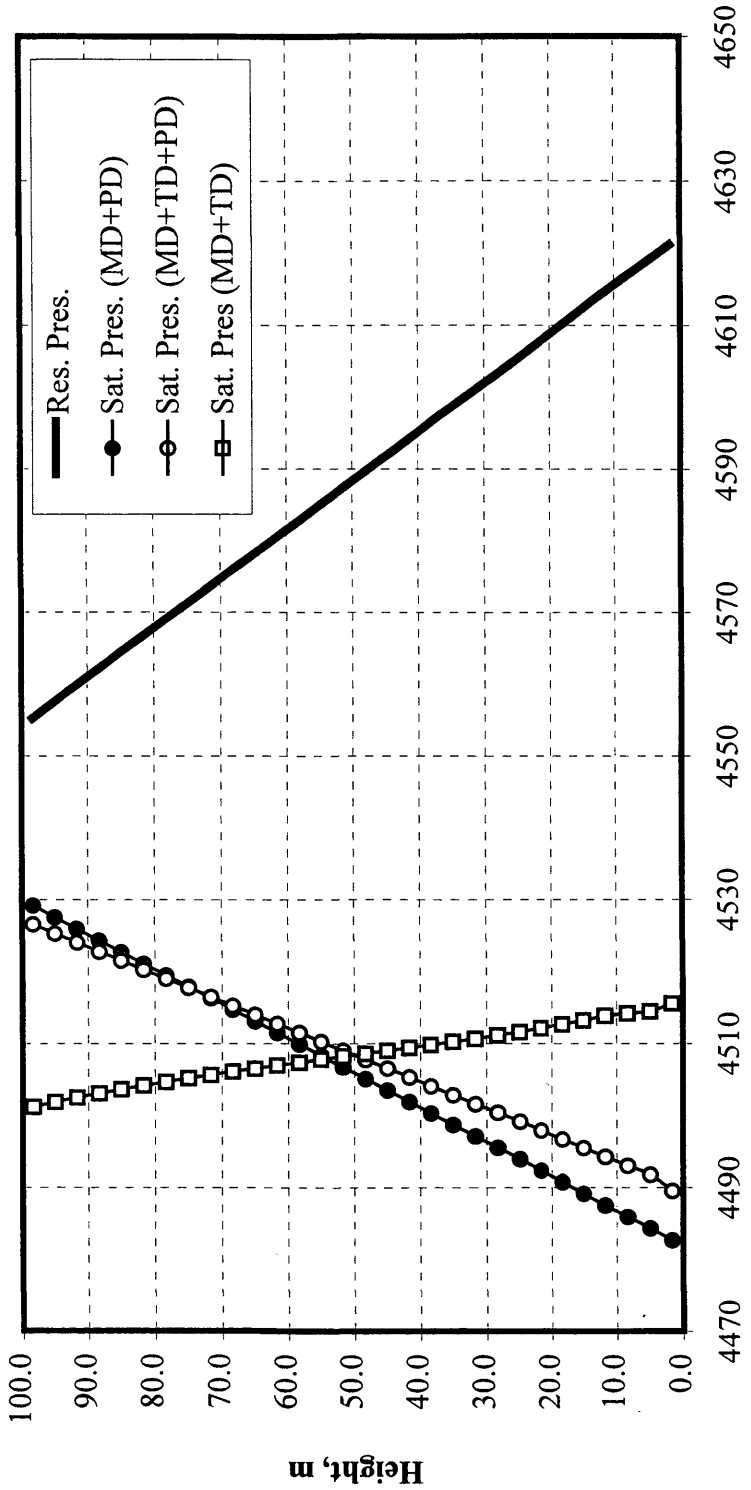

Figure 6.14 Effect of Composition on Saturation Pressure. 10 MM Days.

however, for instance, high thickness, high temperature gradient and fluid near critical point (high thermal diffusion ratios), the variation in compositions can be very important.

With respect to the saturation pressure, when OD, TD, and PD are considered, we can see that the variation of the saturation pressure is around 25 psi between the top at the bottom. This variation is increased to 35 psi when TD is neglected. The same difference becomes –10 psi when PD is neglected.

So far, the case when the matrix block does not have a source or sink, that is, a non-depleted reservoir has been analyzed. In other words, the distribution of components in a reservoir before production was simulated, that is, initial conditions. In addition, it was established above that for practical purposes the compositional gradient could be neglected. Now, a question arises: Can thermal and pressure diffusion be neglected when there are sources or sinks, that is, producer and injector wells? The answer to this question will be given in the following section.

6.4 Three-Component Simulation

The goal of this three-component simulation is to decide whether thermal and pressure diffusion can be neglected in the production stage or if they must be considered. Two simulations were performed from 0 to 50,000 days. In the first case, only molecular

diffusion (MD) was considered. In the second case, molecular, thermal, and pressure diffusion were considered. For both cases, oil was produced at the bottom at 0.001 m^3/day from 0 to 1500 days and then was shut in from 1500 to 50,000 days. The producing well was shut-in to minimize convection so thermal and pressure diffusion could be better observed.

Results of both cases, for a cell at 33 m from the top, are shown in Figures 6.15 to 6.17. As can be seen from these figures, the variation in composition through time is very small. A comparison of both cases demonstrates that composition does not change significantly. The variations in the composition are negligible. After 10,000 days the variation of composition becomes stable for the three components. The difference in mole fraction after stabilization between both cases is 0.0002, 0.00025, and 0.0003 for methane, butane and tetradecane, respectively. Given the results, it was concluded that for a mixture in convective movement, thermal and pressure diffusion can be neglected for the production stage. This agrees with some ideas given by Danesh (1999) and Bedrikovesky (1994). As we will see later, hydrodynamic dispersion, the combination of molecular diffusion and mechanical dispersion, will be the only term considered to analyze the dispersion of an injected component.

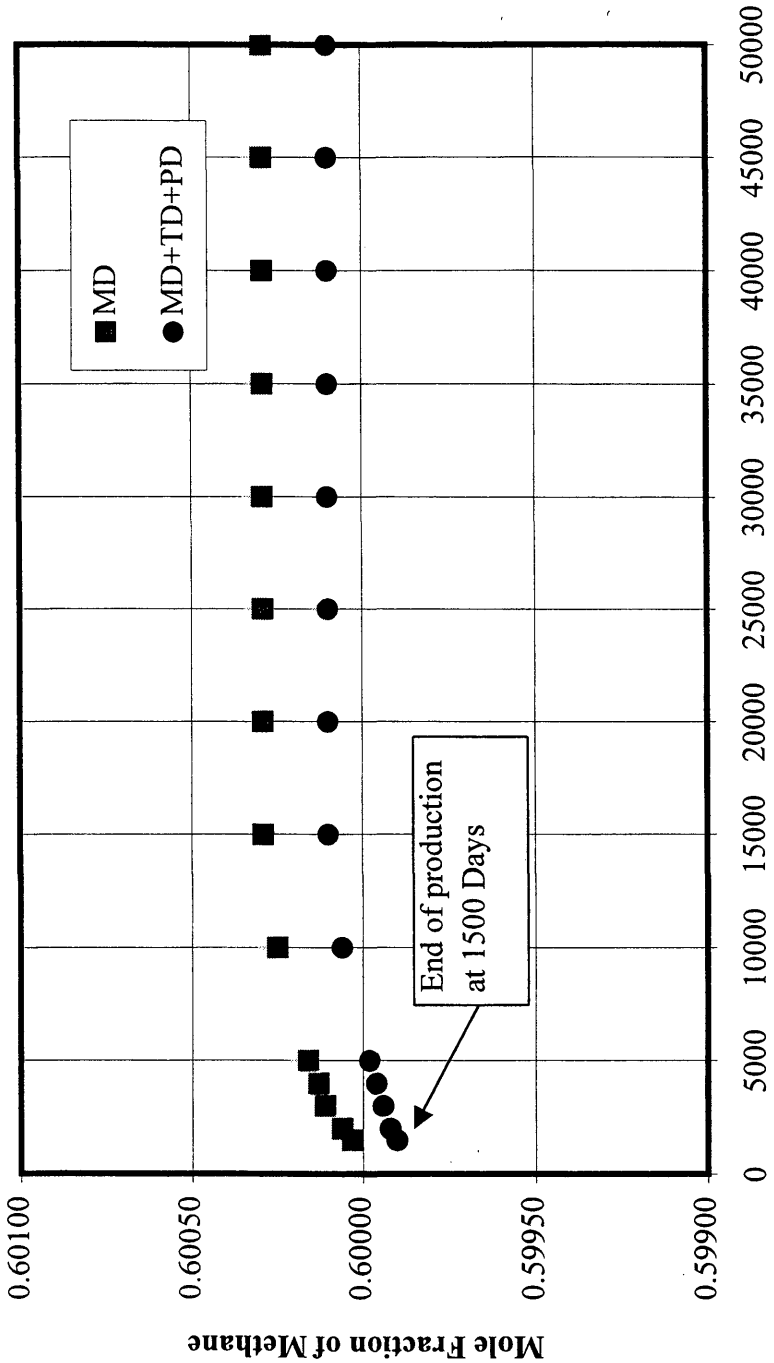

Figure 6.15. Mole Fraction of Methane in the Liquid Phase. Comparing Molecular Difussion (MD) with Molecular (MD), Thermal (TD) and Pressure Difussion (PD). 1500 Days of Production and 48,500 Days for Equilibrium.

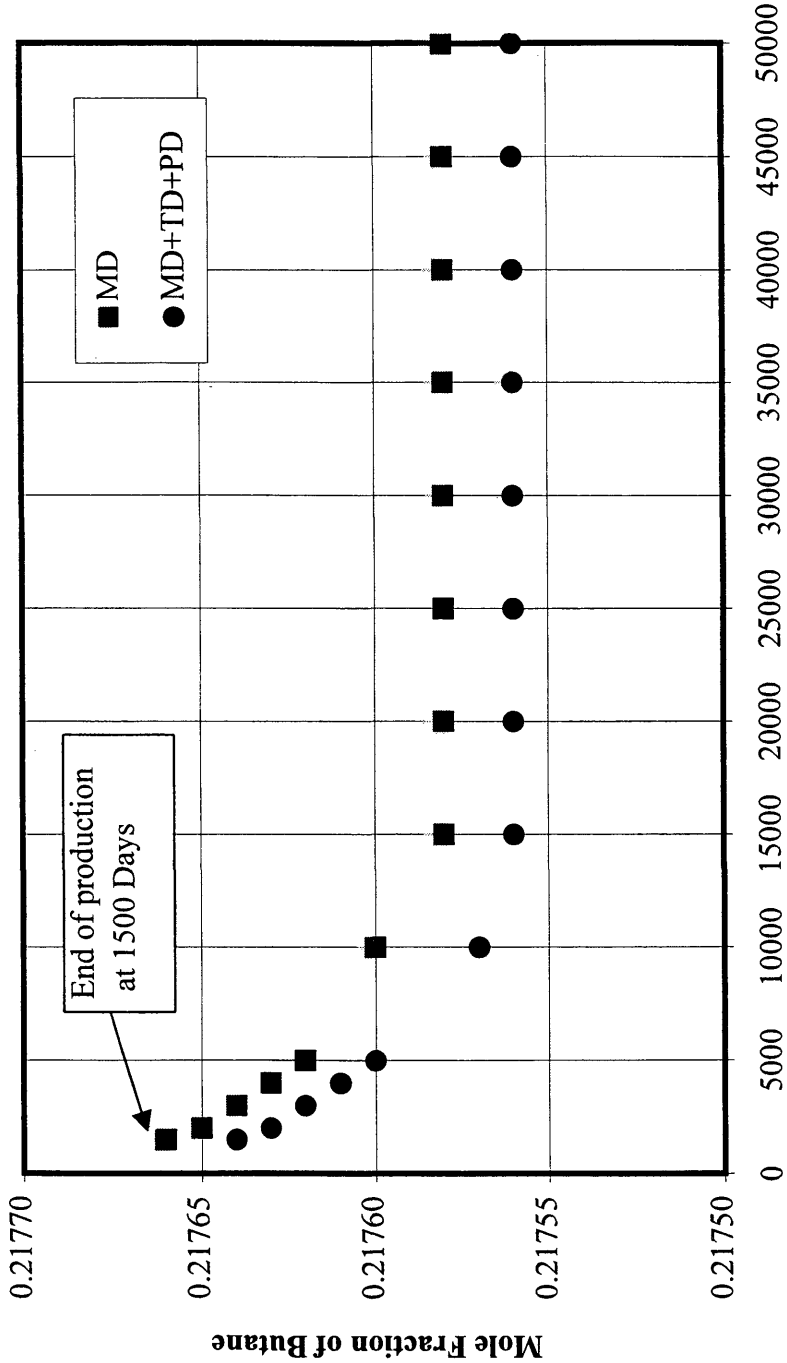

Figure 6.16. Mole Fraction of Butanee in the Liquid Phase. Comparing Molecular Difussion (MD) with Molecular (MD), Thermal (TD) and Pressure Difussion (PD). 1500 Days of Production and 48,500 Days for Equilibrium.

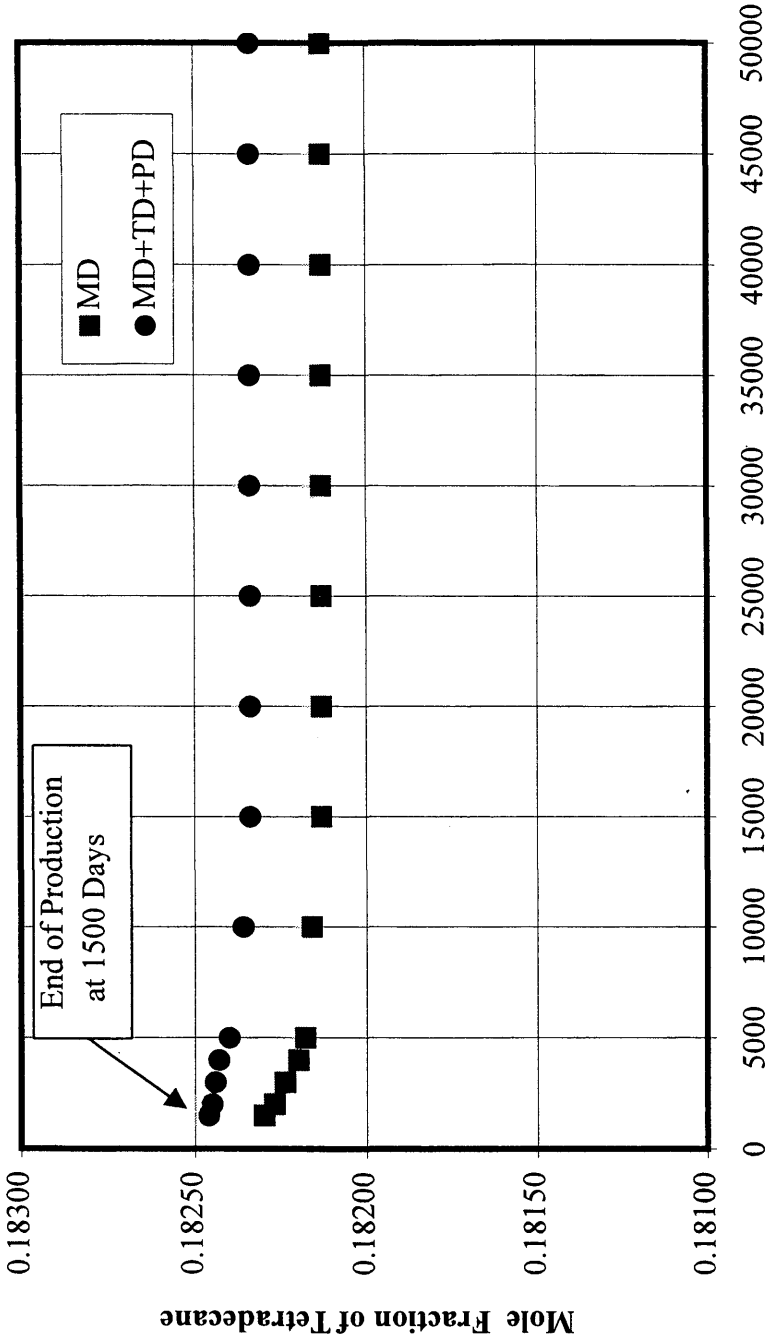

Figure 6.17. Mole Fraction of Tetradecane in the Liquid Phase. Comparing Molecular Difussion (MD) with Molecular (MD), Thermal (TD) and Pressure Difussion (PD). 1500 Days of Production and 48,500 Days for Equilibrium.

6.5 Post Production analysis.

Having shown that neither thermal and pressure diffusion contribute to modify the special distribution of components, the following cases will ignore their effects. Thus, the only term contributing to the diffusion of components under convective motion will be molecular diffusion. Since molecular diffusion is part of the hydrodynamic dispersion term, mechanical dispersion will also be considered. Four more cases are analyzed to simulate the magnitude of the mixing of components due to both diffusion and convective flow in fractured systems. Case Four will be a single matrix block with a vertical fracture in the middle part. Case Five will be a single block with one vertical and three horizontal fractures. Case Six is a single block with one vertical fracture and a different value of matrix porosity for each side of the fracture. (This case is included to study formations with high porosity, for instance, vuggy porosity.) Finally, Case Seven is a single block with a vertical fracture and some layers with low vertical permeability to simulate, for example, stylolites or impermeable barriers. In all cases, nitrogen will be injected at the top, and oil will be produced at the bottom of the fracture. The purpose of injecting nitrogen is to maintain pressure; however, the analysis of its efficiency as a method of recovery is not considered in this work. Since it is important to know the content of nitrogen in the liquid phase, two figures were generated for the four cases at several times: mole fraction of nitrogen in the liquid phase and gas saturation as well as a plot to see the magnitude of the velocity in both phases. These figures are useful in

describing the hydrodynamic dispersion (HD) of nitrogen in naturally fractured reservoirs.

For Cases Four and Five, both figures are presented with and without HD. For simplicity, Cases Six and Seven consider only HD. At the end of this chapter, a plot showing the mass of nitrogen in the liquid phase for the four cases is given. First, Case Four is analyzed, and then the three remaining cases are discussed.

6.5.1 Case 4: Production / Injection Stage –a Single Vertical Fracture

In this section, TD and PD are neglected. Thus, the remaining terms are molecular diffusion and mechanical dispersion. The combination of both terms is called hydrodynamic dispersion (HD). Case Four consists of simulating a single block with a vertical fracture, similar to that shown in Figure 6.4. Table 6.6 presents in detail the data used in this work. Figure 6.18 shows the flow rates, production of oil and injection of nitrogen, for all cases. Oil is produced at the bottom of the fracture and nitrogen is injected at the top. The number of cells in the x- and z-direction was 9 and 33, respectively.

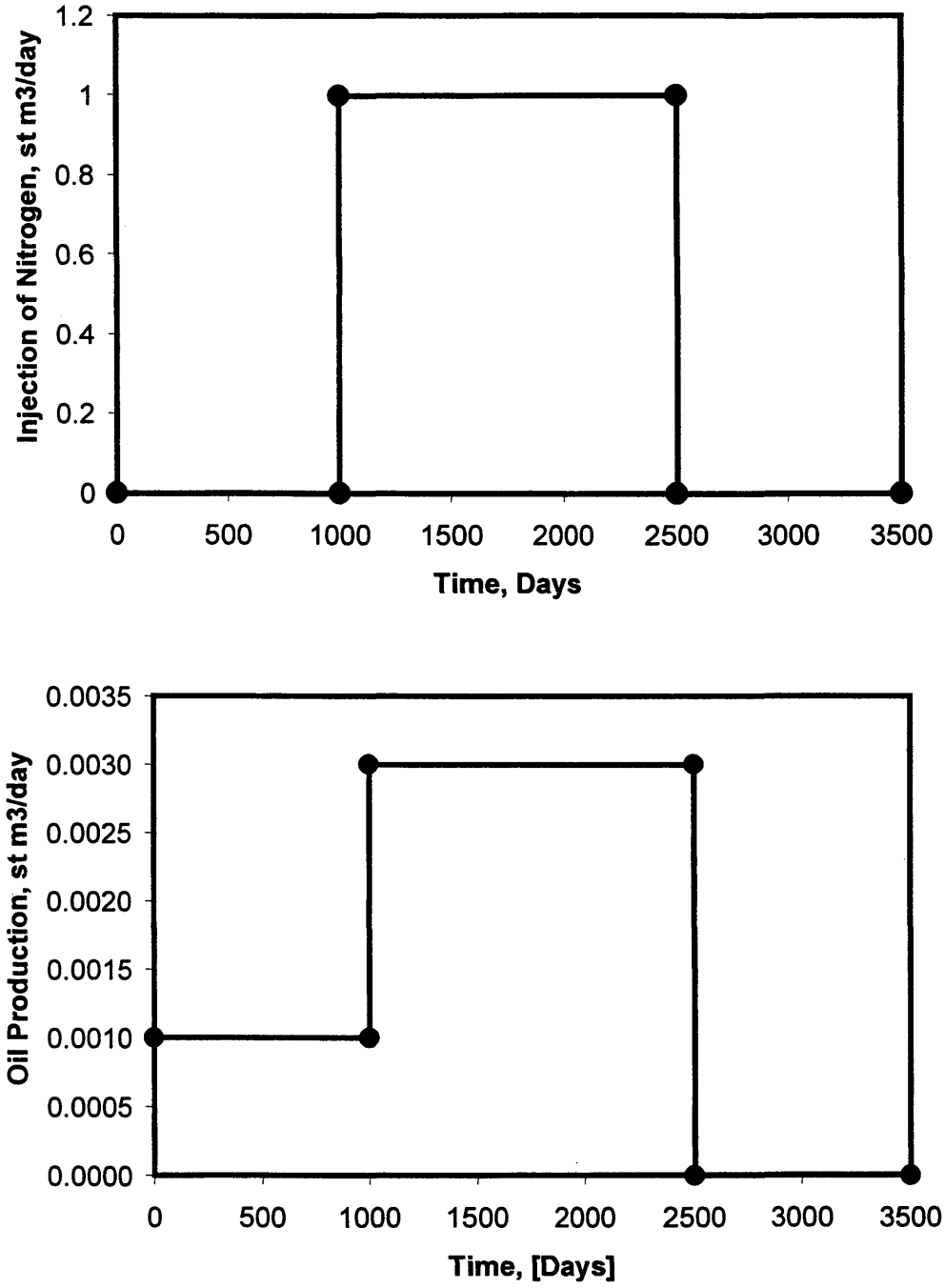

Figure 6.18 Rate of Nitrogen Injection and Oil production

Figures 6.19 and 6.20 show the results after nitrogen injection without hydrodynamic dispersion. First, without HD, Figure 6.19 presents the mole fraction of nitrogen in the liquid phase and Figure 6.20 shows the gas saturation. In Figure 6.19, we see that nitrogen flows immediately to the producer well, at the bottom of the block, without undergoing any nitrogen spread. The small amount of nitrogen around the fracture is due to the pressure gradient between fracture and matrix. After shutting down both wells, at 2500 days, gravity tends to equilibrate the fluid; however, 1000 days of shut-in are not enough to produce a complete segregation of phases. The gas saturation, in Figure 6.20, shows that in the matrix, most of the gas is found above the gas-oil contact in the fracture and is concentrated at the top of the block for all the times.

On the other hand, Figures 6.21 and 6.22 show the same results considering hydrodynamic dispersion. We immediately see the effect of HD on the spreading of nitrogen. Since gas saturation is higher at the top than in the rest of the matrix, the spreading of nitrogen is evident in that location, recalling that a gas easily diffuses into another gas. Notice that the mole fraction of nitrogen in the liquid phase at the top of the block is around 30 %. Comparing Figures 6.21 and 6.22, we see that the mole fraction of nitrogen in the liquid phase increases when gas saturation does. In other words, nitrogen diffuses through the gas phase and then, because of equilibrium, is incorporated in the liquid phase. Recalling that the HD term involves phase saturation (holding constant the remaining terms), as phase saturation increases, the HD term also increases. Thus, there

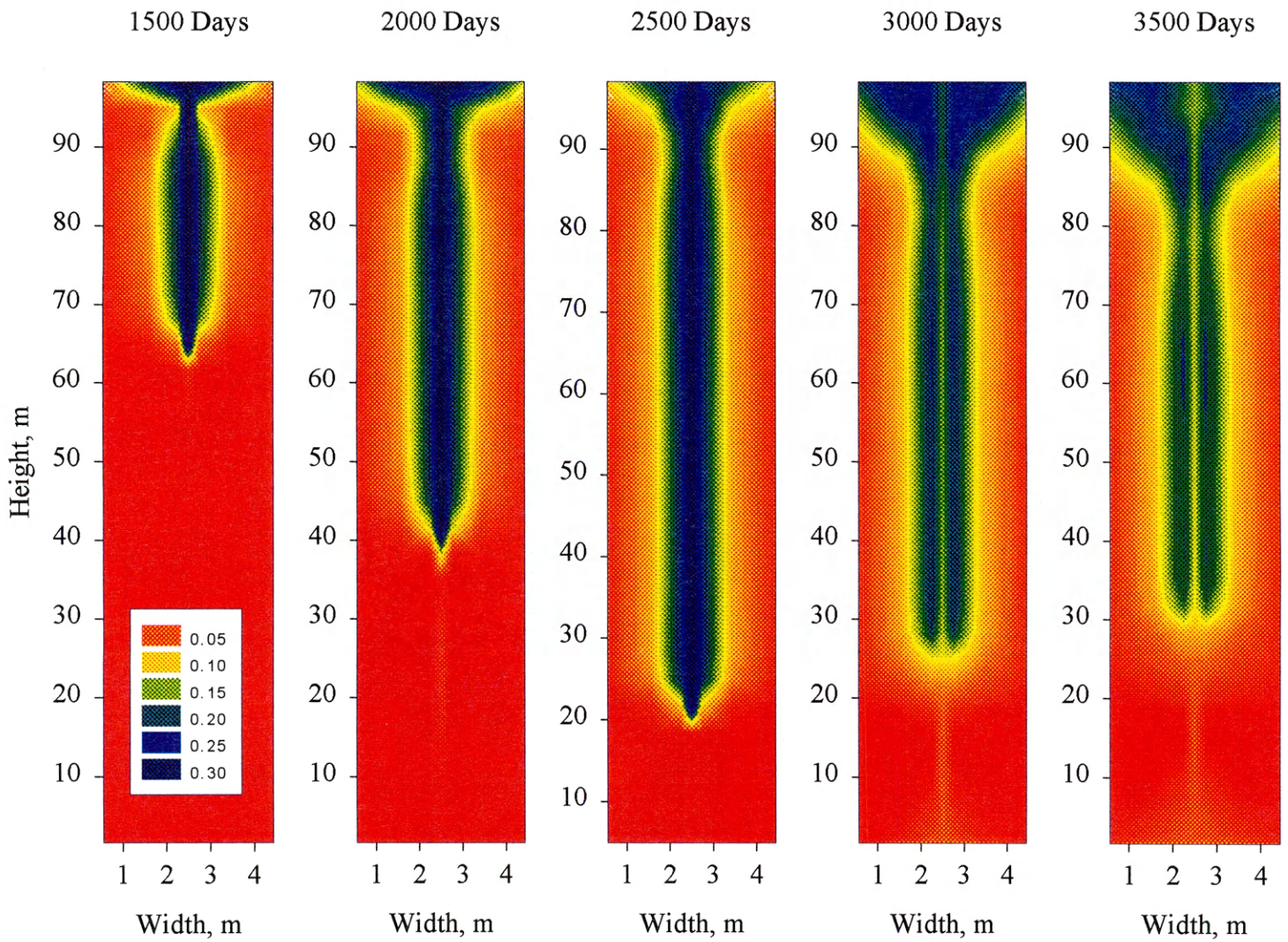

Figure 6.19 Mole Fraction of N2 in the Liquid Phase, Without Hydrodynamic Dispersion

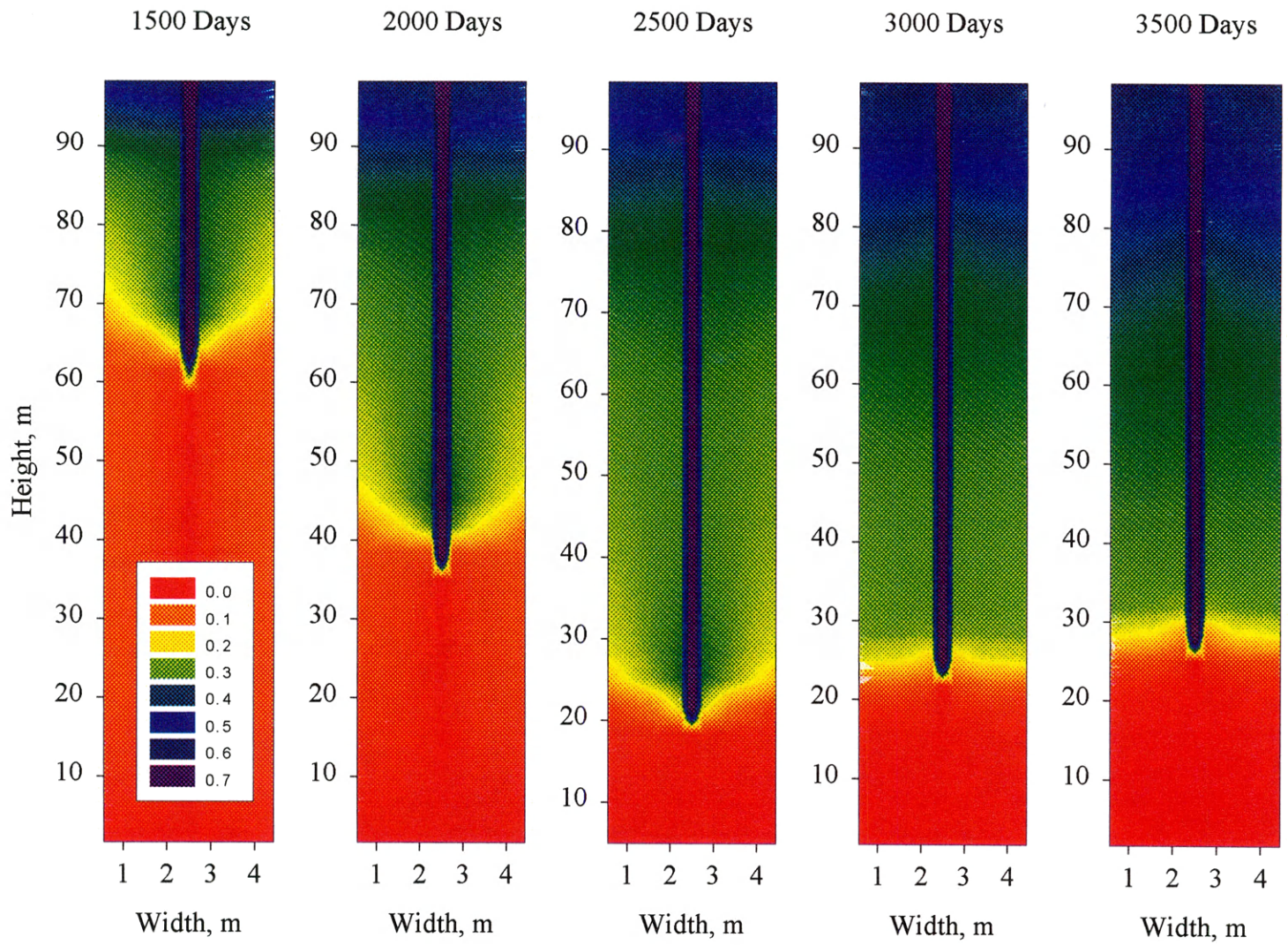

Figure 6.20 One Vertical Fracture. Gas Saturation Without Hydrodynamic Dispersion

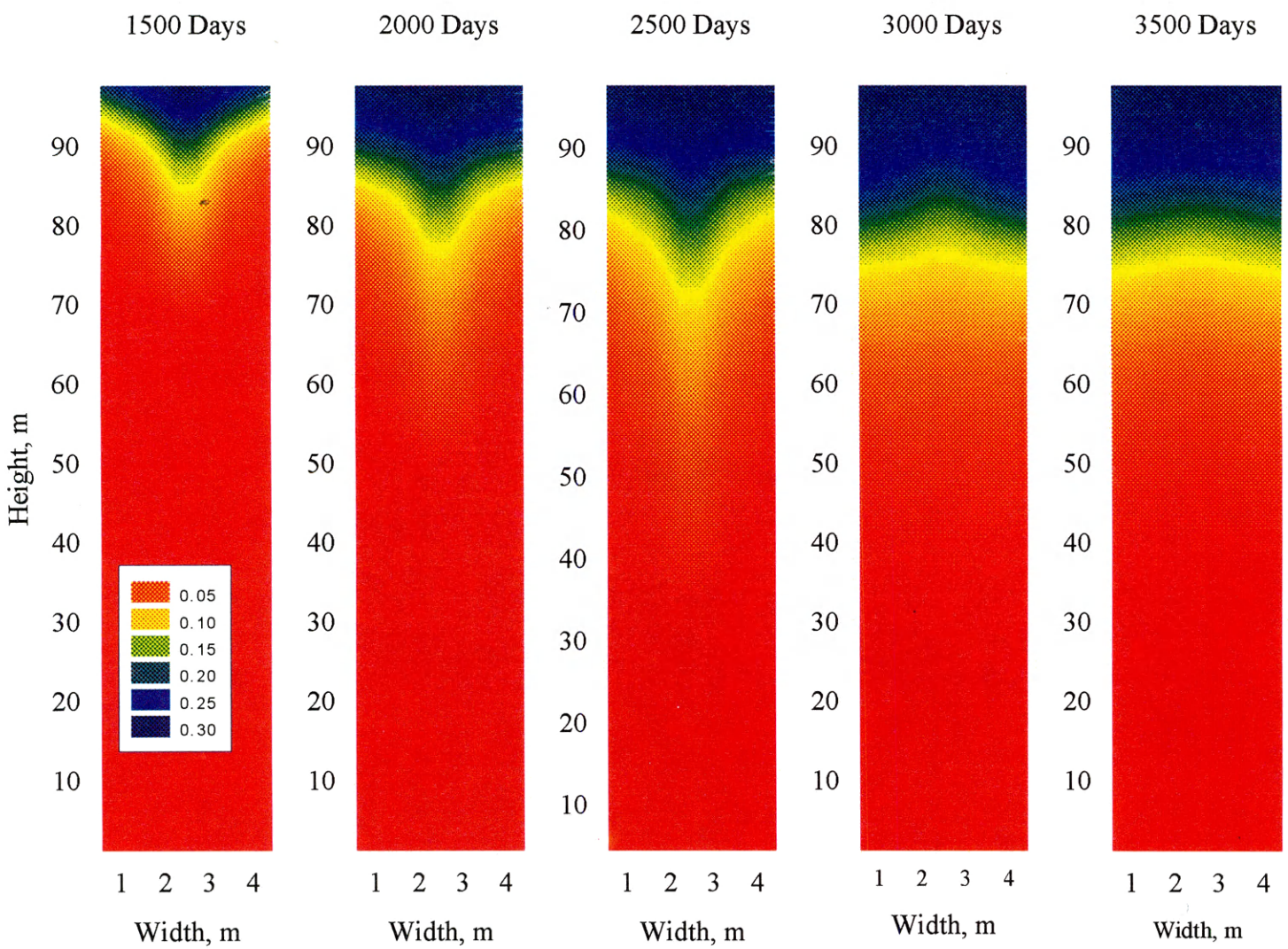

Figure 6.21 Mole Fraction of N2 in the Liquid Phase, With Hydrodynamic Dispersion

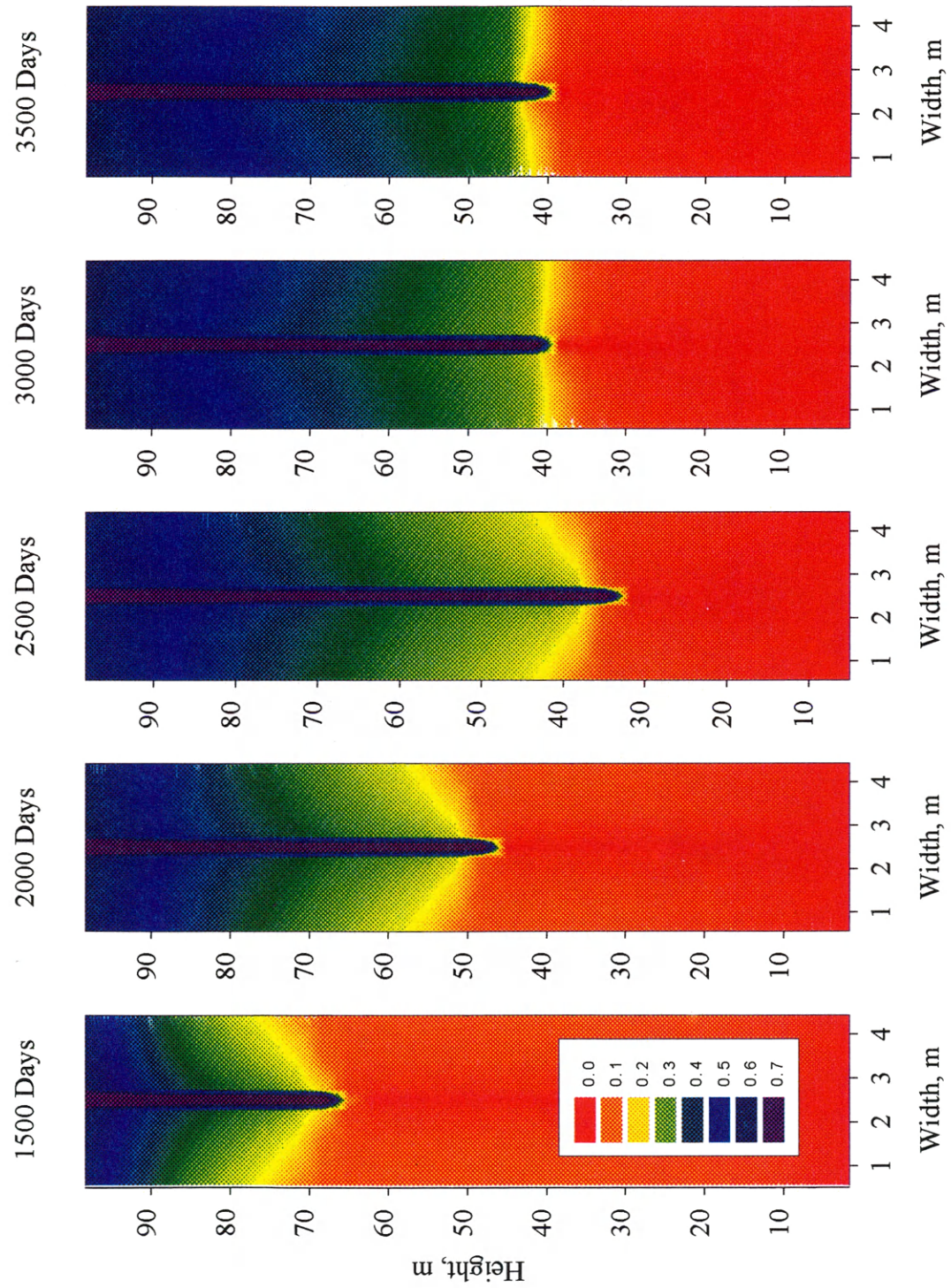

Figure 6.22 One Vertical Fracture. Gas Saturation With Hydrodynamic Dispersion

is more fluid in gas phase in contact with the liquid phase.

By shutting down both wells, the effect of HD on the distribution of nitrogen could be better visualized. Since we want to study the effect of HD at the same time that the reservoir is exploited, the wells were shut-in for 1000 days after 2500 days of production. However, 1000 days of shut-in is not enough to see molecular diffusion effects. After 2500 days, when both wells are shut-in, gravity, capillary and hydrodynamic dispersion act to equilibrate the fluids along the block; however, gravity is the dominant force.

According to the above results, one can conclude that hydrodynamic dispersion must be considered when simulating injection of nitrogen into a fractured reservoir. If HD is ignored, estimates of both time breakthroughs and injected component location can be incorrectly evaluated.

To see the magnitude of the velocity vectors, a plot of the total vector velocities was made. Figure 6.23a and 6.23b show the total magnitude of the gas and liquid velocities, respectively. Regarding the gas phase, it can be seen in Figure 6.23a that the velocity of the gas phase in the fracture is approximately 400 or more times greater than the maximum velocity inside of the matrix block. This small magnitude of the gas velocity inside the matrix block causes a small contribution to the mechanical dispersion term, allowing a larger contribution for the molecular diffusion term. In other words, the

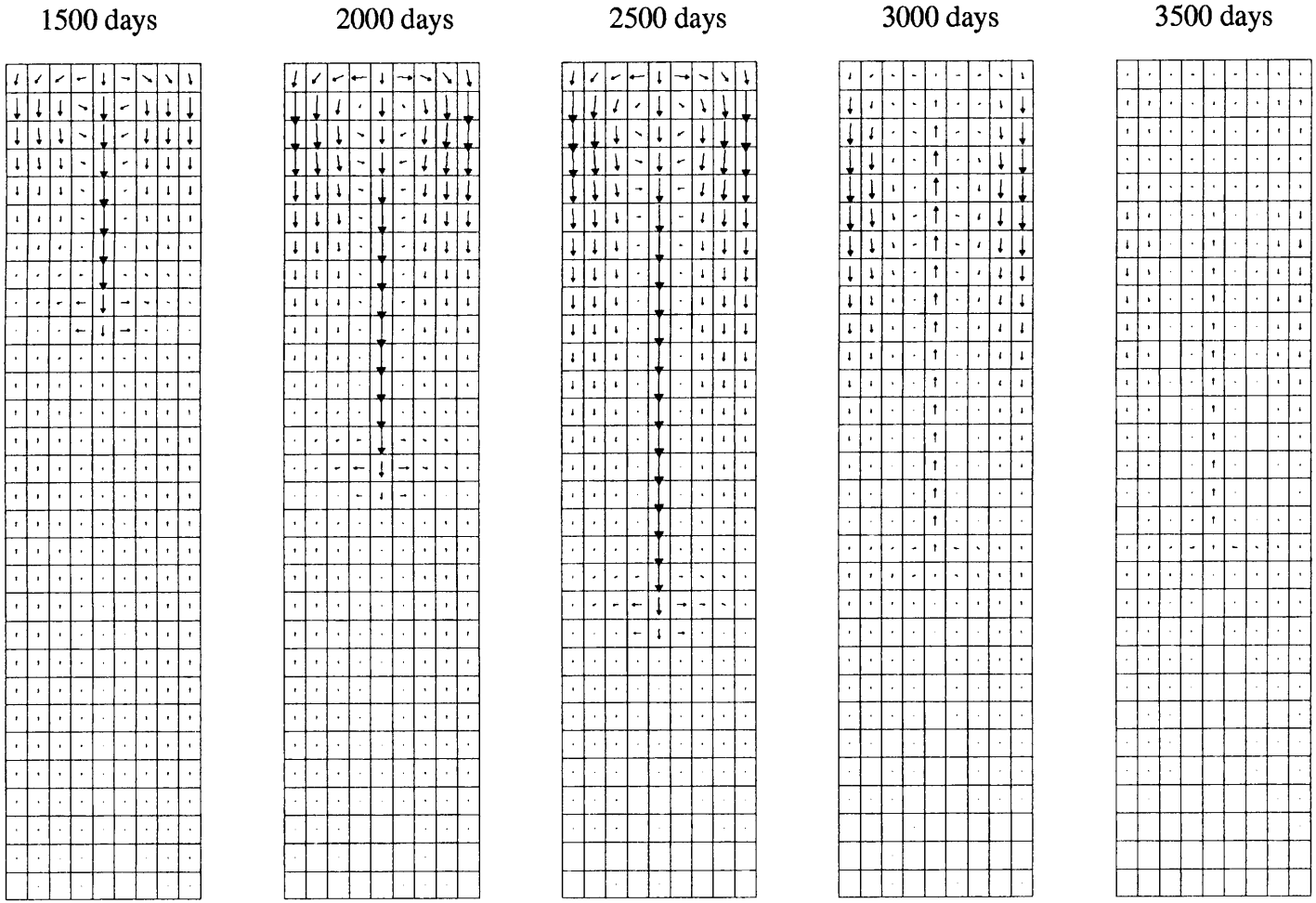

Fig 6.23a Gas Phase Velocity Vector. One Vertical Fracture. Vm is enlarged 400 Times.
Vm(max)=0.01x10-6 m/s; Vf(Max)=5.1x10-6 m/s

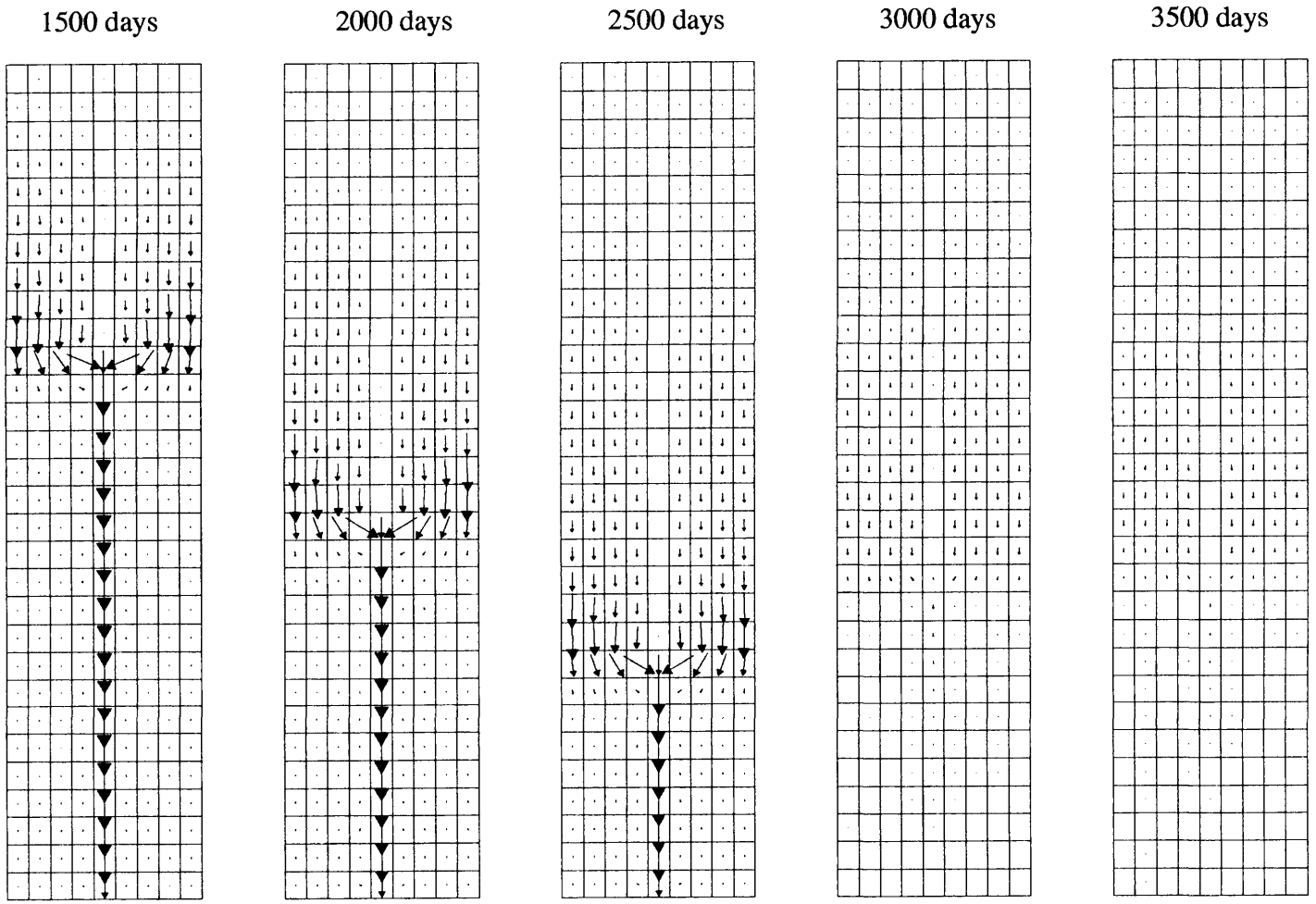

Fig 6.23b Oil Phase Velocity Vector. One Vertical Fracture. Vm is enlarged 400 Times.
Vm(max)=0.02x10-6 m/s Vf(Max)=7.3x10-6 m/s

contribution of molecular diffusion in the hydrodynamic dispersion term will be larger than mechanical dispersion for low velocities; otherwise, the mechanical dispersion term will be larger. The last case is presented in the fracture where the magnitude of the velocity is high. In the fractures, the mixing of components is due mainly to the mechanical dispersion term. Figure 6.23b shows the oil phase velocity. One can see that around the gas-oil contact in the fracture there is a larger pressure drop and therefore, a larger oil phase velocity. Because of a small amount of liquid nitrogen and because the molecular diffusion coefficient for the liquid phase is an order of magnitude smaller than the gas phase, the liquid-liquid diffusion is smaller compared with the gas-gas diffusion.

6.5.1.1 Effect of Fracture Spacing

A simulation was made where matrix block width in x-direction for the 5-meters base case was increased by a factor of 5. Therefore, the matrix block width was increased from 5 meters to 25 meters. The injection/production was also increased by a factor of 5. The simulation results indicate that gas-oil contact moves toward the bottom of the fracture faster, as can be seen in Figure 6.24. Furthermore, when Figure 6.24 results are compared to the 5-meters case results, Figure 6.21, one can observe that for smaller fracture spacing (such as 5 meters versus 25 meters), the gas-oil interface movement is flatter. Therefore, for large fracture spacing, there is a greater chance for earlier gas breakthrough into production wells.

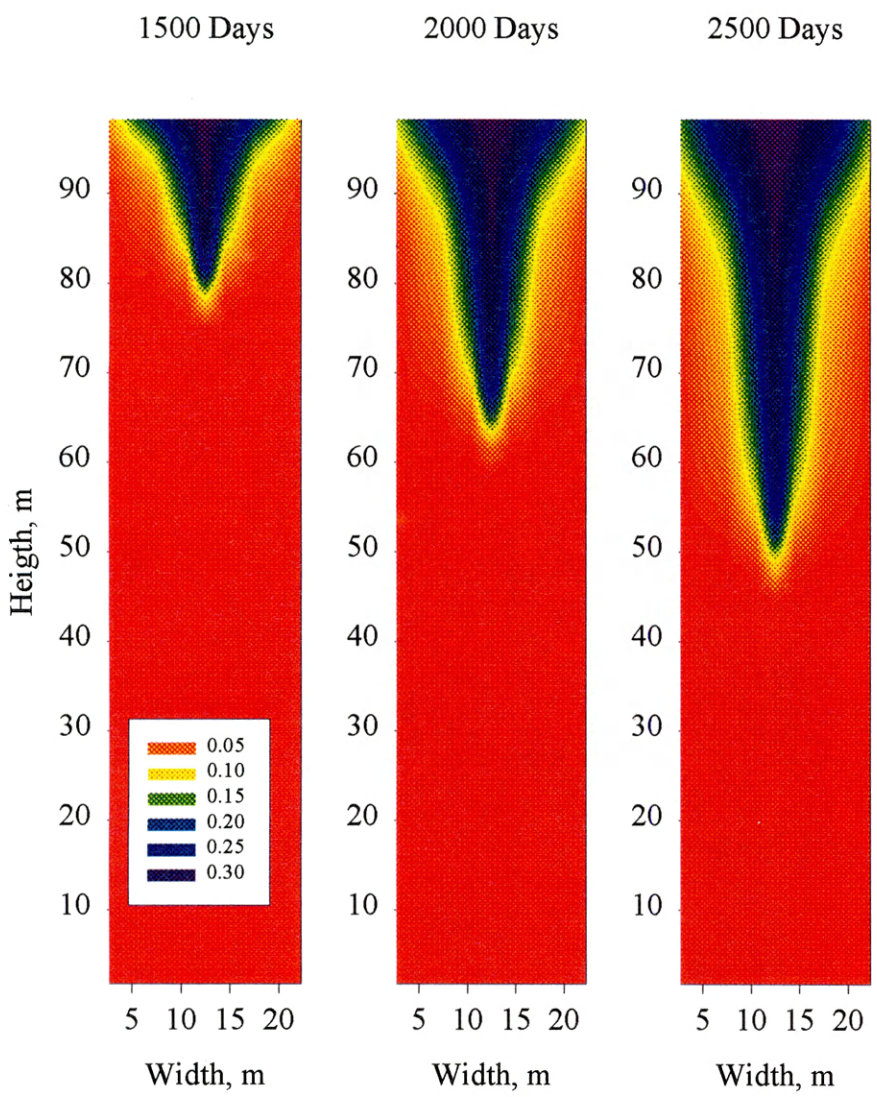

Fig. 6.24. Mole Fraction of Nitrogen in the Liquid Phase With Hydrodynamic Dispersion. 1 Vertical Fracture, Matrix Block 25 m.width.

6.5.1.2 Scaling the Single Matrix Block Results to Full Field

The production and injection rates used for one single matrix block/fracture in the base case (Figure 6.18) can be scaled to full field performance as follow:

Injection:

Area of the matrix block is (5m) x (1m) = $5m^2$ = 53 ft^2. One section is (1mile) x (1mile) which is equal to 27.8 x 10^6 ft^2. The number of blocks per section is 27.8x10^6 / 53, which is equal to 5.2 x 10^5 blocks.

The nitrogen injection was 1.0 st m^3/D = 35.3 scf/D. Therefore, for one section the nitrogen injection rate is calculated as follows:

No. of blocks x Injection rate per block =5.2x10^5 x35.3 scf/D=18.3 MMscf/D/section

Production:

Oil production per block is 0.003 st m^3/D = 0.0188 STB/D. Therefore, the produced oil rate per section can be calculated as show as follows:

No. of blocks x oil rate per block = 5.2 x 10^5 x 0.0188 STB/D = 9776 STB/D/ section

It is, therefore, imperative that while single-matrix block injection and production rates appear to be small, the corresponding field results are large and realistic. For instance, a production rate of 0.00188 STB/D is equivalent to 9776 STB/D per section or 90,000 STB/D for a field consisting of 10 sections. Similarly, an injection rate of 35.3 scf/D per matrix block is equivalent to 18.3 MMscf/D per section and 183 MMscf/D for 10 sections.

6.5.2 Case 5: Production / Injection Stage, Fracture Orientation

The purpose of simulating the block with some horizontal fractures, in addition to the vertical fracture, is to verify that increased contact area between fractures and matrix block results in a greater amount of nitrogen diffusion. The same data given in Table 6.6 were used. Horizontal fractures are located in such a way that the small blocks at the top and the bottom are half as high as those between the two horizontal fractures. Without hydrodynamic dispersion, Figures 6.25 and 6.26 show the mole fraction of nitrogen in the liquid phase and the gas saturation, respectively. The mole fraction of nitrogen in the liquid phase shows results similar to those having no horizontal fractures. The effect of the horizontal fractures is to allow a small amount of nitrogen along the fractures because of the pressure gradients. Nitrogen, however, flows rapidly to the sink. Since HD is ignored, the mole fraction of nitrogen in this case is very similar to Case Four.

The gas saturation for this case also parallels previous results: the gas is concentrated in the fractures, due to their high permeability, and at the top of the block. In the matrix, gas saturation begins to increase above the gas-oil contact present in the fracture. Below this contact, the gas in the matrix is minimal –almost zero.

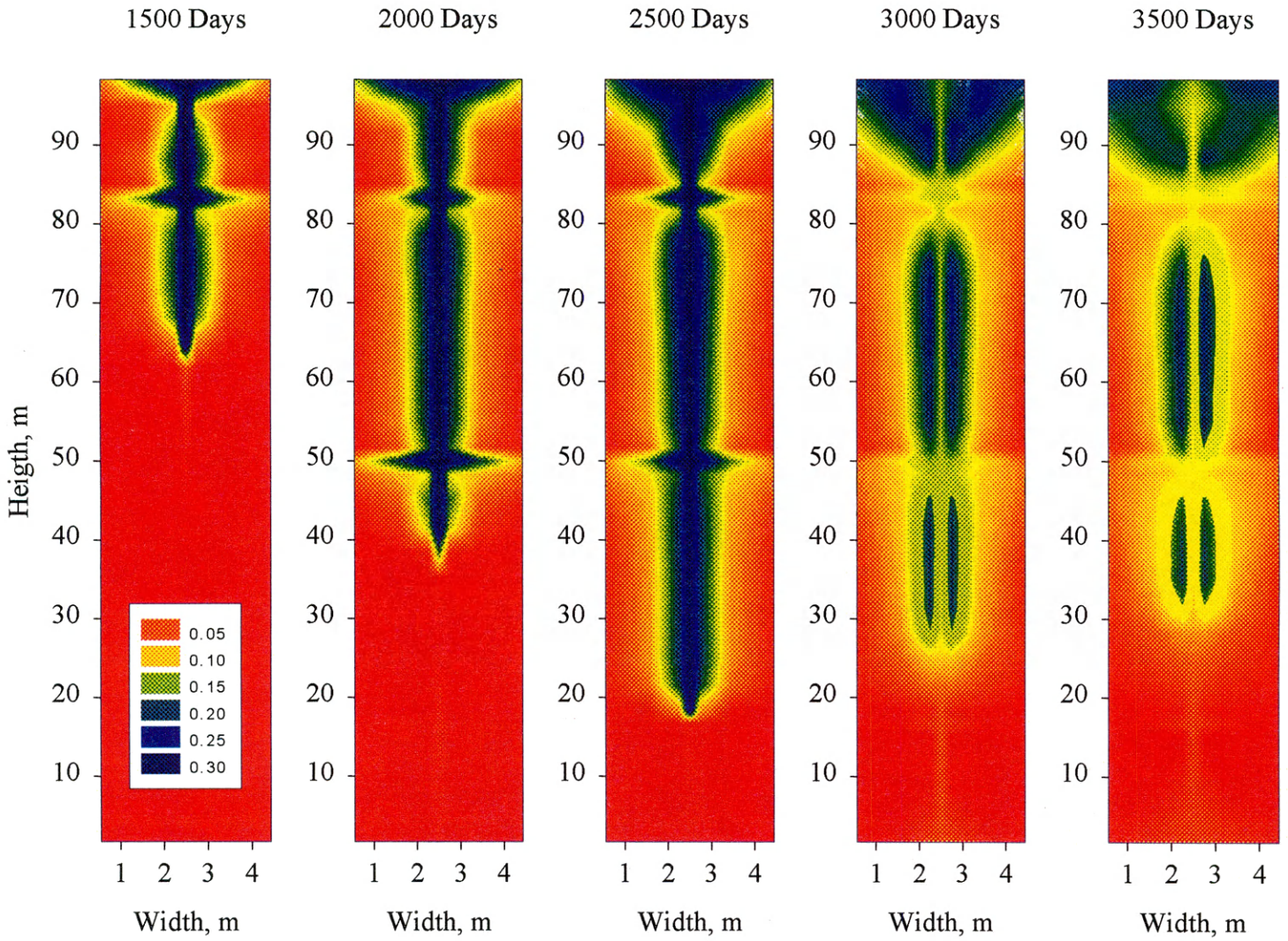

Figure 6.25 One Vertical Fracture and Three Horizontal Fractures. Mole Fraction of N_2 in the Liquid Phase. Without Hydrodynamic Dispersion.

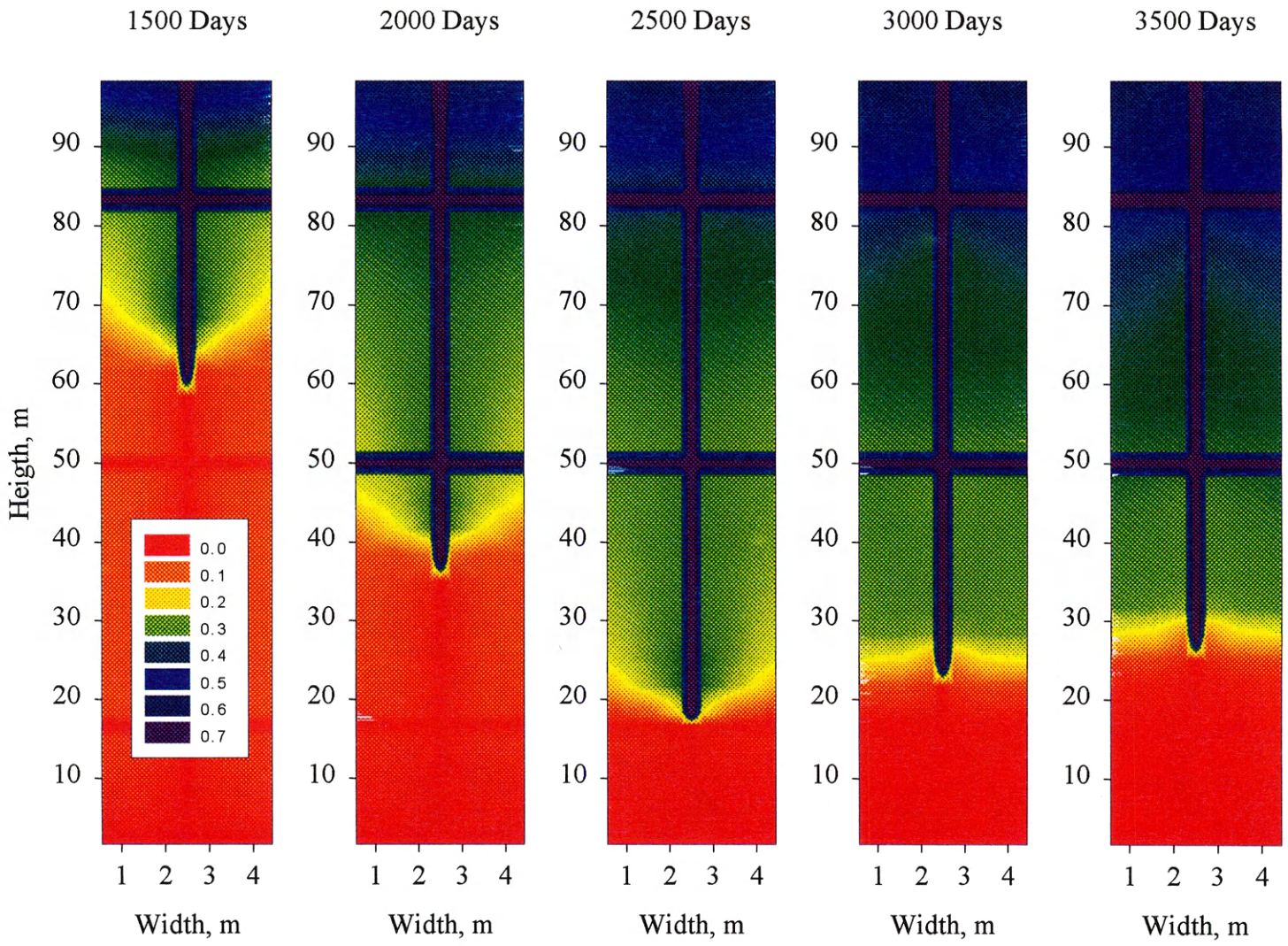

Figure 6.26 One Vertical Fracture and Three Horizontal Fractures. Gas Saturation Without Hydrodynamic Dispersion.

Figures 6.27 and 6.28 present results in which hydrodynamic dispersion is accounted for. Figure 6.27 gives the mole fraction of nitrogen in the liquid phase. Here we can see the same effects as in Case Four. For example, at 2000 days, the highest horizontal fracture barely contributes to the dispersion of nitrogen; nevertheless, the distribution of nitrogen in Figure 6.27 is very different from that in Figure 6.25. Most of the nitrogen is dissolved in both phases at the top of the block. Again, the mole fraction of nitrogen in the liquid phase is around 32 % and hydrodynamic dispersion greatly contributes to the spread of nitrogen. After both wells are shut down, the fluids are equilibrated. This can be seen in the contours of mole fraction of nitrogen at 3000 and 3500 days. Later, the amount of mass of nitrogen in the liquid phase will be compared to Cases Four and Five to demonstrate more clearly the effect of the horizontal fractures where hydrodynamic dispersion is considered.

Figure 6.28 presents gas saturation distribution. Again, gas is concentrated in the fractures and at the top of the block. If one compares both cases (with and without HD), the most important difference is that the oil-gas contact in the fracture advances more rapidly without HD. This advance in the gas-oil contact along the fracture reduces the contact area between matrix and fracture, causing more pressure drop in the matrix block around this contact; thus, more gas is liberated in the matrix. We can see in both figures how the gas saturation in the matrix increases around the gas-oil contact in the fracture.

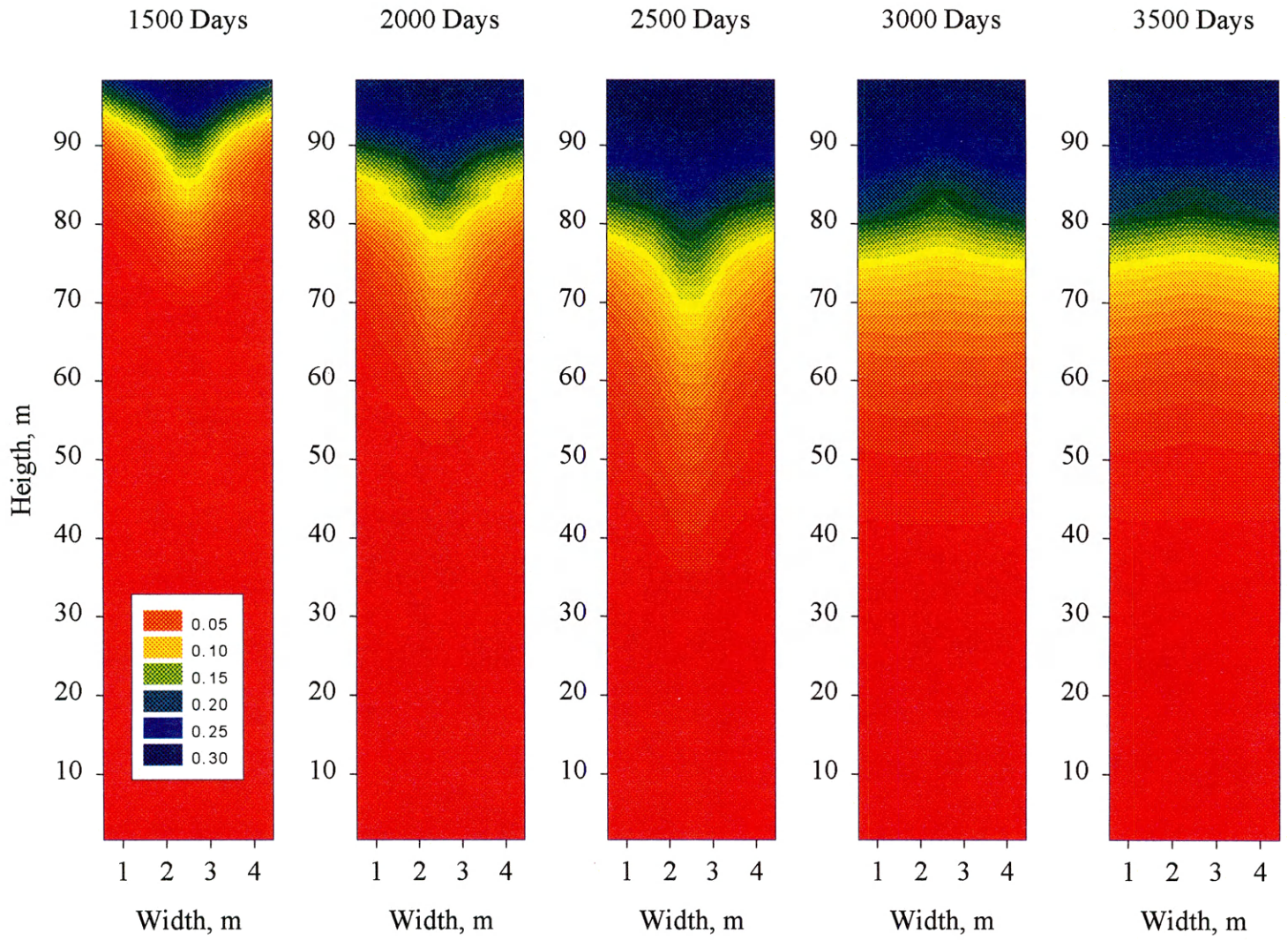

Figure 6.27 One Vertical Fracture and Three Horizontal Fractures. Mole Fraction of N_2 in the Liquid Phase. With Hydrodynamic Dispersion.

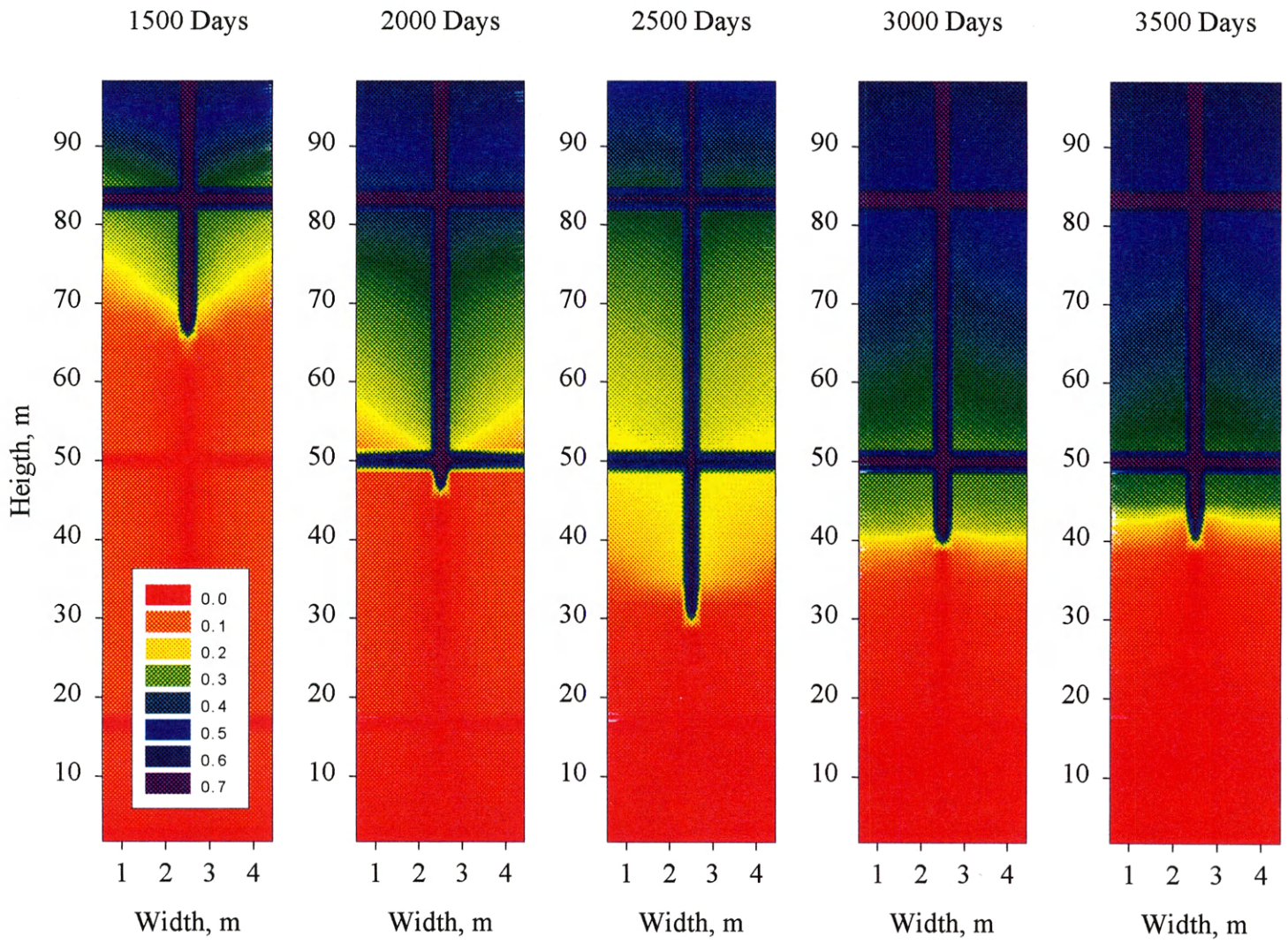

Figure 6.28 One Vertical Fracture and Three Horizontal Fractures. Gas Saturation With Hydrodynamic Dispersion.

In other words, without HD, the gas saturation contours have advanced more. After 2500 days, when both wells are shut down, equilibrium is restored: gas is concentrated at the top in both cases, but gas saturation is greater when HD is considered.

Again comparing Figures 6.27 and 6.28, one arrives at the same results discussed above: nitrogen is first spreading by diffusion in the gas phase and after, due to equilibrium between the liquid and gas phases, it is incorporated into the liquid phase.

6.5.3 Case 6: Production / Injection Stage –Two Porosities

Fractured reservoirs producing from carbonate formations can contain vuggy porosity. The main characteristic of these formations is a moderately high porosity. Porosity plays an important role in the hydrodynamic dispersion term. As we see in Equation 3.12 of Chapter Three, hydrodynamic dispersion is proportional to flow area, ϕS. To simulate the dispersion of nitrogen in high porosity formations, we divide the matrix block into two porosities: the matrix rock to the left side of the fracture was assigned 20% porosity, while the rock to the right side of the fracture 10% porosity. (Note that the total pore volume is the same as in Cases Four and Five). Figure 6.29, the mole fraction of nitrogen in the liquid phase, and Figure 6.30, the gas saturation, show the results for several time steps assuming hydrodynamic dispersion. Before performing this case, it was expected to see more mole fraction of nitrogen in the left side, that is, higher porosity. However,

given the higher pressure drop on the side of lower porosity, nitrogen tends to flow to the lower porosity side. In Figure 6.29 for 2500 days, the contours of the mole fraction of nitrogen are distorted on both sides of the fracture. The contours are slightly skewed to the side of low porosity. After shutting down both wells, molecular diffusion eventually takes place. It can be seen that at 3500 days, the mole fraction of nitrogen in liquid phase is a bit skewed to the side of high porosity.

Gas saturation for the same time-steps is given in Figure 6.30. In this figure, we see more clearly how the pressure drop is higher on the side of lower porosity, that is, on the left side. Because of the higher pressure drop, more gas is released inside the matrix block and more nitrogen is diffused through the gas phase. Thus, more nitrogen in the gas phase is in contact with the liquid, and then, by equilibrium, nitrogen is incorporated into the liquid (see Figure 6.29). It is important to note that a high mole fraction does not mean high amount of mass. This is because the amount of mass is given by $S\phi\xi V_r x_c$, where both the saturation of the phase and the mole fraction are important.

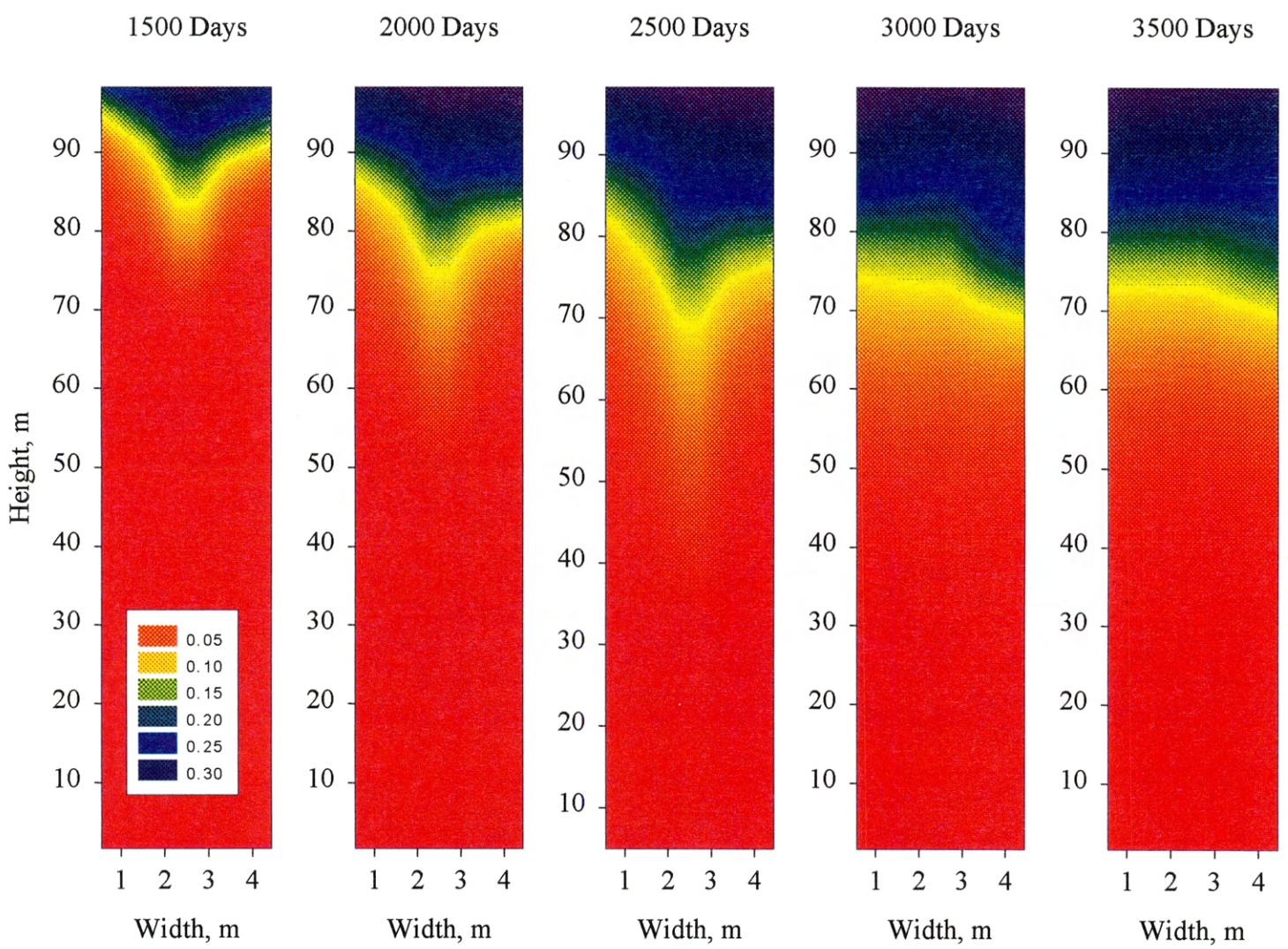

Figure 6.29 Two Porosities. One Vertical Fracture. Mole Fraction of N2 in the Liquid Phase, With Hydrodynamic Dispersion

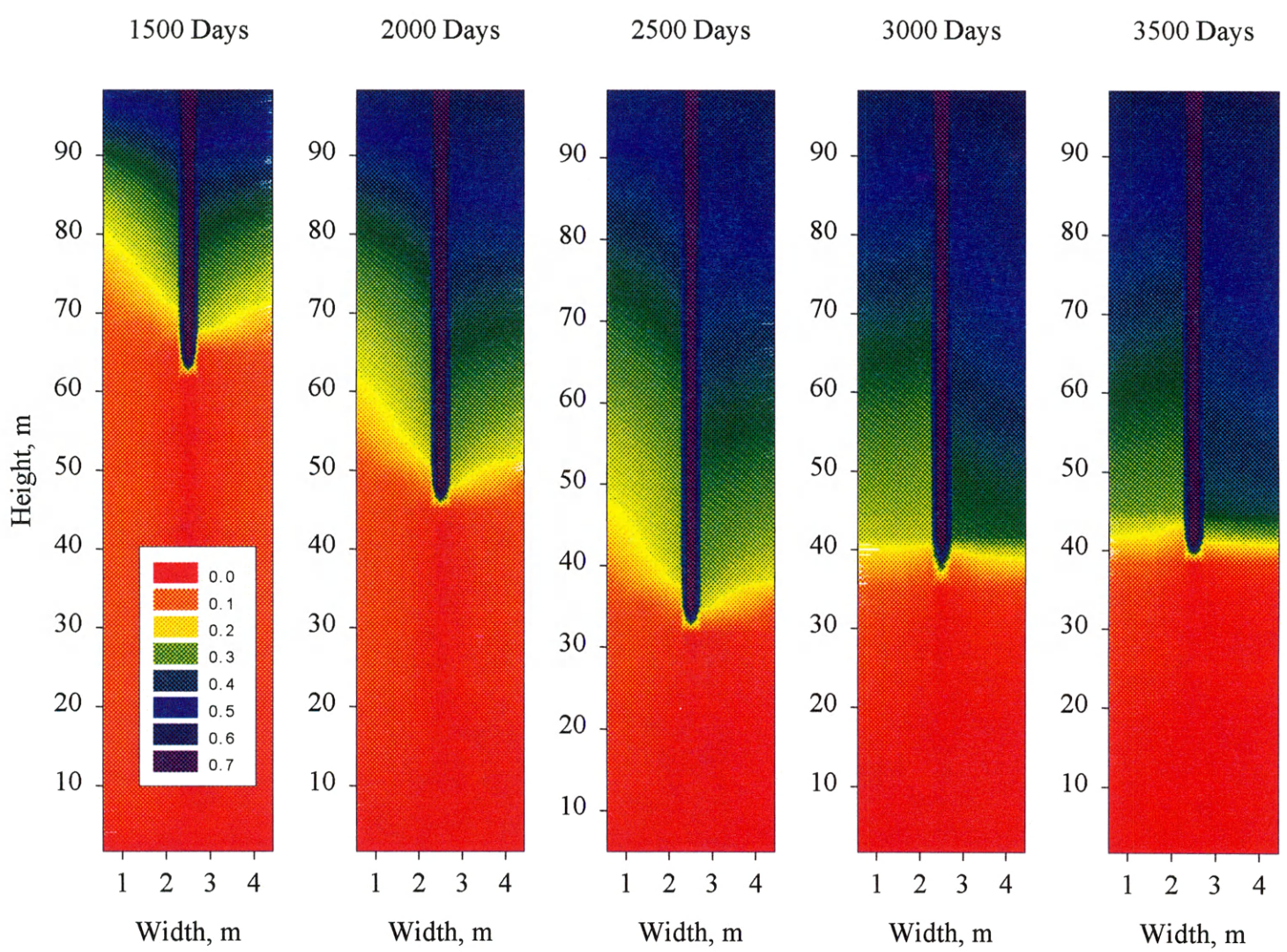

Figure 6.30 Two Porosities. One Vertical Fracture. Gas Saturation With Hydrodynamic Dispersion

6.5.4 Case 7: Production / Injection Stage –Vertical Barriers

Some carbonate formations have stylolitation or clay seams. Their main characteristic is low permeability and, therefore, they restrict the flow. In some cases, they can be impermeable barriers. To simulate a stylolite formation where nitrogen is injected, vertical permeability was set to a very low value in some layers, specifically, 0.1 mD. The thickness of these layers was 100 mm (0.3 ft). Figures 6.31 and 6.32 show the results for the mole fraction of nitrogen in the liquid phase and gas saturation, respectively. In both figures, HD is considered. In Figure 6.31, we see that the upper block contains almost all of the injected nitrogen. Once again, the maximum mole fraction of nitrogen in the liquid phase is around 32%. Stylolites act as barriers, preventing the vertical flow of oil to the bottom of the block, and allowing more time for nitrogen to diffuse into the liquid phase. Both oil and nitrogen flow through the fracture and, after passing the first fracture, nitrogen is again dispersed. The barriers in this ideal case cause a pressure drop in the entire block. Due to the high amount of gas, the dispersion of nitrogen at the top is larger than those of the previous cases. After shutting down both wells, these barriers prevent the equilibrium of fluids along the block. We can see how the fluids tend to segregate through the fracture and later, to the matrix. Due to the vertical barriers, the flow is bypassed in such formations and the diffusion of nitrogen through them is prevented. In other words, there is no convective flow through the barriers, and therefore,

no convective mixing. This is a clear example of the important role played by convective flow in the mixing of components in petroleum reservoirs.

The gas saturation given in Figure 6.32 shows the same behavior as in previous cases. We see how layers with low vertical permeability release more gas, due to a higher pressure drop than in the rest of the matrix. In addition, the gas in the matrix block is liberated as the gas-oil contact in the fracture advances. After shutting down of both wells, the fluid tends to be in equilibrium and the description of equilibrium given for the previous cases also applies for this case.

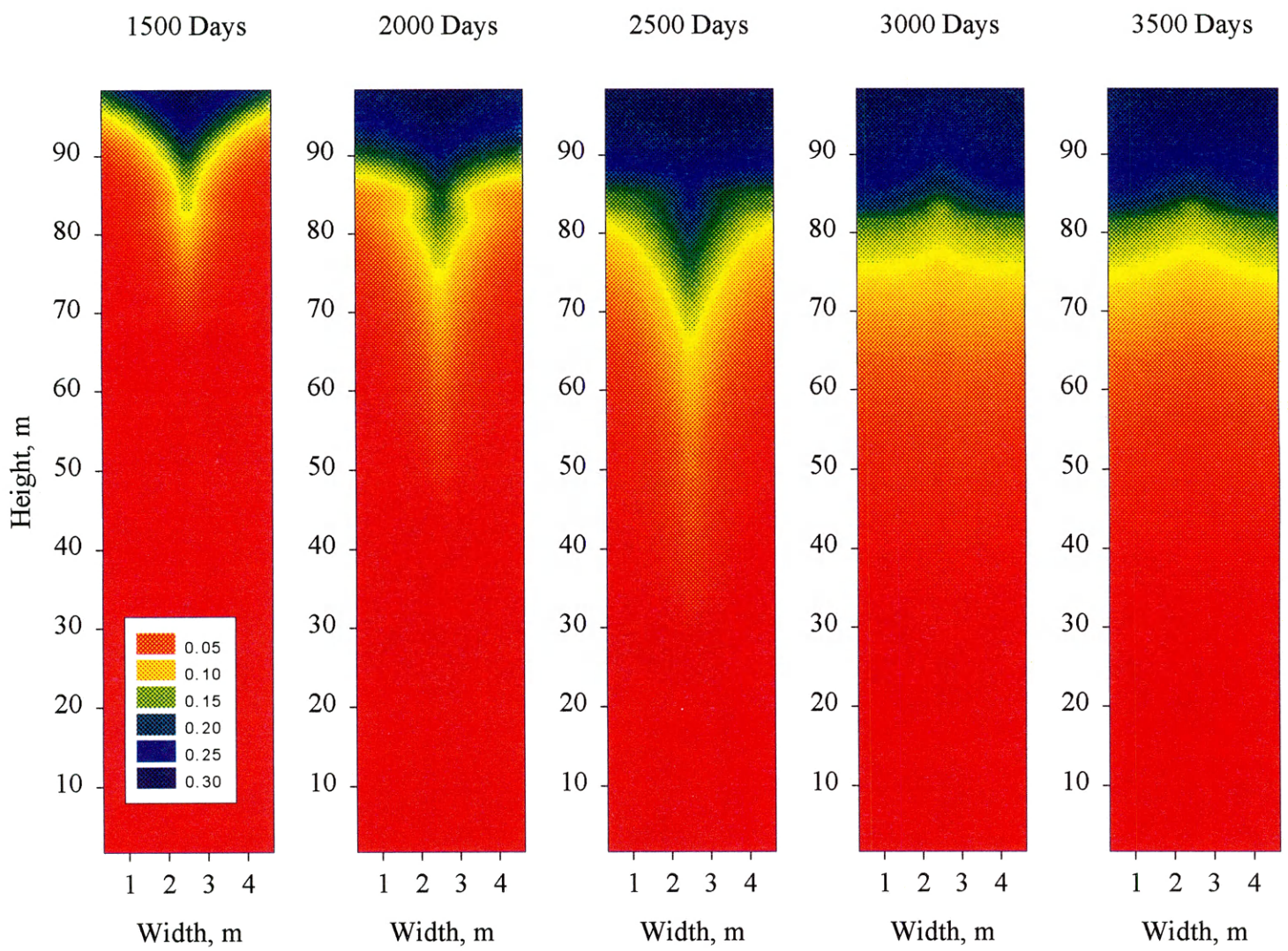

Figure 6.31 Three Horizontal Barriers. One vertical Fracture. Mole Fraction of N_2 in the Liquid Phase.

With Hydrodynamic Dispersion

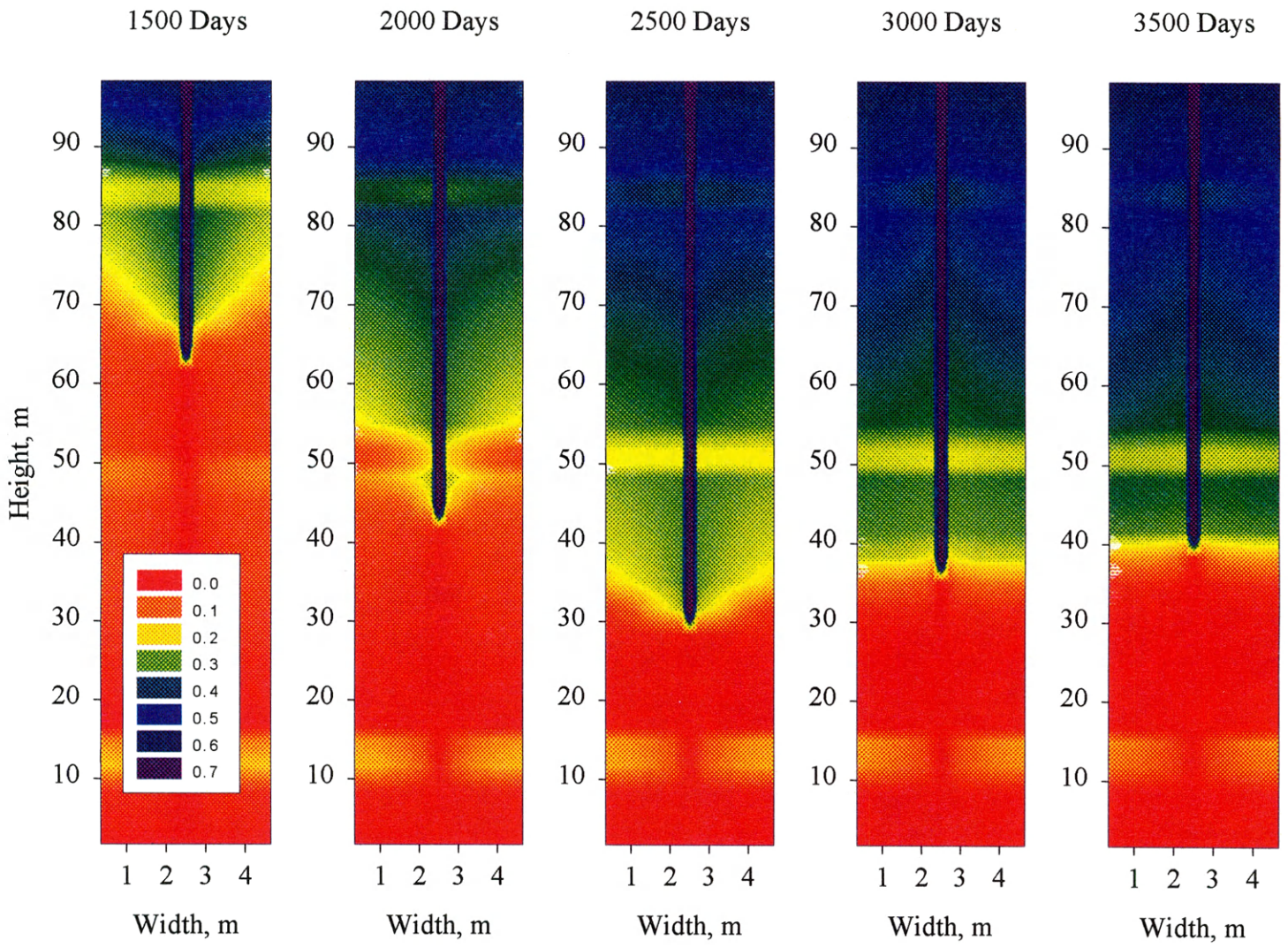

Figure 6.32. Three Horizontal Barriers. One vertical Fracture. Gas Saturation With Hydrodynamic Dispersion

6.6 Mole Fraction and Mass of Nitrogen in the Liquid Phase

In all cases, the maximum mole fraction of nitrogen in the liquid phase was around 32%. If we assume that the composition of the gas is almost 100% nitrogen close to the sink or injector well, then we can establish that, for practical purposes, the maximum mole fraction of nitrogen is:

$$x_{N_2} = \frac{1}{K_{N_2}}$$

where K is the equilibrium constant at the given pressure and temperature in the reservoir. The conditions for pressure maintenance are such that the ratio of both liquid and gas potentials, that is the equilibrium constant, is around 3. Accordingly, the inverse of 3 is approximately 0.33 a number that is very close to 0.32.

As can be seen from the figures for the previous four cases, nitrogen tends to concentrate at the top, near the source where HD is considered. A plot was made to visualize the mass of nitrogen in the liquid phase for all cases. The purpose of this plot is to distinguish from among all cases the mole fraction of nitrogen in the liquid phase. Certainly, the difference will be very small, but if one imagines a real reservoir, that amount of nitrogen could be significant.

It is very important to be able to predict when and how the nitrogen will reach the producing wells. To do this, we need to know the location and amount of nitrogen within the reservoir. In this way, one can anticipate a possible breakthrough of nitrogen in the producing wells. Figure 6.33 shows the amount of mass of nitrogen in the liquid phase for all four cases. Nitrogen mass is normalized by the thickness of the layer.

In the case of vertical barriers, there is more nitrogen at the top and intermediate parts of the block. Nitrogen diffuses more easily through the gas phase; thus, it has more contact with liquid to be in equilibrium. Notice that because of the absence of gas in the lower part of the block (for example, Figure 6.30 or 6.32), the amount of nitrogen in the liquid phase is nil.

With the exception of Case Five (the fracture orientation case), the rest of the cases show a similar amount of nitrogen in the liquid phase. In Case Five, we see the effect of the first horizontal fracture. There is greater mass of nitrogen in the liquid phase when the horizontal fracture exists, than when it does not. The horizontal fracture increases the area of contact between fracture and matrix block, thus increasing the diffusion of nitrogen into the matrix block.

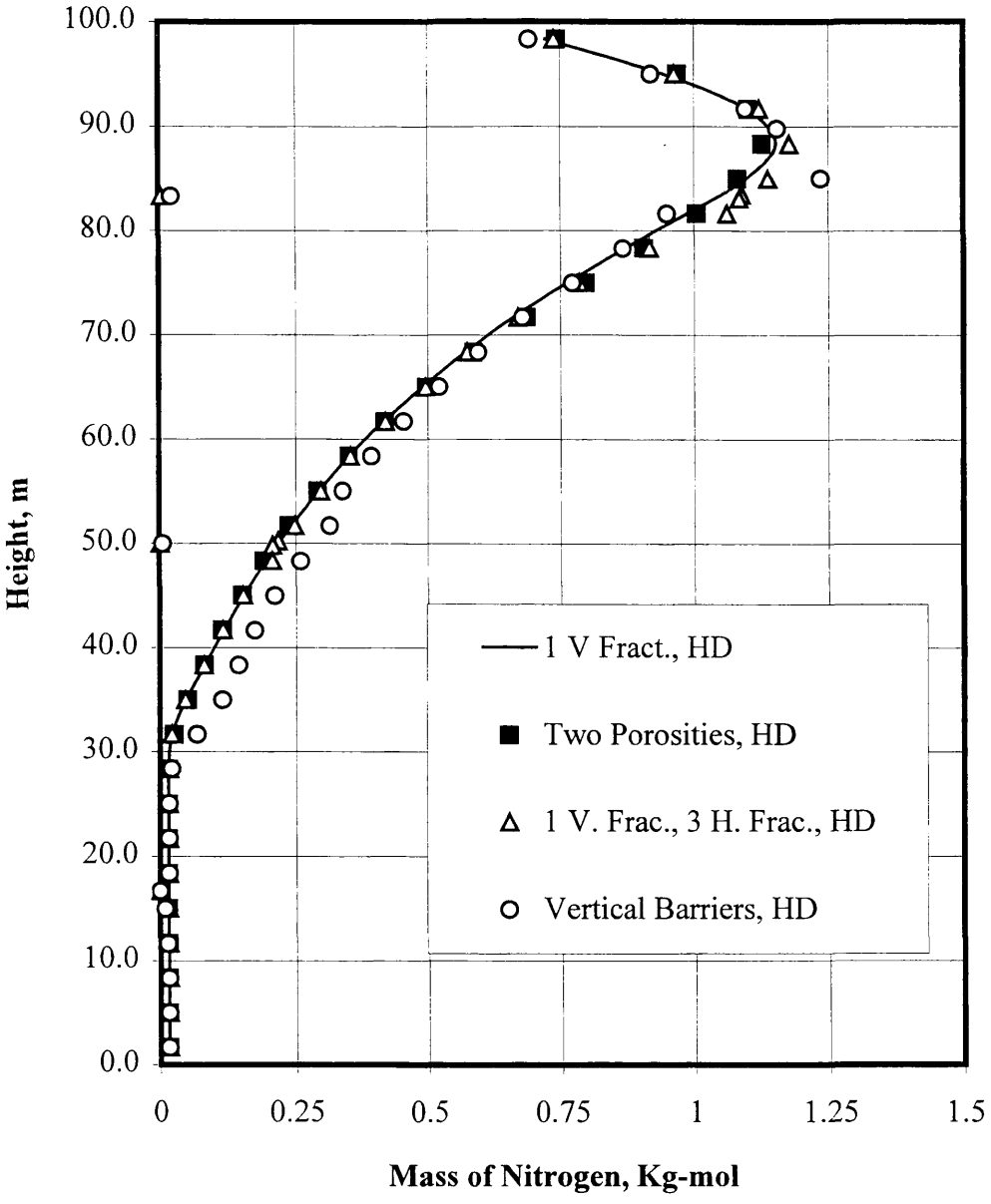

Figure 6.33. Mass of Nitrogene in the Liquid Phase. Per Layer. With Hydrodynamic Dispersion

6.7 Magnitude of the Gas-liquid Molecular Diffusion.

In all cases presented, gas-liquid molecular diffusion has not been included. Thus, the purpose of this section is to discuss gas-liquid diffusion contribution and the magnitude of its effect in the mixing of components. To do so, a special case was run. A matrix block similar to that shown by the Figure 6.4 was used, except that the fracture is located on the right side. The matrix block was divided into 11 cells in the x-direction and 30 cells in the z-direction. Nitrogen is injected at the top cell of the fracture and oil is produced at the bottom cell of the same fracture. Data used for this run are the same as shown in Table 6.6. Oil production and nitrogen injection at surface conditions were the same as the previous cases, 0.001 m^3/day and 1.0 m^3/day, respectively. Results are shown in Figure 6.34. In the first case (schematic 1), gas-liquid molecular diffusion has been included. Recalling that we are allowing gas-liquid diffusion only in the interface between matrix and fracture, that is, between the fracture cells and the first cells inside the matrix block adjacent to the fracture. In the second case (schematic 2), gas-liquid molecular diffusion is suppressed. The third schematic shows the difference in the mole fraction of nitrogen in the liquid phase between the first and second cases. In other words, the contribution and magnitude of gas-liquid molecular diffusion in the mixing of components is shown in the schematic 3. Thus, we can make the conclusion that: the magnitude of the gas-liquid molecular diffusion to mix components is local and small.

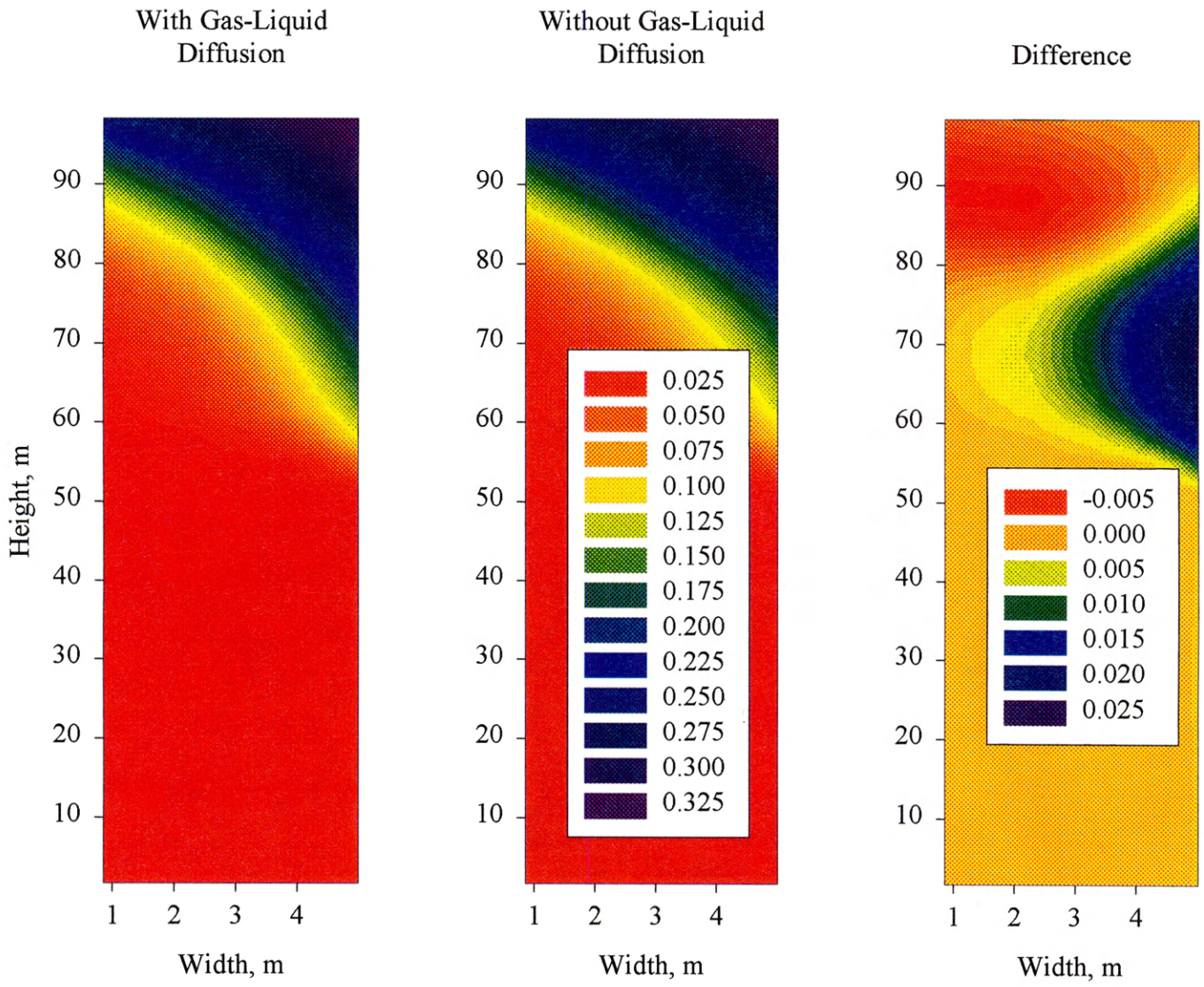

Fig 6.34 Magnitude of Gas-Liquid Diffusion. Mole Fraction of Nitrogen in the Liquid Phase. 2500 Days.

For this example, gas-liquid molecular diffusion contributes locally to less than 2% incremental change in the composition of nitrogen in the oil phase. Therefore, we could say that the contribution of the gas-liquid diffusion is not going to significantly modify the results of the previous cases. It is going to slightly modify the composition of nitrogen in the liquid phase.

CHAPTER 7

CONCLUSIONS AND RECOMMENDATIONS

7.1 Conclusions

The primary objective of this dissertation was to study the significance of the effect of diffusion in the presence of convective mixing of components in fractured reservoirs. Using a numerical simulator and several conceptual models to accomplish this goal, the following are the conclusions:

Primary Conclusions

1. Movements of components resulting from thermal and pressure diffusion are geological time-scale process and are insignificant in the exploitation period. Molecular diffusion, however, has a much shorter time-scale and contributes to mixing of components in the low velocity regions, that is, the interior of matrix blocks.
2. Hydrodynamic dispersion strongly affects the mass transfer processes in producing reservoirs and is, therefore, a significant contributor to the mixing of components on the short-term scale.

3. In compositional modeling, diffusive fluxes (molecular, thermal, and pressure diffusion) can be included when computing the initial compositional gradients. For practical purposes, however, their effects on reservoir performance and modeling could be insignificant.
4. In addition to diffusion and hydrodynamic dispersion of components, viscous, capillary, and gravity forces play a major role in distribution and mixing of components in the reservoir. This statement, as an example, pertains to fluid redistribution after wells are shut-in.

Secondary Conclusions

5. The simulator solves for p^{n+1}, S_g^{n+1} and S_w^{n+1} simultaneously while it solves for fluid composition explicitly. This method drastically reduces computation time compared to the fully-implicit formulation. Furthermore, the procedure is very stable considering that it is used in dual-porosity/dual permeability setting where the fracture cells are very small -- of the order of 10 mm width.
6. The program code can be used to compute compositional gradient, resulting from the contribution from chemical potential and pressure and temperature gradients, for initial reservoir conditions.
7. Thermal diffusion ratios were computed as a function of composition. This approach can also be extended to compute molecular (ordinary) and pressure diffusion coefficients as a function of composition.

8. Gas-to-liquid molecular diffusion mass transfer for a gas-filled fracture adjacent to an oil-saturated matrix was formulated and included in the program code. The input data were assigned based on experimental data and evidence.
9. Gas-oil fluid contact movement in the fracture was modeled in a realistic manner consistent with field practice.

7.2 Recommendations

To further improve and understand the effects of molecular, thermal and pressure diffusion on the compositional gradient and mixing of components, the following is recommended:

1. Apply the methodology of this thesis to a well-characterized reservoir fluid mixture.
2. Include cross-diffusion coefficients in the mathematical model. This could be especially important near the critical point of the fluid mixture.
3. Given significant uncertainty in the estimation of the thermal diffusion ratio, and the fact that none of the available methods have been experimentally verified, we recommend searching for new methods to compute the thermal diffusion coefficient and, when possible, obtain experimental data.

NOMENCLATURE

a	equation-of-state parameter
A	dimensionless equation-of-state parameter
b	equation-of-state parameter
B	dimensionless equation-of-state parameter
B	formation volume factor
C	concentration
D	depth
$D^{GL}{}_c$	molecular diffusion coefficient of component c
$D^{M}{}_c$	molecular diffusion coefficient of component c
$D^{P}{}_c$	pressure diffusion coefficient of component c
$D^{T}{}_c$	thermal diffusion coefficient of component c
f_a	fracture aperture
f_i	fugacity of component i
g	acceleration of gravity
$\overline{g}$	partial molar Gibbs free energy
G	residual function
F	feed moles
I	number of nodes in x-direction
IP	productivity index
J	diffusive flux
J^*	diffusive flux plus mechanical dispersion
$[J]$	Jacobian matrix
k	absolute permeability
$k^{T}{}_i$	thermal diffusion ration of component i
k_{rp}	relative permeability to phase p

K	number of nodes in z-direction
K_i	equilibrium constant of component I
$\mathbf{K}_c$	dispersion coefficient of component c
L	mole fraction of liquid phase
L_{ii}	phenomenological coefficient of component i
m_i	acentric-factor function
M	molecular weight
N_b	total number of nodes
n	number of moles
p	pressure
p_{ci}	critical pressure of component i
Pc	capillary pressure
R	gas constant
q_p	production/injection rate of phase p at res. cond.
$\overline{q}_p$	production/injection rate of phase p at res. cond. per unit of volume rock
Q	molar flow rate
Q^*_i	heat of transport of component i
S	saturation
t	time
T	transmissibility
T_c	critical temperature
$\widetilde{T}$	temperature
t	time
$\overline{u}$	partial molar internal energy
v	molar volume
$\overline{v}$	partial molar volume
V	volume

V	mole fraction of gas phase
Vr	grid block volume
x	related to x-direction
x_c	mole fraction of component c in the liquid phase
y_c	mole fraction of component c in the gas phase
z	related to z-direction
z_c	global mole fraction of component c in the mixture
Z	deviation factor

Greek Letters

δ_1	equation-of-state parameter
δ_2	equation-of-state parameter
δu	iterative change of u
Δ	difference operator
γ	specific weight
α	constant used in eq. 5.1.
$\widetilde{\alpha}$	dispersivity factor
Ω	equation-of-state parameter
ω_i	acentric-factor of component i
ε	tolerance
κ	interaction coefficients
μ	viscosity
μ_i	chemical potential of component i
ξ	molar density
ρ	volumetric density
ϕ	porosity

ϕ_i fugacity coefficient of component *i*

Subscripts

b bubble condition
c component
f fracture
g gas
GL related to gas-liquid diffusion
i grid point
l lower
L liquid
L longitudinal
m matrix
nc number of components
o oil
o base conditions
p phase
r reservoir condictions
rc reduced condition
s surface conditions
T transpose
T tranversal
u upper
V vapor
w water
ν iteration level

ε	tolerance

Superscript

GL	related to gas-liquid diffusion
M	relative to molecular diffusion
n	time step level
o	base conditions
P	relative to pressure diffusion
T	relative to thermal diffusion
T	transpose
T	tranversal
ν	iteration level
*	modified expression

REFERENCES

Abhvani, A.S. and Beaumont, D.N.: "Development of an Efficient Algorithm for the Calculations of Two-Phase Flash Equilibria", *SPE Reservoir Eng.*, 695-702, (Nov 1987).

Aguilera, R.: Naturally Fractured Reservoirs, Penn Well Publishing Co., Tulsa, OK (1995).

Ahmed, T.H.: Hydrocarbon Phase Behavior, Vol.7, Gulf Publishing Co., Houston, TX (1989).

Amyx, J.W., Bass, D.M., and Whiting, R.L. : Petroleum Reservoir Engineering, Mcgraw-Hill Book Company, Inc., New York, NY, (1960).

Aziz, K. and Settari, A.: Petroleum Reservoir Simulation, London,UK, *Applied Science Pub.*, (1979).

Barenblatt, G.I., Zheltov, I. P., and Kochina, I.N.: "Basic Concepts in the Theory of Seepage of Homogenous Liquid in Fissured Rocks", *PMM*, Vol. 24, No. 5, (1960).

Bear, J.: Dynamics of Fluid in Porous Media, *Elsevier*, New York, NY, (1972).

Bear, J.:"Modeling Flow and Contaminant Transport in Fractured Reservoir," in Flow and Contaminant Transport in Fractured Rock, Bear J. Ed., Academic Press, (1993).

Bedrikovetsky, P.: Mathematical Theory of Oil and Gas Recovery", *Kluwer Academic Publisher,* (1993).

Belery, P. and Da Silva, F. V.: "Gravity and Thermal Diffusion in Hydrocarbon Reservoirs," paper presented at the Third Chalk Research Program, Copenhagen, June 11-12, (1990).

Bird, R. B., Stewart, W. E. and Lightfoot, E. N.: Transport Phenomena, Wiley International Edition, New York, (1960).

Boersma, D.M. and Hagoort, J.: "Displacement Characteristics of Nitrogen vs. Methane Flooding in Volatile-Oil Reservoirs", *SPERE*, (Nov. 1994).

Branco, C.M.: "Simulador Compositional de Reservatorios com Formulacao Implicita em pressao e Saturacoes e semi implicita em composicoe", Tese de Mestrado, Universidade Estadual de Campinas, Campinas, (July 1991).

Branco, C.M. and Rodriguez, F.: "A Semi-Implicit Formulation for Compositional Reservoir Simulation" Paper SPE 27053 presented at the III Latin American and Caribbean Petroleum Engineering Conference of SPE, Buenos Aires, Arg, 377-391, (April 1994).

Charbeneau, R.J.: Groundwater Hydraulic and Pollutant Transport, *Prentice-Hall*, New Jersey, (2000).

Coats, K.H.: "Use and Misuse of Reservoir Simulation Model," *J. Pet. Tech.* 1391-1393 (Nov.1969).

Coats, K. H.: "An Equation of State Compositional Model," *Soc. Pet. Eng. L.* 363-76 (Oct.1980).

Coats, K.H.: " Implicit Compositional Simulation of Single Porosity and Dual-Porosity Reservoirs", SPE 18427, Proc. Tenth SPE Reservoir Simulation Symposium, 239-275, (Feb 1989).

Dake, L.P.: Fundamentals of Reservoir Engineering , *Elsevier*, New York,(1979).

Danesh, A.: PVT and Phase Behavior of Petroleum Reservoir Fluids, *Developments in Petroleum Science, Elsevier*, Amsterdam, (1998).

Da Silva F. and Belery, P.: "Molecular Diffusion in Naturally Fractured Reservoirs: A Decisive Recovery Mechanism", SPE 19672, Presented at the 64th annual conference held in San Antonio, TX, (1989).

Edmister, W. and Lee, B.: Applied Hydrocarbon Thermodynamics, Vol. 1.,*Golf Publishing Company,* 2nd Ed. (1984).

Firoozabadi, A.: Thermodynamics of Hydrocarbon Reservoirs, First Edition, McGraw Hill, New York, (1999).

Firoozabadi, A., Ghorayeb K., and Shukla, K.:" Theoretical Model of Themal Diffusion Factors in Multicomponent Mixture", *Aiche Journal,* 46, No. 5. 892-900, (2000).

Firoozabadi, A., and Thomas, K.L.:"Sixth Comparative solution Project: Dual-Porosity Simulators", *J. Pet. Tech.,* 710-19, (1990)

Festoy, S. and Van Golg-Racht, T.D.: "Gas Gravity Drainage in Fractured Reservoir Through New Dual-Continuum Approach", *SPE Reservoir Engineering*, 271-279,(Aug. 1989).

Fried, J. and Combarnous, M.: "Dispersion in Porous Media", *Advances in Hydrosciences*, Vol 7, V.T. Chow, Ed. Academic Press, 169-281,(1971).

Fung, L.S.: "Simulation Block to Block Process in Naturally Fractured Reservoir," *SPERE* (Nov. 1991).

Fussel, L.T. and Fussel, D.D.: "An Iterative Technique for Compositional Reservoir Simulator," *Soc. Pet. Eng. J.,* 211-220; Vol. 19, (Aug. 1979).

Fussel, D.D. and Yanosik, J.L.:"An Iterative Sequence for Phase-Equilibrium Calculations Incorporing the Redlich-Kwong Equation of State", *Soc. Per. Eng, J.,* 173-182. (June 1978).

Gelhar, L.W., Welty, C. and Rehfeldt, K.R.: "A Critical Review of Data on Field-Scale Dispersion in Aquifers," *Water Resour. Res.,* 28(7), 1955-74, (1992).

Ghorayeb, K. and Firoozabadi, A.: "Numerical Study of Natural Convection and Diffusion in Fractured Porous Media", *SPEJ*, 5(1), (March 2000).

Gilman, J.R. and Kazemi, H.: "Improvement in Simulation of Naturally Fractured Reservoir", *Soc. Pet. Eng. J.*, 695-707, (Aug. 1983).

Gilman, J.R. and Kazemi, H.: "Improved Calculations for Viscous and Gravity Displacement in Matrix Blocks in Dual-Porosity Simulators', *J. Pet. Tech.* 60-70, (Jan. 1988).

Glasstone, G., Laidler, K.J., and Eyring, H.: Theory of Rate Processes, McGraw-Hill Company, Inc., New York, (1941).

Graves, R.M. : "Notes for Advanced Rock Properties", PE-508, Petroleum Engineering Department, Colorado School of Mines, Golden, CO, (2000).

Hashem, Y.K. : "Explicit Composition Implicit Pressure and Saturation Simulation of Dual-Porosity/Permeability Reservoir", PhD Thesis, *Colorado School of Mines*, (1998).

Hasse, T.: Thermodynamics of irreversible processes, Dover Publication Inc., NewYork, (1990).

Hill, A.C. and Thomas, G.W.: "A new Approach for Simulating Complex Fractured Reservoirs", Paper SPE 13537 presented at the 1985 SPE Reservoir Simulation Symposium, Dallas, Feb 10-13.(1985).

Hoffman, J. D.: Numerical Methods for Engineers and Scientists, McGraw Hill, New York (1992).

Jacqmin, D. "The interaction of Natural Convection and Gravity Segregation in Oil/Gas Reservoir," paper SPE 16703 presented at the 1987 62nd SPE Annual Technical Conference and Exhibition, Dallas, (Sept. 1987).

Kazemi, H.: "Notes for Compositional Simulation", PE-614, Petroleum Engineering Department, Colorado School of Mines, Golden, CO, (1999).

Kazemi, H.: "Notes for Dual porosity Reservoirs", PE-614K, Petroleum Engineering Department, Colorado School of Mines, Golden, CO, (1999).

Kazemi, H. and Gilman, J.R.:"Multiphase Flow in Fractured Petroleum Reservoirs", in Flow and Contaminant Transport in Fractured Rock, Bear J. Ed., Academic Press, London, UK, (1993).

Kazemi, H. and Merril, L.S.: "Numerical Simulation of Water Imbibition in Fractured Cores", *Soc. Pet. Eng. J.,* 175-82; (Jun. 1976).

Kazemi, H., Merril, L.S., Potefield, K.L., and Zeman, P.R.: "Numerical Simulation of Water-Oil Flow in Naturally Fractured Reservoirs", *Soc. Pet. Eng. J.,*317-26,(Dec. 1976).

Kazemi, H.:"Pressure Transient Analysis of Naturally Fractured Reservoirs with Uniform Fraacture Distribution", *Soc. Pet. Eng. J.,* 451-462; *Trans.*, AIME, Vol. 246, (Dec. 1969).

Kazemi, H., Vestal, C.R. and Sank, G.D.: "An Efficient Multicomponent Numerical Simulator", *Soc. Pet. Eng. J.*, 355-368; (Oct. 1978).

Lake, L.W., Pope, G.A., Carey, G., and Sepehrnoori, K.:"Isothermal, Multiphase, Multicomponent Fluid Flow in Permeable Media", *In Situ*, 8(1). 1-40 (1984).

Lorenz, J., Bray, B.G., and Clark, C.R.: "Calculating Viscosities of Reservoir Fluids From Their Composition," *JPT* (Oct 1964) 177-184. Trans., AIME, Vol. 225.

McCain, W.D. Jr.: The Properties of Petroleum Fluids, Penn Well Publishing Company, 2nd Edition, Tulsa, Oklahoma (1990).

Michelsen, M.: "The Isothermal Flash Problem. I. Stability," *Fluid Phase Equilibria*, Vol. 9, 1-19, (1982)

Michelsen, M. and Heidemann, R.: "Calculations of Critical Points from Cubic Two-Constants Equations of State," *AIChe J.*, Vol 27, 521-523, (May 1981).

Minkowycz, W.L., Sparrow, E.M., Scheider, G.E. and Pletcher, R.H.: Handbook of Numerical Heat Transfer, *Wiley Publication*, New York, 24-26,(1988).

Nghiem, L. and Li, Y.: " Phase Equilibrium Calculations for Reservoir Engineering and Compositional Simulation", *First and Second Int. Forum on Reservoir Simulation*, Leoben, Austria, 427-500, (1989).

Peaceman, D.W.: Fundamentals of Numerical Reservoir Simulation, *Elsevier*, Scientific Publisher Company Inc. New York (1989).

Peng, D. Y. and Robinson, D. B.: "A New Two-constant Equation of State," *Ind. Eng. Chem. Fund.* (1976), Vol. 15, 59.

Perkins, T. K. and Johnston, O.: "A Review of Dispersion in Porous Media", *Soc. Pet. Eng. J.*, 70-78, (March 1963).

Prausnitz, J. M., Lichtenthaler, R. N. and de Azevedo, E. G,: Molecular Thermodynamics of Fluid-Phase Equilibria, Second Edition, *Prentice-Hall Inc.*, Englewood Cliffs, N.J. (1986).

Renner, T.A.: "Measurement and Correlation of Diffusion Coefficients for CO_2 and Rich-Gas Applications," *SPE Reservoir Engineering*, 517-523, (May 1988).

Ridlich, O. and Kwong. J.: "On the Thermodynamics of Solutions. An Equation of State. Fugacities of Gaseous Solutions," *Chemical Reviews,* Vol. 44, 233-247, (1949).

Riley, M.F. and Firoozabadi, A.: "Compositional Variations in Hydrocarbons Reservoirs with Natural Convections and Diffusion", *AIChE J.*, Vol 44, 452. (1988).

Rossen, R.H. and Shen, E.:"Simulation of Gas/Oil Drainage and Water/Oil Imbibition in Naturally Fractured Reservoir", *SPE Reservoir Engineering,* 464-470, (Nov. 1989)

Sahimi, M.: Flow and Transport in Porous Media and Fractured Rocks, *VCH,* Weinheim, Germany, (1995).

Saidi, A. M.: Reservoir Engineering of Fractured Reservoir, *TOTAL edition*, Paris 1987.

Sherman, A.H.: "NSPIV, A Fortran Subroutine for Sparse Gaussian Elimination with Partial Pivoting", *ACM Trans. Math. Software*. (1989).

Shukla, K., and Firoozabadi, A.: "A New Model of Thermal Diffusion Coefficient in Binary Hydrocarbon Mixtures," *Ind. Eng. Chem. Res.*, Vol. 37, 3331, (1998).

Sigmund, P.M.: "Prediction of Molecular Diffusion at Reservoir Conditions. Part I", *The Journal of Canadian Petroleum",* 48-57, (April 1976).

Sonier, F., Souillard, P. and Blaskovick, F.T.: "Numerical Simulation of Naturally Fractured Reservoir", *SPERE*, 1114-22, (Nov 1988).

Stone, H.L.: "Estimation of Three-Phase Relative Permeability and Residual Oil Data," Presented at the 24th Annual Technical Meeting of the Petroleum Society of CIM, Edmonton, (May 1973).

Thomas, G.W.: Principles of Hydrocarbon Reservoir Simulation, *Printice Hall*, Englewood Cliffs, NJ, (1982).

Thomas, L.K., Dixon, T.N., and Pierson, R.: "Fractured Reservoir Simulation", *Soc. Pet. Eng. J.,* 42-52; (Oct. 1983).

Van Golf Racht, T.D.: "Fundamentals of Fractured Reservoir Engineering," *Elsevier Scientific Publishing*, New York, (1982).

Warren, J.E. and Root, P.J.: "The Behavior of Naturally Fractured Reservoirs", *Soc. Pet. Eng. J.,* 245-255, (Sept. 1963).

Witherspoon, P., Wang, J., Iwa K., and Gale, J.E.: "Validity of Cubic Law for fluid flow, a deformable rock fracture,", *Water resour. Res.* 1016-1024, 16, (1980).

Yamamoto, R.H., Padgett, J.B and Ford, W.T.: "Compositional Reservoir Simulator for fissured System-The single-Block Model", *Soc. Pet. Eng. J.*, 113-128, (Jun 1971).

Instructions to use the CD

1. To read the appendices is necessary to have *Microsoft Word* 97. To read the ASCII files is necessary to have any Editor, for example, *WordPad.*

2. The CD contains three folders: Appendices, Case_4, and Simulator.

3. The folder "Appendices" contains all appendices cited in the thesis. The folder "Case_4" contains the results for the Case Four (Thesis, pp. 128). The Folder "Simulator" contains an executable file and a set of data to reproduce Case Four.

4. Any question or request contact Victor H Arana O (vharana@yahoo.com)